energies

MDPI

*Review*

# Nanofluids in Thermal Energy Storage Systems: A Comprehensive Review

**Mohamed Shameer Peer, Mario Cascetta, Luca Migliari and Mario Petrollese ***

Department of Mechanical, Chemical and Materials Engineering, University of Cagliari, 09123 Cagliari, Italy; mohameds.peermohamed@unica.it (M.S.P.); mario.cascetta@unica.it (M.C.); luca.migliari@unica.it (L.M.)
* Correspondence: mario.petrollese@unica.it; Tel.: +39-0706755118

**Abstract:** Nanofluids, which consist of nanosized particles dispersed in a base fluid, represent a promising solution to improve the performance of thermal energy storage systems. This review offers a comprehensive overview of nanofluids and their applications in thermal energy storage systems, discussing their thermal properties, heat transfer mechanisms, synthesis techniques, and application in latent heat storage systems. Various types of nanofluids are examined, including metal oxide, carbon-based, and metallic nanofluids, highlighting their effects on thermal conductivity, latent heat and the phase change temperature. A review of experimental and numerical studies showcases the performance of thermal energy storage systems incorporating nanofluids and the factors influencing their thermophysical characteristics and energy storage capacity. Finally, the key findings of current research are summarized, as well as the challenges and the potential future directions in nanofluid-based thermal energy storage systems research, emphasizing the need to optimize nanoparticle concentration and long-term durability.

**Keywords:** nanofluids; nanoparticles; heat transfer; thermal energy storage; phase change material



Academic Editor: Antonio C.M. Sousa

Received: 17 December 2024
Revised: 22 January 2025
Accepted: 31 January 2025
Published: 4 February 2025

**Citation:** Peer, M.S.; Cascetta, M.; Migliari, L.; Petrollese, M. Nanofluids in Thermal Energy Storage Systems: A Comprehensive Review. *Energies* **2025**, *18*, 707. https://doi.org/10.3390/en18030707



## 1. Introduction

Currently, the transition to a decarbonized and sustainable energy sector, crucially facilitated by integration of Renewable Energy Sources (RES) into the energy combination, is regarded as an essential and urgent strategy for addressing climate change [1]. In fact, traditional energy systems dependent on fossil fuels pose serious risks to the environment due to climate-altering emissions. According to the Energy Institute [2], global energy-related greenhouse gas emissions reached a new all-time high of over 40 gigatons in 2023. While renewable energy sources continued to expand rapidly, reaching record levels in 2023, the dominance of fossil fuels in the global energy mix remained stubbornly high, hovering around 80%.

Thermal energy storage (TES) offers a promising solution to address fluctuations in Renewable Energy Sources (RES) production, particularly on the long-term (up to seasonal) scale. There is a widespread consensus that TES is one of the most appropriate options for long-term energy storage systems, primarily because of its low capital investment requirements [3,4]. By capturing and reserving surplus heat for future use, TES systems can enhance grid stability, diminish dependence on fossil fuels, and support a sustainable energy future.

The global demand for TES is influenced by several factors, such as geographical location, climate, and energy consumption patterns. Regions rich in renewable energy sources,

like solar and wind, present greater potential for TES applications [5]. It is also driven by the need to mitigate climate change impacts, support renewable energy integration, enhance energy efficiency, and adapt to evolving energy demands in both heating and cooling applications across diverse regions [6]. The demand for TES is also influenced by shifting energy consumption driven by urbanization, industrialization, seasonal heating and cooling requirements, and the addition of intermittent RES [7]. However, TES requirements and challenges differ widely by region. For instance, in arid and semi-arid areas, TES can be employed to accumulate solar thermal energy for heating and cooling applications. In colder climates, TES is often used to capture excess heat from industrial processes or district heating systems [8].

TES has diverse applications across multiple sectors, including buildings, industry, and power generation. In the building sector, TES can capture and store surplus solar thermal energy for heating and cooling, helping to lower fossil fuel reliance and reduce energy costs [9]. In industrial settings, TES can recover waste heat from processes, boosting energy efficiency and decreasing greenhouse gas emissions. Within the power sector, TES can be combined with renewable energy sources to offer long-term flexible solutions, thereby enhancing grid stability and reliability [10].

Although TES shows great potential, several obstacles limit its broader adoption. These challenges mainly include the high up-front costs as well as the limited efficiency when compared to other types of storage systems. However, ongoing research and development efforts are helping to address these issues, making the future of TES increasingly promising [11]. Government policies and incentives are also vital, as they can encourage TES deployment by creating supportive market conditions and lowering financial barriers. Augmenting the efficiency of TES is of paramount importance in the changeover to a sustainable energy landscape [12]. TES efficiency is contingent upon various factors, including the thermal characteristics of storage materials, system design, and integration with existing energy infrastructure. The selection of high-capacity materials with favorable heat transfer characteristics is crucial to improve thermal retention and minimize energy losses [13].

Nanofluids, a mixture composed of nanoparticles like metal oxides, metals or carbon-based materials dispersed in traditional heat transfer fluids, have been recognized as an auspicious solution to the problem of improving the performance of TES systems [14]. These advanced fluids exhibit significantly improved thermal conductivity and heat transfer capabilities compared to their conventional counterparts, making them particularly well-suited for applications demanding highly efficient heat transfer [15].

The thermal characteristics of nanofluids are improved with respect to those of traditional heat transfer fluids due to several reasons, such as the increased surface area, which enhances heat transfer, and the modified flow properties, that facilitate better convective heat transfer [16]. The stability aspect and uniform scattering of nanoparticles in base fluid are vital factors affecting the performance of nanofluids, as they influence thermal conductivity and help prevent sedimentation. Researchers are actively exploring different formulations of nanofluids to optimize these attributes, ensuring they maintain stability and effectiveness across various operating conditions [17].

The number of publications related to thermal energy storage research from 2001 to 2025, as shown in Figure 1, demonstrates a significant upward trend based on data retrieved from the Scopus database. From 2001 to 2013, the growth in research output was gradual, with annual publications remaining below 100. However, from 2014 onward, the field experienced a notable surge, reflecting increased global interest and advancements in thermal energy storage technologies. This upward trajectory peaked in 2024 with over 500 publications, marking the highest output within the observed period. The sharp

decline in 2025 is likely due to incomplete data collection for that year, as it may not yet fully represent the total number of indexed publications. Overall, the trend underscores the growing importance of thermal energy storage as a pivotal research area in the context of sustainable energy and climate change mitigation.

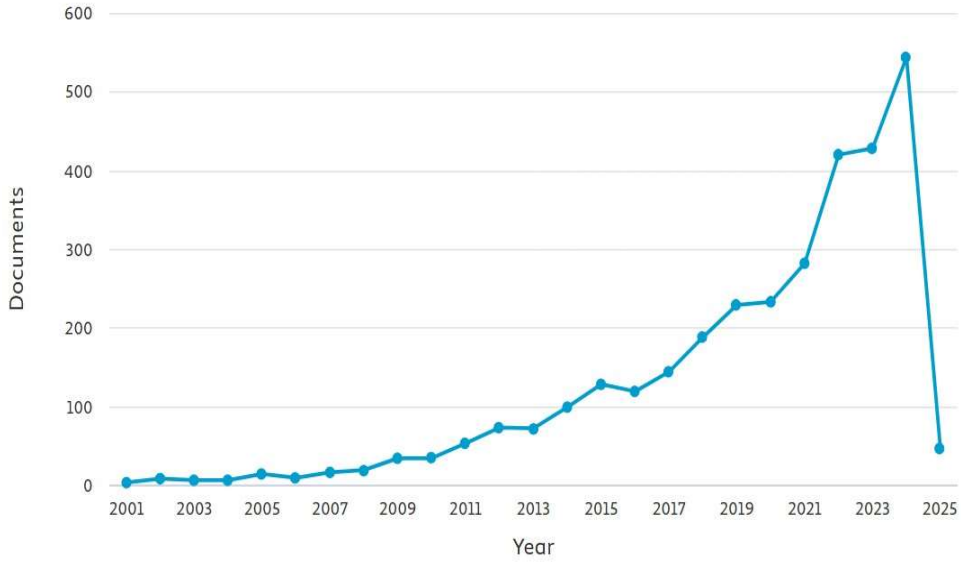


**Figure 1.** Nanomaterial research publications for thermal energy storage from the year 2001 to 2025: an annual analysis.

Overall, the paper seeks to synthesize existing research and provide insights into how nanofluids can improve the efficiency and effectiveness of TES, thereby helping the development of sustainable energy solutions. Given these premises, the novelty of this paper is providing a comprehensive review of TES systems based on nanofluids. The structure of the paper is as follows: In Section 2, the paper begins by classifying and briefly describing thermal energy storage (TES) systems, setting the stage for understanding the challenges that nanofluids might help address. Section 3 explores the topic of nanofluids, covering their synthesis methods (Section 3.1), thermophysical properties (Section 3.2), and heat transfer mechanisms (Section 3.3). In Section 4, the paper focuses on how nanofluids are applied within thermal energy systems. Section 5 discusses the ongoing challenges in nanofluid research which still need to be tackled. Section 6 states the limitations and future directions in nanoparticle-based PCM systems and thermal storage systems. Lastly, Section 7 concludes the paper and looks ahead at the future potential of nanofluids.

## 2. Thermal Energy Storage Systems

TES systems can be broadly classified into three main categories: sensible heat storage (SHS), latent heat storage (LHS), and thermochemical heat storage (TCHS), as illustrated in Figure 2. SHS retains energy by increasing the temperature of a medium, such as water or rocks without inducing a phase change. LHS relies on phase change materials (PCM) which absorb and emit energy while in phase transition [18]. These transitions include solid–liquid, liquid–gas, solid–gas, and solid–solid changes. Among them, solid–liquid PCMs are increasingly used for their reliability and high energy storage capacity. While liquid–gas and solid–gas transitions offer higher energy density, they are often limited by complex system requirements. Solid–solid transitions, which involve changes in crystalline structure, present unique advantages such as no leakage, enhanced long-term stability, and simpler containment. Polymers and specific alloys are examples of materials that make this method suitable for compact and dependable energy storage applications. TCHS uses

reversible chemical reactions or sorption processes to store and release heat, offering high energy density and long-term storage capabilities [19].

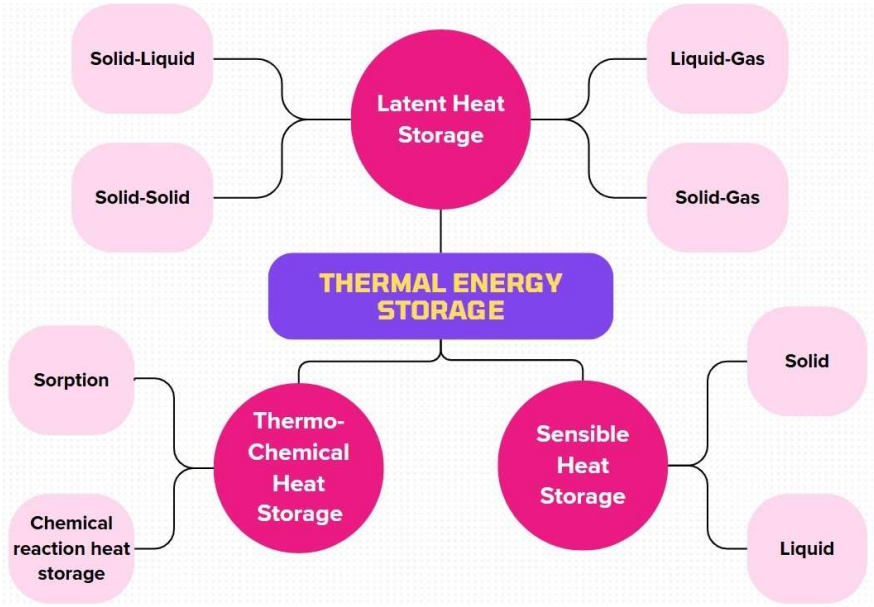


**Figure 2.** Types of TES.

### *2.1. Sensible Heat Storage (SHS)*

Sensible heat storage is a highly cost-effective method for storing thermal energy. It includes storing heat energy inside the material's sensible heat capacity, as its temperature changes, as shown in Figure 3. SHS is a TES subcategory that elevates material temperature without phase change to store heat [20]. This versatile and commonly used TES technology finds applications in space cooling and heating, and domestic hot water as well as industrial settings. SHS systems capture heat by temperature increment of storage media such as metals, rocks, concrete, water or molten salts. The quantity of heat captured through SHS is linked to the material's weight and its temperature rise [21]. SHS systems offer a combination of simplicity and affordability, making them a popular choice. SHS systems boast high efficiency levels, typically recovering between 70% and 90% of stored energy [22]. While SHS systems excel in efficiency, they typically store less heat per unit volume compared to other TES technologies like LHS. SHS systems can be primarily categorized into liquid-based and solid-based depending on their storage medium.

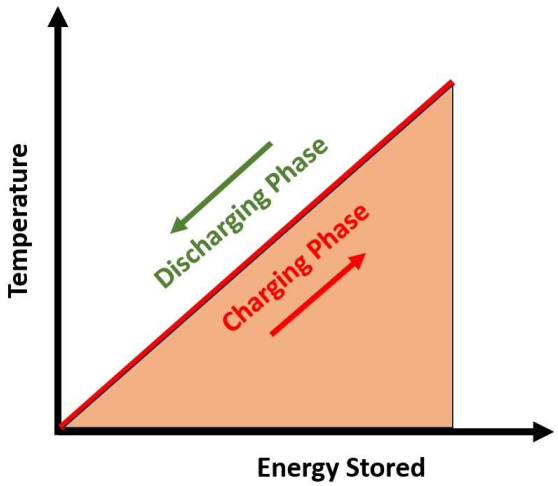


**Figure 3.** Sensible Heat Storage reaction.

Liquid-based storage includes water and organic liquids. Water's widespread availability, low cost, and effective heat transfer properties make it a preferred option [23]. Organic fluids provide flexibility and store a significant amount of energy [24]. Moreover, some systems combine water [25] with organic liquids, such as fatty acids or paraffin waxes to achieve a broader range of temperature and higher density of energy. This elasticity allows them to be used effectively in applications with considerable temperature swings.

Solid-based storage systems employ materials like concrete [26], rocks [27] or metals [28] as the heat storage medium. These materials offer distinct benefits compared to liquid-based SHS. In fact, rocks, readily available and affordable, present a cost-effective option for heat storage. Concrete's growing popularity stems from its seamless integration into building constructions. Moreover, under high pressure and temperature conditions, solid-based storage systems exhibit minimal leakage risk [29]. In harsh environments, solids demonstrate exceptional resilience, tolerating a varied temperature range. For effective cooling and heating, SHS acts as the best source by blending seamlessly with concrete for building structures [30]. While solid-based heat storage systems offer several advantages, they also come with certain drawbacks [29] with respect to liquid-based heat storage:

- solid-based SHS can store less heat per unit mass or volume due to inferior specific heat capacity and energy density;
- because of the formation of hotter and colder regions within the storage medium, it can be challenging to maintain and achieve constant distribution of temperature;
- factors like conduction and radiation cause self-discharge in solid-based SHS, leading to a gradual loss of heat periodically;
- while solid-based SHS may be less expensive up-front, they often have elevated enduring operational and maintenance expenses compared to liquid-based SHS.

### *2.2. Latent Heat Storage (LHS)*

Latent heat storage mainly retains heat through the phase change process, where temperature remains nearly constant. This method is closely associated with the latent heat of material, as illustrated in Figure 4. Latent Heat Storage accomplishes heat storage by employing PCMs. This procedure entails the absorption or release of a substantial quantity of heat, referred to as latent heat of vaporization or fusion. LHS offers several advantages over SHS, specifically increased energy storage capacity [31], swift storage and release capacity [32], sleek and compact design [33] and decreased susceptibility to temperature variations [34].

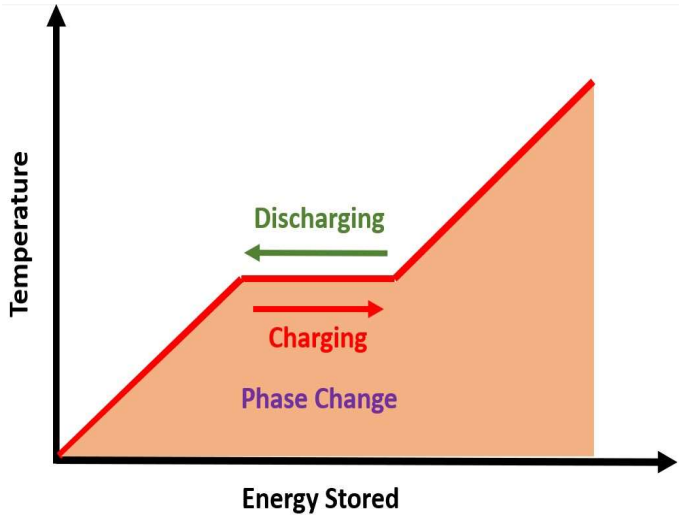


**Figure 4.** Latent Heat Storage reaction.

LHS are categorized into organic and inorganic types based on the kind of PCM used. Organic phase-changing materials undergo a distinctive temperature-based phase transformation, shifting from liquid to a solid state and from solid to liquid state, accompanied by latent heat release or absorption. Within the realm of TES, organic PCMs have gained prominence in construction applications, mainly due to their temperature transition phase falling within the human-safe range. Importantly, PCMs exhibit a broad range of temperature for changing phase, expanding their versatility in diverse applications. They are also significantly safer for various applications due to toxic- and corrosion-resistance properties. Moreover, the versatility of organic phase-changing materials is evident in their diverse forms, enabling tailored applications to suit various contexts [35]. Commonly employed organic PCMs are paraffins [36], fatty acids [37], eutectic mixtures [38], polymers [39], esters [40], sugar alcohols [41] and fatty alcohols [42].

Inorganic phase change materials primarily consist of water, molten salts, hydrated salts and metal alloys. Hydrated salts and water are predominantly utilized in low-temperature applications [43]. Metals and alloys offer significant advantages for development in latent heat energy storage systems, including high energy storage density, minimal volume change during melting, excellent thermal conductivity, and thermal stability that is tens to hundreds of times better than other PCMs [44]. Meanwhile, for cold storage, inorganic PCMs are primarily composed of hydrated, molten salts, and other inorganic compounds [45]. Inorganic phase change materials offer advantages over organic ones, including higher latent heat, a wider high-temperature range, and lower cost [46]. However, inorganic phase change materials also face challenges such as supercooling and phase separation, which can directly or indirectly impact their heat storage capacity [47]. The benefits and disadvantages of organic and inorganic PCMs [48] are listed in Table 1.

**Table 1.** Benefits and drawbacks of organic and inorganic PCMs [48].

| Organic PCMs | Inorganic PCMs |
|---|---|
| Benefits | Benefits |
| Low supercooling<br>Non-corrosive<br>Stable thermal performance<br>Wide range of available melting points | High latent heat<br>High phase change enthalpy |
| Drawbacks | Drawbacks |
| Inflammability<br>Lower thermal conductivity<br>Potential for degradation over time<br>Low phase change enthalpy | Prone to supercooling<br>Risk of phase separation and phase segregation<br>Can be corrosive<br>Lack of thermal stability |

### *2.3. Thermo-Chemical Heat Storage (TCHS)*

Thermo-chemical heat storage (TCHS) uses reversible processes of chemical reactions for heat storage and retrieval [49]. This process includes the exchange of heat between a chemical reaction and its surroundings, enabling the storage and retrieval of energy. To fully understand the adsorption or desorption cycle, it is essential to carefully analyze the equilibrium temperature, which directly influences the cycle process. The release of ions from solids initiates when the system temperature surpasses the equilibrium temperature [50]. TCHS systems are of two types depending on their interaction with the environment.

Open TCHS System—The material acts as a heat-storing medium, absorbing reactants during the endothermic phase and releasing them during the exothermic phase. During the charging phase of the cycle, the adsorbent material undergoes a process of heat absorption

as it binds with incoming reactants. As discharge progresses, the absence of new reactants results in the desorption of previously adsorbed reactants, accompanied by the release of heat. The constant supply of heat makes the open system suitable particularly for applications like cooling or heating of space. By dynamically controlling reactant flow, the system can flexibly adjust its heat storing and rate of release, optimizing performance according to needs. The flexibility of open systems in reactant supply means they are less dependent on storage capacity [49].

Closed TCHS System—Fixed adsorbent reactants exhibit reversible heat exchange through chemical reactions [50]. The system exhibits closed-loop thermal management, maintaining its temperature balance within a defined boundary. This system consists of two primary phases: charging and discharging. During the charging phase, the reactant is adsorbed by adsorbent material, primarily through a reversible chemical process or adsorption. This reaction absorbs heat from its surroundings, saving it as chemical potential energy within the system. The gathered heat from this exothermic reaction is suitable for practical implementation in a range of applications, including heating and air conditioning of space [51].

### 2.4. Challenges in TES

TES systems encounter various challenges that can significantly hinder their efficiency and overall effectiveness, many of which may be alleviated through the application of nanofluids.

Challenges in SHS:

- Low Energy Density: Sensible heat storage typically has lower energy storage density, meaning large volumes of material are needed to store significant amounts of energy [29].
- Thermal Losses: As SHS systems primarily rely on temperature changes for energy storage, maintaining consistent heat transfer efficiency is challenging [52].
- Slow Heat Transfer: The rate of heat absorption and release is often slow due to limited heat conductivity of the storage material [53].

Challenges in LHS:

- Low Thermal Conductivity: Many phase change materials (PCMs) used in LHS systems have poor thermal conductivity, slowing down the heat transfer process [47,48].
- Supercooling and Phase Separation: Some PCMs exhibit supercooling (cooling below their freezing point without solidifying), and phase separation (where different phases of the material separate), which can hinder performance [48].
- Limited Melting and Freezing Cycles: PCMs degrade over time with repeated melting and freezing cycles, reducing their effectiveness [48].

Challenges in TCHS:

- Low Energy Density: While TCHS systems can store large amounts of energy, the materials used often suffer from low energy density when compared to SHS and LHS systems [54].
- Kinetics of Chemical Reactions: The rate of the chemical reactions involved in thermochemical storage can be slow, limiting the system's responsiveness [55].
- Complex System Design: The need to control reaction conditions, such as pressure and temperature, makes TCHS systems complex and potentially costly [56].

How Nanofluids Alleviate These Challenges:

While nanofluids are commonly incorporated to augment the performance of LHS systems by improving heat transfer and reducing supercooling and phase separation, they also offer potential benefits in SHS and TCHS systems. Nanofluids can enhance thermal

conductivity, speed up energy transfer, and improve the efficiency and stability of the entire TES system across all three types.

- Optimized Energy Density: The addition of nanofluids improves heat transfer rate and thermal response, allowing for higher energy storage density compared to conventional systems [57].
- Improved Heat Transfer Efficiency: The enhanced thermal properties of nanofluids allow for better heat distribution, minimizing thermal losses during the cycles of charging and discharging [58].
- Enhanced Heat Transfer: Nanofluids increase thermal conductivity of the liquid phase, improving heat transfer rate during the phase change process, thus speeding up the energy storage and retrieval processes [58].
- Enhanced Thermal Conductivity: Nanofluids, which are suspensions of nanoparticles in liquids, improve the thermal conductivity of base fluids, resulting in faster heat transfer and more effective energy storage and retrieval [57,59].
- Reduced Supercooling: By adding nanoparticles in PCM, nanofluids can reduce the degree of supercooling, improving the overall efficiency of the system [60].
- Prevention of Phase Separation: Nanoparticles can act as nucleating agents, promoting a more uniform phase change process and reducing the tendency for phase separation [61].
- Improved Thermal Stability: Nanofluids improve the thermal stability and lifespan of PCMs by reducing the repeated thermal cycling effects [62].
- Enhanced Reaction Rates: Nanoparticles can provide a large surface area that promotes faster chemical reactions, improving the rate of energy storage and release [63].

## 3. Nanofluids

By incorporating nanoparticles into base liquids, nanofluids are created as advanced heat transfer media. They exhibit superior thermophysical characteristics and enhance heat transfer efficiency, making them suitable for various industrial and technological uses. This section examines the methods of synthesizing nanofluids, their properties, and heat transfer characteristics. It emphasizes the synthesis approaches, discusses their thermophysical properties and correlations.

### *3.1. Synthesis Techniques*

The techniques used to prepare nanofluids significantly impact their thermal properties. A variety of material mixtures can be employed for specific applications. These include nitrides, metal nanoparticles, metal carbides, oxides and nonmetals without and with surfactants. These materials can be dispersed into various base fluids like water, ethylene glycol (EG) and oil [59]. The following equation (Equation (1)) (Stokes' Law) states that the terminal velocity of a spherical object falling through a fluid is directly proportional to the square of its radius, the difference in density between the object and base fluid, and the viscosity of the fluid.

$$\mathrm{V} = \frac{2R^2}{9}(\rho_P - \rho_L) \times g \tag{1}$$

where V—velocity of sedimentation of particles, μ—viscosity of fluid, $R$—spherical object radius, $\rho_P$ and $\rho_L$ are the particle and fluid density and $g$ is gravitational acceleration. From the above equation, it is observed that lower sedimentation velocity of nanoparticles contributes to improved nanofluid stability. This is due to the reduction in R, elevating μ, and minimizing the difference between $\rho_P$ and $\rho_F$. To prevent nanoparticle accumulation while preparing nanofluids, it is essential to ensure the use of smaller-sized nanoparticles. The latter are characterized by lower sedimentation velocity, thus reducing the risk of

aggregation and increasing the dispersion of particles in the fluid. These aspects help uphold uniform properties and thermal performance [64].

Nanoparticle sedimentation is strongly influenced by the Stokes regime, a flow condition where viscous forces control inertial forces, distinctive of low Reynolds numbers. Within this regime, particles show expectable laminar motion, and their suspension stability depends on the equilibrium between sedimentation and counteracting forces like Brownian motion and electrostatic repulsion. The Stokes regime confirms that particles trail the streamlines of the fluid, avoiding quick sedimentation, which is critical for preserving nanofluid performance over time [65].

Reducing sedimentation velocity lessens particle clustering and guarantees uniform dispersion. For example, nanoparticles under 50 nm lead to improved Brownian motion, which avoids settling and advances stability. The interaction between particle size, Brownian motion and the Stokes regime is very important for nanofluid design [66]. Moreover, adjusting the base fluid properties, such as increasing viscosity or incorporating surfactants, further reduces sedimentation, which stabilizes the fluid for longer periods [67].

The Stokes regime also helps in augmenting nanoparticle suspension through the design of nanofluids along with low sedimentation rates. The Stokes number, defined as the dimensionless ratio of the particle relaxation time to the characteristic timescale of the flow, provides an understanding of particle–fluid interactions. The Stokes Number provides an insight into particle–fluid relations, where $S_t < 1$ specifies that particles follow fluid streamlines and persist in suspension. This equation forecasts and regulates particle dynamics in nanofluids. Applying the Stokes regime to nanofluids ensures better thermal properties and operational efficiency in heat transfer applications [68]. The preparation of nanofluids involves two primary methods: one-step and two-step.

#### 3.1.1. One-Step Method

The one-step method involves directly creating nanomaterials within a fluid without going through a separate dispersion process. This technique uses either liquid chemistry or physical methods to achieve this. A team of researchers conducted in-depth research on this method for preparing metal nanofluids. They developed techniques that involve condensation through direct evaporation that efficiently create nanofluids [69]. Nanofluids with enhanced stability can be produced using concurrent production and dispersal of nanoparticles in base fluid which decreases nanoparticle agglomeration. The one-step method, while offering certain advantages, is often hindered by the need for sophisticated and costly equipment. This limitation can restrict its widespread application in industrial settings. The one-step preparation methods investigated by previous researchers are reported in Table 2.

**Table 2.** Summary of studies on one-step methods of nanofluid preparation.

| Ref | Base Fluids | Nanomaterial | Key Findings |
| --- | --- | --- | --- |
| [70] | Water | Nanocarbon | The one-step synthesis of nanocarbon utilizes an $O_2$–$C_2H_2$ flame to generate carbon-based nanoparticles, which are then mixed and condensed with water. The process includes precise control of flame ratios and water flow, followed by continuous stirring, homogenization, and ultrasonic treatment to ensure optimal dispersion and suspension of the nanoparticles. |

**Table 2.** *Cont.*

| Ref | Base Fluids | Nanomaterial | Key Findings |
|---|---|---|---|
| [71] | EG | Cuprous oxide | Cuprous oxide nanofluid was synthesized via reduction of copper sulfate in ethylene glycol with ammonium hydroxide and ribose, followed by pH adjustment and heating at 70 °C. Key reaction parameters like reducing agent concentration and microwave irradiation were optimized. |
| [72] | Oil | Ag/Si | Silica-based nanofluids were prepared using a one-step method by magnetic stirring at 130 °C for 2 h, with silica concentrations ranging from 0.07 to 4.4 wt%. Silver nanoparticles supported on silica were similarly synthesized by adding silver nitrate and silica to the base fluid, followed by stirring at 130 °C for 2 h to prevent oxidation and facilitate nanoparticle formation. |
| [73] | Oil | SiC | Nanofluids in this study were prepared using the Electrical Explosion Welding (EEW) method, where electrical explosion of thin wire electrodes in liquid media (e.g., water, oil, glycerin) simultaneously produces and distributes nanoparticles. The process allows for the use of various liquids and surfactants, ensuring long-term stability of the nanofluid, and is particularly cost-effective for large-scale nanoparticle production. |
| [74] | Distilled Water | $NaNO_3$-$KNO_3$ | Metal oxide nanoparticles were synthesized directly in molten $NaNO_3$-$KNO_3$ eutectic by thermal decomposition of metal nitrate precursors, ensuring no contamination due to shared anions with the solvent. Aluminum nitrate was identified as the optimal precursor. |
| [75] | Oil | CuO | EEW method involves using high voltage and current to convert thin conductive wires into nanoparticles under liquid, offering the ability to produce a wide range of metallic nanocolloids. This environmentally friendly method ensures excellent dispersion of nanoparticles in various liquids like water, oil, and glycerin, without the need for surfactants. |
| [76] | Deionized water | Graphene | Graphene nanofluids were prepared by dispersing graphite powder in deionized water and exfoliating the mixture using a high-speed homogenizer at 10,000 rpm for one hour. After centrifugation, the supernatant was collected as the final nanofluid. |
| [77] | EG | Cu | Copper nanofluid was synthesized by reducing copper sulfate in ethylene glycol with fructose, followed by pH adjustment and heating to 70 °C. Microwave heating was also tested to examine its effect on synthesis. Copper nanoparticles were separated by centrifugation, washed, and dried. |

#### 3.1.2. Two-Step Method

Figure 5 represents the two-step method involves two distinct phases: production stage, which focuses on creating the nanoparticles themselves, and dispersion stage, where the nanoparticles are introduced into base fluid, and dispersed evenly to form the nanofluid. The synthesis of nanotubes or nanoparticles using physicochemical techniques should be performed first, followed by dispersion of the nanoscale powders into the base liquid. Unlike the single-step methods, the two-step methods inherently involve the formation of clusters of nanoparticles [78]. The formation of nanoparticle clumps in nanofluids can

impede their normal fluid dynamics and thermal conductivity. Ball milling and ultrasonic vibration are among the dispersion techniques essential for achieving optimal results in the two-step method [79].

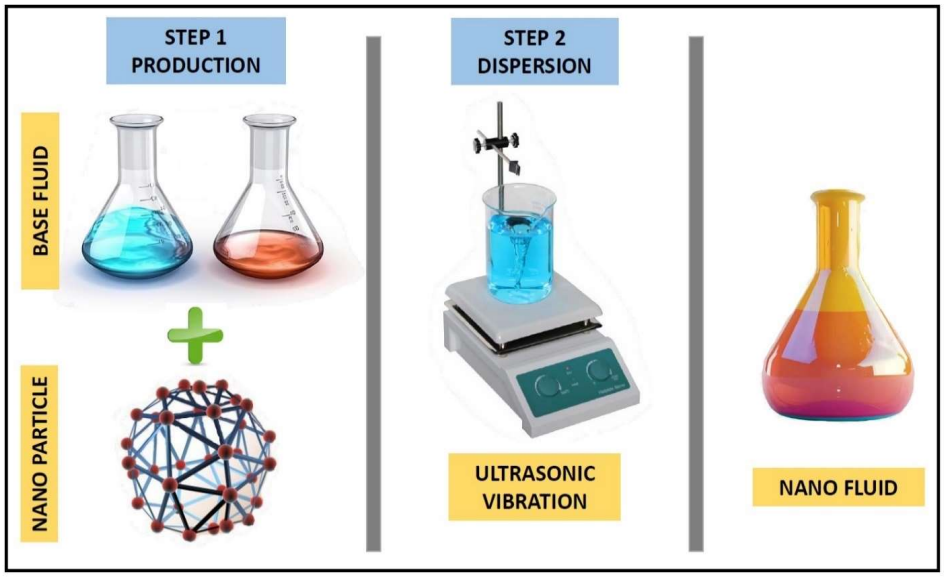


**Figure 5.** Preparation of nanofluid.

Recently, the two-step method has gained significant popularity in industrial applications due to lower costs for production compared to the single-step method. Despite advancements, agglomeration of nanoparticles remains a challenge in the two-step method, leading to ongoing instability issues in suspensions [80]. A study compared Ag nanofluids prepared using two different methods for their thermal application [81]. The two-step preparation methods investigated by previous researchers are listed in Table 3.

**Table 3.** Summary of studies on two-step methods of nanofluid preparation.

| Ref | Base Fluids | Nanomaterial | Key Findings |
|---|---|---|---|
| [78] | Water | Cu/CuO | Hybrid nanofluids were prepared using a two-step method by mixing copper and copper oxide nanoparticles with water as the base fluid. Various weight fractions of nanoparticles (Cu and CuO) were tested, with concentrations ranging from 2 g/L to 4 g/L to achieve optimal stability for low-temperature applications. |
| [82] | Water | $Al_2O_3$ | The two-step method involves dispersing nanoparticles like aluminum oxide ($Al_2O_3$) in deionized water using sonication, homogenization, or magnetic stirring for uniform distribution. Surfactants may be used to enhance stability, with $Al_2O_3$ concentrations ranging from 0.1% to 0.6% in the base fluid. |
| [83] | Oil | $CeO_2$/CuO | The $CeO_2$-CuO hybrid nanolubricant was prepared using the two-step method by dispersing nanoparticles in base fluid to achieve various volume fractions (0.25% to 1.5%). The mixture was stirred with a magnetic stirrer for 1 h and exposed to ultrasonic waves for 1.5 h to prevent agglomeration and ensure stability. |

**Table 3.** *Cont.*

| Ref | Base Fluids | Nanomaterial | Key Findings |
|---|---|---|---|
| [84] | DI water | CuO/GNP | The two-step method was used to prepare hybrid nanofluid-based phase change materials (NFPCMs) by adding oxygen-functionalized GNPs and CuO nanoparticles to the base PCM. The mixture was stirred and ultrasonicated, followed by probe sonication to enhance stability. A nucleating agent and surfactant were also added to improve homogeneity and stability, with no visible sedimentation observed after three days. |
| [85] | Water | $TiO_2$/Graphene Oxide | $TiO_2$ and GO nanofluids were prepared using the two-step method, where $TiO_2$ nanoparticles at varying concentrations were dispersed in water with cetyltrimethylammonium bromide to prevent agglomeration. The mixture was sonicated and stirred for uniformity, followed by the addition of 20 wt% GO dispersion. The final mixture was heated in an oil bath at 80 °C with magnetic stirring for 6 h. |
| [86] | EG/Oil | MWNT | CNT nanofluids were prepared by dispersing multi-walled carbon nanotubes into ethylene glycol or synthetic engine oil using magnetic agitation and ultrasonication. N-hydroxysuccinimide (NHS) was used as a dispersant in the engine oil-based suspensions. Volume concentrations ranged from 0.2 to 1.0 vol.% in ethylene glycol and 1.0 to 2.0 vol.% in engine oil. |
| [87] | Oil | MgO/ZnO | ZnO and MgO nanofluids were prepared without surfactants using the two-step method, with concentrations ranging from 0.125% to 1.5%. The nanoparticles (40 nm) were dispersed by magnetic stirring for 3 h, followed by ultrasonic processing at 20 kHz for 1 h. The nanofluid showed excellent stability for at least two weeks, with no visible sedimentation observed. |
| [88] | Water | MWCNT/$Fe_2O_3$ | Hybrid $Fe_2O_3$ and MWCNTs nanofluids (80% $Fe_2O_3$, 20% MWCNTs) were prepared using the two-step method. Dispersion was optimized by adjusting pH, conductivity, sonication parameters and dispersion to nanoparticle weight ratios (0.4–1.0) at a 0.1% concentration. Hybrid nanofluids were then formulated with volume concentrations ranging from 0.1% to 1.5%. |

The one-step and two-step methods have different advantages and limitations that make them appropriate for diverse use cases. The one-step method leads to improved stability and control but is often stalled by its high costs and inadequate scalability; the two-step method is more cost-effective and better suited for large-scale applications, although at the expense of stability and control [89]. Benefits and drawbacks of the two methods are summarized in Table 4.

### *3.2. Thermophysical Properties*

Nanofluids, characterized by enhanced thermophysical properties and stability, hold great promise for a diverse range of applications [90]. This potential is rooted in their ability to significantly outperform conventional fluids in various domains.

**Table 4.** Benefits and drawbacks of one-step and two-step methods.

| One-Step Method | Two-Step Method |
|---|---|
| Benefits | Benefits |
| High stability<br>Reduced agglomeration<br>No need for storage, drying, or oxidation<br>Greater control over the process | Well-suited for large-scale production<br>Suitable for oxide nanoparticles<br>Cost-effective |
| Drawbacks | Drawbacks |
| Not ideal for large-scale production<br>Lower thermal conductivity<br>Suitable only for low vapor pressure liquids | Prone to rapid agglomeration<br>Limited control over dispersion<br>High surface energy requiring extra treatment |

#### 3.2.1. Thermal Conductivity

Thermal conductivity is the measure of a nanofluid's capability to conduct heat. It is defined as the rate at which heat passes through a material (unit thickness) when subjected to a unit temperature gradient. It has been demonstrated that thermal conductivity of fluids like water, kerosene, and ethylene glycol, has been improved by incorporating little nano-suspended elements [91]. This is the reason why the use of nanoparticles in PCMs is often aimed at enhancing thermal conductivity. This property is crucial for efficient heat transfer and can improve the performance of PCM-based TES systems. Nanofluids, colloidal dispersions of nanomaterials in base fluid, exhibit unique thermal properties. Various researchers have developed diverse models to estimate the thermal conductivity of a nanofluid. A list of these models is presented in Table 5.

**Table 5.** Developed equations for thermal conductivity of nanofluids.

| Ref | Nanomaterial | Models |
|---|---|---|
| [92] | $Al_2O_3$ & Cu | $\frac{k_{nf}}{k_{bf}} = \frac{k_{np}+2k_{bf}+2(k_{np}-k_{bf})\phi}{k_{np}+2k_{bf}-(k_{np}-k_{bf})\phi}$ |
| [93] | $Al_2O_3$ & Cu | $\frac{k_{nf}}{k_{bf}} = \frac{\frac{k_{Cu}\phi_{Cu}+k_{Al_2O_3}\phi_{Al_2O_3}}{\phi}+2k_{bf}+2(k_{Cu}\phi_{Cu}+k_{Al_2O_3}\phi_{Al_2O_3})-2k_{bf}\phi}{\frac{k_{Cu}\phi_{Cu}+k_{Al_2O_3}\phi_{Al_2O_3}}{\phi}+2k_{bf}-(k_{Cu}\phi_{Cu}+k_{Al_2O_3}\phi_{Al_2O_3})+k_{bf}\phi}$ |
| [94] | Ag & MgO | $\frac{k_{nf}}{k_{bf}} = \frac{0.1747\times10^5+\phi_{nf}}{0.1747\times10^5-0.1498\times10^6\phi_{nf}+0.1117\times10^7{\phi_{nf}}^2+0.1997\times10^8{\phi_{nf}}^3}$ |
| [95] | $Al_2O_3$ & ZnO | $\frac{k_{nf}}{k_{bf}} = a_0 + a_1T + a_2T^2 + a_3R + a_4R^2 + a_5\phi + a_6\phi^2$ |
| [96] | $Al_2O_3$ & $TiO_2$ | $\frac{k_{nf}}{k_{bf}} = \frac{k_{np}+2k_{bf}+2\phi(k_{np}-k_{bf})}{k_{np}+2k_{bf}-\phi(k_{np}-k_{bf})}$ |
| [97] | SWCNT & $Al_2O_3$ | $\frac{k_{nf}}{k_{bf}} = 0.008379\times[\phi^{0.4439}\times T^{0.9246}]+0.963$ |
| [98] | MWCNTs & COOH | $\frac{k_{nf}}{k_{bf}} = aT^b + c\phi^d + e(T\phi)^f - g$ |
| [99] | $Al_2O_3$ & Fe | $\frac{k_{nf}}{k_{bf}} = (\frac{k_{np}+2k_{bf}+2\phi(k_{np}-k_{bf})(1+\beta)^3}{k_{np}+2k_{bf}-\phi(k_{np}-k_{bf})(1+\beta)^3})$ |
| [100] | $Al_2O_3$ & Cu | $\frac{k_{nf}}{k_{bf}} = \frac{(9.6128+\phi)}{-0.00010759T^2+9.3885} - \frac{0.0041099}{\phi}$ |
| [101] | $Al_2O_3$ & Fe | $\frac{k_{nf}}{k_{bf}} = (4.97\phi^2+2.72\phi+1)$ |
| [102] | Graphite & $SiO_2$ | $\frac{k_{nf}}{k_{bf}} = 0.852870218\times(1+\phi)^{6.591412917}\times T^{0.052797513}\times(\frac{m_{np2}}{m_{np1}})^{0.022254808}$ |

#### 3.2.2. Density

Density is a key factor influencing various fluid properties, such as friction factor, Reynolds number and pressure loss. A study used blended nanofluid in which lower pressure drop was observed for a $H_2O$/MWCNT blend in comparison to a $H_2O$/CuO-MWCNT blend due to the lower CuO density [103]. The study reveals that pressure can vary when nanofluid density varies. Another group of researchers found that change in density plays a major role in elevating the pumping power of nanofluid [104]. Adding surfactant can also have a minor impact on nanofluid density. The hike in nanofluid density is a result of the nanomaterials occupying space within the base fluid [105]. Also, the hybrid nanomaterials show lower density when compared to other nanomaterials. Table 6 provides theoretical equations for nanofluid density, which have been investigated through both experimental and theoretical approaches.

**Table 6.** Correlation models for density of nanofluids.

| Ref | Nanomaterial | Model |
|---|---|---|
| [93] | $Al_2O_3$ & Cu | $\rho_{nf} = \rho_{Cu}\phi_{Cu} + \rho_{bf}(1-\phi) + \rho_{Al_2O_3}\phi_{Al_2O_3}$ |
| [106] | $Al_2O_3$ & $TiO_2$ | $\rho_{nf} = (1-\phi)\rho_{bf} + \phi\rho_{np}$ |
| [107] | MWCNTs & $Fe_3O_4$ | $\rho_{nf} = \rho_{bf}(1+\phi)^{0.03279}[\frac{T}{60}]^{0.0003355}$ |
| [108] | $Al_2O_3$ & Fe | $\rho_{nf} = (1-\phi)\rho_{bf} + \phi\rho_{np}$ |
| [109] | Nanodiamond & $Fe_3O_4$ | $\rho_{nf} = \rho_{bf}[(1+\phi)^{0.427\times10^{-1}}(\frac{T_{min}}{T_{max}})^{0.95\times10^{-4}}]$ |
| [110] | $Al_2O_3$ & Cu | $\rho_{nf} = \rho_f(1-\phi) + \rho_1\phi_1 + \rho_2\phi_2$ |
| [111] | Nanodiamond & $Fe_3O_4$ | $\rho_{nf} = \rho_{bf}[(1+\phi)^{0.414\times10^{-1}}(\frac{T_{min}}{T_{max}})^{0.1106\times10^{-3}}]$ |
| [112] | Ag & MgO | $\rho_{nf} = \left(1-\phi_{nf}\right)\rho_{bf} + \phi_{Ag}\rho_{Ag} + \phi_{MgO}\rho_{MgO}$ |
| [113] | $TiO_2$ & Cu | $\rho_{nf} = (1-\phi_2)[(1-\phi_1) + \phi_1(\frac{\rho_s}{\rho_f})]\rho_f + \rho_{s2}\phi_2$ |
| [114] | $Al_2O_3$ & Cu | $\rho_{nf} = \rho_{np}\phi + \rho_{bf}(1-\phi)$ |
| [115] | Graphite & $SiO_2$ | $\rho_{nf} = \rho_{np1}\phi_{np1} + \rho_{np2}\phi_{np2} + \rho_{bf}(1-\phi_{np1}-\phi_{np2})$ |
| | | $\rho_{nf} = (\frac{m}{V})_{nf} = \frac{m_{bf}+m_{nf}}{V_{bf}+V_{np}} = \frac{\rho_{bf}V_{bf}+\rho_{np}V_{np}}{V_{bf}+V_{np}}$ |
| [116] | - | $\rho_{nf} = (1-\phi)\rho_{bf} + \phi\rho_{np}$ |
| | | $Where: \phi = \frac{V_{np}}{V_{bf}+V_{np}} \approx \frac{V_{np}}{V_{bf}}$ |

#### 3.2.3. Viscosity

The viscosity of nanofluids is a crucial factor affecting their application in various ways. The variation in viscosity directly influences movement characteristics and other associated factors. For instance, Li et al. demonstrated that by increasing EG/ZnO concentration in a nanofluid, a hike in viscosity can be observed and when the temperature is increased there is a decrease in viscosity [117]. Loulijat et al. proved that an Ag-$H_2O$ nanofluid's shear viscosity decreases as temperature increases, which is due to the improved Brownian motion of water molecules, which reduces the overall viscosity [118]. The nanofluid's viscosity is also significantly influenced by the spacing between particles and the extent of their combination, rather than solely by their size [119]. According to Hossein et al., the viscosity of carbon nanotubes decreases as their aspect ratio increases [120]. As larger nanofluid particles have elevated thermal conductivity the interfacial thermal resistance is decreased. Table 7 reports various equations used to estimate nanofluids' viscosity.

**Table 7.** Viscosity equations used by authors for nanofluids.

| Ref | Nanomaterial | Models |
|---|---|---|
| [88] | MWCNT & $Fe_2O_3$ | $\frac{\mu_{nf}}{\mu_{bf}} = 1.031 + 0.0025T + 0.1386\phi$ |
| [92] | $Al_2O_3$ & Cu | $\mu_{nf} = \frac{\mu_{bf}}{(1-\phi_{Al_2O_3}-\phi_{Cu})^{2.5}}$ |
| [93] | $Al_2O_3$ & Cu | $\frac{\mu_{nf}}{\mu_{bf}} = (k_2\phi^2 + k_1\phi + 1)$ |
| [94] | Ag & MgO | $\frac{\mu_{nf}}{\mu_{bf}} = (1 - 7214\phi_p^2 + 32.795\phi_p - 0.1941 \times 10^8 + 714600\phi_p^3\phi_p^4)$ |
| [106] | $Al_2O_3$ & $TiO_2$ | $\mu_{nf} = \frac{\mu_{bf}}{(1-\phi)^{2.5}}$ |
| [113] | $TiO_2$ & Cu | $\mu_{nf} = \frac{\mu_{bf}}{(1-\phi_2)^{2.5}(1-\phi_1)^{2.5}}$ |
| [121] | MWCNTs & $SiO_2$ | $\frac{\mu_{nf}}{\mu_{bf}} = a_4\phi^4 + a_3\phi^3 + a_2\phi^2 + a_1\phi + a_0$ |
| [122] | MWCNTs & ZnO | $\frac{\mu_{nf}}{\mu_{bf}} = A + B\phi + C\phi^2 + D\phi^3$ |
| [123] | $Al_2O_3$, CuO & $TiO_2$ | $\frac{\mu_{nf}}{\mu_{bf}} = (0.955 - 0.00271 \times T + 1.858 \times \frac{\phi}{100} + (705 \times \frac{\phi}{100})^{1.223})$ |
| [124] | Graphite & $SiO_2$ | $\frac{\mu_{nf}}{\mu_{bf}} = (1.00527 \times (1+\phi)^{9.36265} \times (T)^{0.00035} \times (\frac{m_{np1}}{m_{np2}})^{-0.028935}$ |
| [125] | MWCNTs & $SiO_2$ | $\frac{\mu_{nf}}{\mu_{bf}} = a_0 + a_1\phi + a_2\phi^2 + a_3\phi^3$ |
| [126] | $TiO_2$ & $SiO_2$ | $\frac{\mu_{nf}}{\mu_{bf}} = 37(0.1 + \frac{\phi}{100})^{1.59}(0.1 + \frac{T}{80})^{0.31}$ |
| [127] | MgO & MWCNTs | $\mu_{nf} = 3.371 \times \exp(-0.000371T^2 + 0.5782\phi)$ |
| [128] | MWCNTs & ZnO | $\frac{\mu_{nf}}{\mu_{bf}} = 796.8 + 12.88T + 76.26\phi + 0.7694\phi T + \frac{-196.9T - 16.53\phi T}{\sqrt{T}}$ |

#### 3.2.4. Specific Heat Capacity

Specific heat capacity is defined as the quantity of heat required to raise the temperature of a unit mass of nanofluid by one degree Kelvin. In nanofluids, this property is influenced by the specific heat capacities of both base fluid and dispersed nanoparticles, along with their respective volume fractions. For this reason, there is no homogeneous effect on the specific heat of a nanofluid in comparison with the base fluid. For instance, while comparing specific heat capacity between water and $Al_2O_3$ nanofluids, a small deviation was observed by Alade et al. with various volume fractions [129]. Li et al. proved that adding increasing amounts of β-cyclodextrin carbon nanotubes to ethylene glycol results in a decrease of specific heat capacity, where a 0.1 vol% EG concentration exhibited the greatest decrease, 9.07%, which was less than with pure EG [130]. On the other hand, Rizvi et al. demonstrated an increase in specific heat capacity of $Li_2CO_3$-$Na_2CO_3$ of up to 25.1% and $Li_2CO_3$-$K_2CO_3$ up to 21.1% [131]. As the concentration of particles and the temperature of activated EG/carbon graphene increases, the specific heat also increases [132]. The equations for determining the specific heat capacity of nanofluids are presented in Table 8.

**Table 8.** Correlations proposed by researchers for specific heat of nanofluids.

| Ref | Nanomaterial | Models |
|---|---|---|
| [93] | $Al_2O_3$ & Cu | $C_{p,nnf}\rho_{hnf} = C_{p,Cu}\rho_{Cu}\phi_{Cu} + C_{p,Al_2O_3}\rho_{Al_2O_3}\phi_{Al_2O_3} + C_{p,bf}\rho_{bf}(1-\phi)$ |
| [105] | Graphite & $SiO_2$ | $C_{p,nf}\rho_{hn} = C_{p,np1}\rho_{np1}\phi_{np1} + C_{p,np2}\rho_{np2}\phi_{np2} + C_{p,bf}(1 - \rho_{np1}\phi_{np1} - \rho_{np2}\phi_{np2})$ |
| [106] | $Al_2O_3$ & $TiO_2$ | $C_{p,nf} = C_{p,bf}\frac{(1-\phi)\rho_{bf}}{\rho_{nf}} + C_{p,np}\frac{\phi\rho_{np}}{\rho_{nf}}$ |
| [107] | Nanodiamond | $C_{p,nf} = C_{p,bf}(1+\phi)^{-0.0143}(\frac{T}{50})^{0.14\times10^{-4}}$ |
| [109] | Nanodiamond & $Fe_3O_4$ | $C_{p,nf} = C_{p,bf}(1+\phi)^{-0.148\times10^{-1}}(\frac{T_{min}}{T_{max}})^{-0.537\times10^{-4}}$ |
| [110] | $Al_2O_3$ & Cu | $C_{phnf} = \frac{(\rho C_p)_f(1-\phi)+(\rho C_p)_1\phi_1+(\rho C_p)_2\phi_2}{\rho_f(1-\phi)+\rho_1\phi_1+\rho_2\phi_2}$ |

**Table 8.** *Cont.*

| Ref | Nanomaterial | Models |
|---|---|---|
| [133] | $Al_2O_3$ & Fe | $C_{p,nf} = C_{p,bf}\frac{(1-\phi)\rho_{bf}}{\rho_{nf}} + C_{p,np}\frac{\phi\rho_{np}}{\rho_{nf}}$ |
| [134] | $Al_2O_3$ | $C_{p,nf} = \frac{(1-\phi)\cdot\rho_{bf}\cdot C_{p,bf}+\phi\cdot\rho_p\cdot C_{p,p}}{\phi\cdot\rho_p+(1-\phi)\cdot\rho_{bf}}$ |
| [135] | CuO & $SiO_2$ | $C_{p,nf} = C_{p,bf}(1-\phi) + C_p\phi$ |
| [136] | $Al_2O_3$ | $C_{p,nf} = 0.8429(1+\frac{T_{nf}}{50})^{-0.3037}(1+\frac{r_p}{50})^{0.4167}(1+\frac{\phi_p}{100})^{2.272}$ |
| [137] | CuO & $SiO_2$ | $C_{p,nf} = \frac{(\rho C_p)_p\phi+(\rho C_p)_f(1-\phi)}{\rho_{bf}(1-\phi)+\rho_p\phi}$ |
| [138] | MgO, ZnO & $ZrO_2$ | $\frac{C_{p,bf}(T)-C_{p,nf}(T)}{C_{p,bf}(T)} = \frac{\phi_p+A^{C_p(T)}_{C_{p,p}(T)}}{B+\phi_p}$ |

#### 3.2.5. Stability

While a small quantity of nanoparticles can markedly enhance the properties of a bulk fluid when they are evenly distributed and stable, nanoparticle aggregation is the primary cause of nanofluid instability [139]. This unexpected phenomenon is attributed to the intermolecular forces of Van der Waals attraction and the interaction between particles and their extensive surface area [140]. Agglomeration in nanofluids poses a significant challenge to their practical applications. The agglomeration process can diminish the desired thermal conductivity. Additionally, the augmented frictional resistance caused by agglomeration leads to higher pressure drops, which can adversely impact the flow behavior of nanofluids [141]. The stability of nanofluids is paramount for achieving optimal system performance. The challenge of maintaining nanofluid stability hinders the full realization of their potential applications [142]. The stability of nanofluids can often be assessed visually. Stable nanofluids typically exhibit a uniform appearance, while unstable nanofluids may appear heterogeneous.

The sedimentation assessment method comprises images capturing the sedimentation process in nanofluids to investigate their stability. A lengthier sedimentation time shows superior nanofluid stability, as stable nanofluids have consistently dispersed nanoparticles with no precipitation. This method, which is among the easiest nanofluid stability assessment techniques, analyses sedimentation volume over time by adding nanofluid into a transparent glass tube. Smaller nanoparticles display slower sedimentation rates compared to larger particles, as their deposition rate is diminished. The sedimentation process can also be analyzed by photographing the fluid, showing a visual evaluation of stability. Due to the microscopic size of nanoparticles, visual assessment of nanofluid stability can be unreliable. Consequently, additional characterization techniques are necessary for accurate stability prediction [140]. Table 9 summarizes the techniques used for stabilization and its respective stability indicators.

**Table 9.** Nanofluid stabilization and its stability indicators.

| Ref No | Base Fluid/Nanofluid | ϕ (%wt) | PS (nm) | Surfactants | Stabilization Techniques | Stability Indicator |
|---|---|---|---|---|---|---|
| [143] | DW/MWCNT | 0.15 | 10–20 | COOH | MS, US | ζ = 41.40 mV |
| [144] | Water/GNPs | 0.1 | 2 | SDS, CTAB, BS | Water bath, US | >2 months |
| [145] | Water/$Al_2O_3$ | 1–3 | 25 | SDS | USB, US | ζ = −47.90 mV |
| [146] | DW/Al & Cu | 0.3 | 80, 40 | SDS | MS, US | ζ = −41.20 and −38.40 mV |
| [147] | Water/$Al_2O_3$ | 1–3 | 45 | SDBS | MS, US | ζ = −38.60 mV |

**Table 9.** *Cont.*

| Ref No | Base Fluid/Nanofluid | ϕ (%wt) | PS (nm) | Surfactants | Stabilization Techniques | Stability Indicator |
|---|---|---|---|---|---|---|
| [148] | Water/CNT | 0.1–1 | 10–20 | PVP, SDS | MS, US | $\zeta = -63.20$ mV |
| [149] | Water/SWCNT | 0.1 | 20–50 | SDBS | US | 2 months |
| [150] | Water-EG (60:40)/Graphene | 0.1–0.3 | 123–424 | HCl + NaOH | US | 3 weeks |
| [151] | DW/rGO-Ag | 0.0005–0.05 | - | SDBS | US | >2 weeks |
| [152] | Water/MWCNT-$CeO_2$ | 0.25–1.5 | <30 | SDBS, SDS, CTAB, DDC, and PVP | US | >1 month |
| [153] | DW/Cu, Fe, Ag | 0.1 | 30–50 | No surfactant | Sonication | 5 days |
| [154] | Water/Cu, Zn, Al | 40–240 ppm | 49 | No surfactant | MS, Sonication | $\zeta = 34.60 - 38.60$ mV |

### *3.3. Heat Transfer*

This section reports research on the enhancement of heat transfer which is achievable via nanofluids. Mechanisms of enhancement include natural convection, forced convection and mixed convection. The improved heat transfer capabilities of nanofluids can be attributed to several factors, including the following:

- Increased thermal conductivity: The nanoparticles possess greater thermal conductivity compared to most base fluids, allowing for more efficient heat transfer.
- Enhanced turbulence: The presence of nanoparticles can initiate fluid flow turbulence, promoting heat transfer by disrupting thermal boundary layers.
- Brownian motion: The random motion of nanoparticles within fluid can increase the rate of heat transfer by promoting energy exchange.

As with thermophysical properties, numerous researchers have derived heat transfer correlations for various nanofluid combinations by fitting their experimental or numerical data. Circular tube geometry offers significant insights into the design of heat exchange systems. Consequently, it remains the most widely utilized geometry in heat transfer devices [155]. Convective heat transfer occurs in a tube of circular shape with constant heat flux due to the temperature gradient between the nanofluid-incorporating working fluid near the wall of tube and the fluid at its core. This concept allows for the analysis of the flow's hydrodynamic and thermal characteristics and their correlation with the Nusselt number (*Nu*) [156]. Previous researchers have derived Nusselt number correlations for various modes of heat transfer, like natural convection, forced convection, and mixed convection.

#### 3.3.1. Natural Convection

Natural convection is the process of heat transfer driven by buoyancy forces, where fluid motion is caused by temperature differences within the fluid. Nanofluids influence natural convection heat transfer by enhancing thermal conductivity, viscosity, and heat capacity, which alter buoyancy forces, flow patterns, and heat transfer rates. While improved thermal conductivity and modified buoyancy typically enhance convection, increased viscosity and improper nanoparticle concentrations can suppress fluid motion, making the overall impact highly dependent on the specific nanofluid composition and operating conditions [157].

A numerical study of $Al_2O_3$-Cu flow through a sinusoidally corrugated chamber filled with pure water and various hybrid fluids has been developed by Takabi et al. They investigated the effects of nanoparticle volume fraction (0 vol% to 2 vol%) on heat transfer rates at various Rayleigh numbers. The results demonstrated that nanofluids significantly improved heat transfer compared to pure water, augmenting the enclosure

cooling and lowering temperatures on a heated surface [94]. The convective flow through a nanofluid across a porous medium (saturated) along a vertically propagating permeable plate has been explored statistically. It was found that skin friction coefficient increased and the Nusselt number dropped as the nanoparticle volume % increased [158]. For TES applications, the behavior of hydrothermal and entropy analysis for a buoyancy of water and MgO-Ag has been investigated. The fin-equipped octagonal cage was filled with a nanofluid. The analysis shows that entropy increases with nanoparticle concentrations and Rayleigh numbers and decreases with magnetic numbers. Additionally, it was shown that as fin length increases, entropy reduces [159].

The impact of a heat-generating cylinder and an $Al_2O_3$/Cu nanofluid with water with natural convection was studied numerically by Mokaddes Ali. The combination of nanoparticles with base fluid improved heat transfer efficiency by approximately 21.98 percent for 1% concentration and approximately 86.06% for 5% concentration, compared with a pure base fluid [160]. Nayak et al. conducted a numerical study of $TiO_2$-Cu flow in a C-shaped enclosure filled with water. The researchers investigated the effects of $\phi$ (2%) on heat transfer and fluid flow. The results verified that introducing nanoparticles enhanced the thermal conductivity of the base fluid (water), leading to increased surface temperatures and decreased temperature profiles within the nanofluid. At high Rayleigh and Lewis numbers, the streamline functions became less pronounced [161]. Since the majority of solar energy-based systems rely on HTF's natural flow, mono-nano fluids have been used in multiple investigations as HTF in solar-based TES systems. However, nanofluids provide a viable alternative to solar-powered thermal storage units. Moreover, studies have shown that nanofluids outperform natural convection systems in solar collector systems.

An investigation of convective flow of a CuO nanofluid with water in a porous medium observed that heat transfer was enhanced by higher buoyancy forces [162]. In contrast, heat transfer diminished with increasing Hartmann number and eccentricity. Based on numerical results, a Nusselt number correlation was developed for volume concentration ($0 \leq \phi \leq 0.4\%$), Rayleigh number ($100 \leq \mathrm{Ra} \leq 1000$), eccentricity ($0.7 \leq \varepsilon \leq 0.9$) and Hartmann number ($0 \leq \mathrm{Ha} \leq 20$). The correlation (Equation (2)) for natural convective heat transfer is as follows:

$$\begin{aligned} Nu_{nf} = \quad & -1.410 + 10.820\,\varepsilon + 0.430\,a + 2.3 \times 10^{-4} Ra_{nf} + 5.30 \times 10^{-3} Ha + 5.20\,\varepsilon a \\ & +1.40 \times 10^{-4} \varepsilon Ra_{nf} - 0.0430\,\varepsilon Ha - 4.60 \times 10^{-4} a Ra_{nf} + 6.050 \times 10^{-3} a Ha \\ & +1.6 \times 10^{-7} Ra_{nf} Ha - 11.9\varepsilon^2 - 0.63a^2 + 6.5 \times 10^{-7} Ra_{nf}^2 + 9.1 \times 10^{-4} Ha^2 \end{aligned} \quad (2)$$

Natural convection of $Fe_3O_4$ nanofluid/water was simulated in [163] using a single-phase numerical model. A correlation for the assessment of Nusselt number was proposed (Equation (3)) for volume concentration ($0 \leq \phi \leq 0.1\%$), Rayleigh number ($102 \leq \mathrm{Ra} \leq 106$), Hartmann number ($0 \leq \mathrm{Ha} \leq 80$), aspect ratio ($0.2 \leq \mathrm{AR} \leq 0.8$) and inclination angle ($0 \leq \mathrm{a} \leq 90^\circ$):

$$Nu_{nf} = \left(C_1 + C_2 Ra_{nf} + C_3 Ra_{nf} Ha\right) \exp\left(C_4 \phi AR + \left(C_5 + C_6 Ra_{nf} + C_7 Ra_{nf} Ha\right) AR^2\right) \quad (3)$$

A constant heat flux was applied to $Al_2O_3$ nanofluid/water, and an experimental investigation was conducted to study the resulting natural convection [164]. The results revealed that the primary factor contributing to the improved natural convection heat transfer of nanofluids was the relative rise in thermal conductivity, compared to other thermophysical properties. A correlation has been proposed, based on least-square regression

analysis of the *Nu* results, for volume concentration ($0 \leq \phi \leq 4\%$), and Rayleigh numbers ($6.21 \times 10^5 \leq \mathrm{Ra} \leq 2.56 \times 10^8$).

$$Nu_{nf} = CRa_{nf}^{n}\left(\frac{Pr_{nf,hw}}{Pr_{nf}}\right)^{m}\left(\frac{\beta_{nf,hw}}{\beta_{nf}}\right)^{q} \quad (4)$$

where $C$, $n$, $q$ and $m$ are constants.

#### 3.3.2. Forced Convection

Instead of being largely driven by the forces of natural buoyancy, forced convection occurs when the fluid moves as a result of an external force, allowing a fluid to transfer heat more effectively. It is crucial to consider that the concentration and type of nanoparticles, the fluid flow conditions, and other geometrical features of a system all affect how effective nanofluids are in forced convection heat transfer. To attain intended heat transfer increase, experimental and numerical investigations have often been done to optimize nanofluid mixture as well as operating parameters for particular applications.

Khosravi et al. analyzed the rate of generation of entropy in a solar receiver numerically. They employed Pt-GNP nanofluid as the working fluid and utilized neural networks to investigate the effects of input parameters, like wave amplitude, nanoparticle concentration, and Reynolds number. The study revealed that increasing these input factors significantly reduced the rate of thermal entropy generation, suggesting that optimizing these parameters could lead to more efficient and less energy-dissipative solar receivers [165]. Abdelrazek et al. assessed the thermal performance of MWCNTs-$Al_2O_3$/distilled water with nanofluid in a fully developed turbulent flow regime within an annular channel [166]. The study combined experimental and numerical approaches, utilizing ANSYS CFD Fluent to perform 3D numerical simulations. The researchers focused on the concentric configuration of the annular channel and examined the effects of nanoparticle concentration on convective heat transfer enhancement. They detected that the addition of nanofluids significantly improved heat transfer compared to the base fluid (DW). The maximum improvement in convective heat transfer was achieved at nanoparticle concentrations of 0.050 wt%, 0.0750 wt%, and 0.10 wt%, with corresponding increases of 2.98%, 4.86%, and 6.49%, respectively.

As discussed in this section on nanofluids in forced convective systems, the incorporation of nanoparticles has demonstrated a remarkable enhancement in heat transfer efficiency. The presence of these nanoscale particles within the base fluid significantly improves the system's ability to transfer heat, leading to a variety of benefits like increased energy efficiency, diminished system size, and enhanced performance in applications ranging from electronics cooling to solar energy systems. Forced convective heat transfer of nanofluids chiefly depends on the *Re*, *Pr*, particle volume concentration and particle diameter. Nusselt number correlations proposed by various studies for the forced convection of various types of nanofluids and counterflow heat exchangers are presented in Table 10.

**Table 10.** Nusselt number correlations for forced convection proposed in previous studies.

| Ref No | Nanofluid | ϕ/ψ (%) and PD (nm/μm) | Correlation | Re | Boundary Condition |
|---|---|---|---|---|---|
| [167] | Cu | $0.3 \leq \phi \leq 2.0$ (100 nm) | $Nu_{nf} = 0.4328(1.0 + 11.285\phi^{0.754}Pe_p^{0.218})Re_{nf}^{0.333}Pr_{nf}^{0.4}$ | $800 \leq Re \leq 25{,}000$ | CHF |
| [168] | $Al_2O_3$ | $1 \leq \psi \leq 6$ (150 nm) | $(Nu_x)_{nf} = 4.36 + [ax_+^{-b}(1+\psi^c)\exp^{-dx}][1 + e.(\frac{d_p}{d_{ref}})^{-f}]$ | $500 < Re < 2000$ | CHF |

**Table 10.** *Cont.*

| Ref No | Nanofluid | ϕ/ψ (%) and PD (nm/μm) | Correlation | Re | Boundary Condition |
|---|---|---|---|---|---|
| [169] | $TiO_2$ | $0.05 \leq \phi \leq 6$ (150 nm) | $Nu_{nf} = 0.00218 Re_{nf}^{1.0037} P_{nf}^{0.5} (1+\phi)^{154.6471}$ | $4.8 \times 10^3 \leq Re \leq 3.05 \times 10^4$ | CWT |
| [170] | Graphitic | $2 \leq \psi \leq 2.5$ (1–2 μm) | $Nu_{nf} = 1.86 Re_{nf}^{0.333} Pr_{nf}^{0.333} (\frac{D_h}{L})^{0.333} (\frac{\mu_{bulk}}{\mu_{wall}})^{0.14}$ | $5 \leq Re \leq 110$ | CWT |
| [171] | CuO, $SiO_2$ | $1 \leq \phi \leq 10$ (20–100 nm) | $Nu_{nf} = 0.065(Re_{nf}^{0.65} - 60.22)(1 + 0.0169\phi^{0.15}) Pr_{nf}^{0.542}$ | $3 \times 10^3 \leq Re \leq 1.7 \times 10^4$ | CHF |
| [172] | $Fe_2O_3$ | $0 \leq \phi \leq 0.06$ (30 nm) | $Nu_{nf} = 0.02327 Re_{nf}^{0.8} Pr_{nf}^{0.4} (1+\phi)^{1.969}$ | $16{,}000 < Re < 30{,}000$ | CHF |
| [173] | Ag | $0.3 \leq \phi \leq 0.9$ (100 nm) | $Nu_{nf} = 0.023 Re_{nf}^{0.8} Pr_{nf}^{0.3} + (0.617\phi - 0.135) Re^{0.445\phi - 0.37} P_r^{1.081\phi - 1.305}$ | $900 < Re < 12{,}000$ | CWT |
| [174] | MWCNT | $\phi = 0.0111\%$ (20 nm) | $Nu_{nf} = 0.3762 Re_{nf}^{0.6681} Pr_{nf}^{0.4}$ | $182 < Re < 956$ | CHF |
| [175] | GNP | $0.1 \leq \psi \leq 2$ (2.5 nm) | $Nu_{nf} = 0.026 Re_{nf}^{0.806} Pr_{nf}^{0.401} (1+\phi)^{0.5}$ | $6.7 \times 10^3 \leq Re \leq 2.8 \times 10^4$ | - |

#### 3.3.3. Mixed Convection

Mixed convection occurs when both natural and forced convection are significant factors in fluid flow. The optimal use and efficiency of nanofluids in mixed convection systems can vary depending on factors like the specific nanoparticle types, concentration, and the properties of the base fluid. To determine the best formulation for mixed convection applications, researchers often conduct numerical simulations and experimental studies to optimize nanofluid performance. A numerical study of the generation of entropy with a horizontally flowing nanofluid of Cu-$Al_2O_3$ with water was carried out by Hussain et al. [176]. The study discovered that entropy formation and heat transfer rates significantly improved through increasing the volume of nanoparticles and Reynolds number. The Bejan number, on the other hand, showed the reverse pattern, declining as the *Re* and nanoparticle concentration increased. Zahan et al. conducted a numerical study on heat transfer of water-based hybrid nanofluids comprising varying concentrations of $Al_2O_3$ and Cu nanoparticles within a triangular enclosure with a sinusoidal wavy bottom surface [110]. The results of their investigation revealed a minor rise in the average Nusselt number for $Al_2O_3$-Cu/water hybrid nanofluids compared to conventional nanofluids. This enhancement in heat transfer could be due to synergistic effect of two types of nanoparticles, which leads to upgraded thermal conductivity and convective heat transfer within the hybrid nanofluid.

A numerical investigation of the impact of radiation on $MoS_2$-GO/water nanofluid flow was conducted. The study found that skin friction increased due to buoyancy-assisted flow, but decreased in both buoyancy-aiding and buoyancy-opposing flows. The decrease in skin friction was attributed to the yaw angle [177]. Another numerical study of Cu-$Al_2O_3$/water nanofluid flow through a porous medium under mixed convection conditions was investigated. The study found that increasing $\phi$ in the Cu-$Al_2O_3$/water nanofluid led to improved heat transfer performance. The nanofluid outperformed conventional nanofluids in terms of heat transfer [178].

Hussain et al. numerically examined the heat transfer performance of water-based hybrid nanofluids having $Al_2O_3$ and Cu flowing through a wavy channel within a fixed cylinder [179]. Their study found that the maximum heat transfer was observed at $\phi$ 0.05%. Additionally, as the *Re* increased, the fluid flow transitioned from slow to fast regime. These findings highlight the ability of hybrid nanofluids to enhance heat transfer in wavy channel flows, particularly at higher nanoparticle concentrations and Reynolds numbers. Xiav et al. used a nanofluid (MWCNT-SWCNT) flow to investigate the effects of nonlinear mixed convection under varying slip boundaries on heat and mass transfer analysis [180]. The results show that greater ranges of the mixed convection increase the rate of transmission.

It was also observed that at nanoparticle concentrations of 0.03% there is an improvement in both fluid velocity and the thickness of the momentum barrier layer.

While there have been numerous studies on the forced convective heat transfer of nanofluids, the number of studies proposing models for heat transfer in natural and mixed convection is significantly smaller. Mixed convective flow of dilute nanofluids considering a Prandtl number in the range ($0.5 \leq Pr \leq 7$) was mathematically modeled in [181]. A correlation for Nusselt number prediction (Equation (5)) was developed, incorporating the thermophoresis parameter ($N_t$) and Brownian diffusion parameter ($N_b$).

$$Nu_{nf} = C + C_{Nb}N_b + C_{Nt}N_t \quad (5)$$

where $C$, $C_{Nt}$ and $C_{Nb}$ are constants.

A study [182] investigated mixed convection of $Al_2O_3$ nanofluids in various regions of an inclined copper pipe with a diameter of 6.35 mm. In the horizontal part of the tube, heat transfer decreased with increasing particle volume fraction. However, in the vertical section, the Nusselt number remained relatively unaffected by changes in particle volume fraction. The correlations for mixed convection were proposed for both vertical (Equation (6)) and horizontal (Equation (7)) tube configurations. The correlations are valid for nanoparticle volume fractions between 0 and 4%, Reynolds numbers between 350 and 900, and Rayleigh numbers between $5 \times 10^5$ and $9.6 \times 10^5$.

$$\text{For vertical tube, } Nu_{nf} = Nu_{con}\,(1 + 52 \times 10^4\, Gr/Re_{nf})^{0.28} \quad (6)$$

$$\text{For horizontal tube, } Nu_{nf} = Nu_{con}\,(1 - \phi^{0.625})\,(1 + 5.25 \times 10^{-5}\, Ra_{nf}{}^{1.06})^{0.135} \quad (7)$$

#### 3.3.4. Turbulent Heat Transfer Using Nanofluids

The study of heat transfer in turbulent flow conditions represents important challenges due to the involvement of high Rayleigh and Reynolds numbers and because of its complex fluid dynamics. Nanofluids incorporated with base fluids have resulted in enhancement of heat transfer performance in turbulent flows due to their unique thermophysical properties [183]. Experimental investigations have highlighted the impact of $\gamma$-$Al_2O_3$ and CuO-water-based nanofluids on turbulent heat transfer and associated pressure drop performance in circular tubes. The addition of nanoparticles to the base fluid has shown a significant enhancement in the convective heat transfer rate under turbulent flow conditions. However, this improvement is often accompanied by an increase in pressure drop, attributed to the altered viscosity and density of the nanofluid [184,185].

Using $Al_2O_3$-water-based nanofluid as the heat transfer fluid, a 2D axisymmetric-forced turbulent convection numerical study was conducted in a straight circular tube. The results were validated with experimental data and concluded that greater nanoparticle concentrations lead to higher heat transfer coefficients but result in increased pressure drops [186]. The turbulent heat transfer and pressure drop characteristics of semicircular and trapezoidal corrugated channels were analyzed using $SiO_2$-water nanofluids with 1% and 2% volume fractions over a Reynolds number range of 10,000 to 30,000. An increase in the Reynolds number enhanced turbulent intensity and flow mixing, which significantly improved turbulent heat transfer performance. Furthermore, a higher nanoparticle volume fraction in the fluid increased its thermal conductivity, intensifying the heat transfer rate and resulting in an elevated Nusselt number [187].

The turbulent heat transfer performance was investigated by varying both the nanofluid concentration (from 0.0625% to 1%) and the flow rate, with Reynolds numbers ranging from 3200 to 19,000. It was found that increasing the flow velocity amplifies turbulence intensity and flow mixing, which enhances turbulent heat transfer performance.

To further improve the thermal efficiency of the heat exchanger, the nanoparticle volume fraction was increased. This increase in nanoparticle concentration led to higher density and viscosity in the working fluid, further intensifying turbulent heat transfer [188]. The study investigated turbulent heat transfer in nanofluids (MWCNT, GNP, $SiO_2$, ZnO in water as base fluid) through an axisymmetric abrupt expansion heat exchanger. Experiments were conducted at Reynolds numbers between 4000 and 16,000, with a constant wall heat flux of 12,128.56 $W/m^2$. The results showed that the Nusselt numbers were higher than in fully developed pipe flow, indicating enhanced turbulent heat transfer, despite the recirculating velocities being a small fraction of the bulk mean velocity [189].

The turbulent heat transfer properties of $Fe_3O_4$ nanofluids in a circular pipe were investigated, where the nanofluids consisted of a mixture of $Fe_3O_4$, ethylene glycol (EG), and deionized water (DIW). The $Fe_3O_4$ nanoparticles were treated with citric acid to improve their dispersion. The study examined the performance of these nanofluids over volume fractions ranging from 0.0 wt% to 1.2 wt%. It was found that effective convective heat transfer (CHT) required significant adjustments in heat flux, fluid flow rate, and temperature. Additionally, the CHT coefficient of the nanofluid was observed to be 7% lower than that of the base liquid [190]. The turbulent heat transfer properties of $Fe_3O_4$/MWCNT nanofluids with distilled water were investigated over concentrations ranging from 0.1 to 0.3 wt%. At a Reynolds number of 22,000 and a 0.3 wt% concentration, a maximum enhancement of 31% in the Nusselt number (Nu) was observed, along with a 1.18-fold increase in pumping power [191]. The turbulent heat transfer properties of $Fe_3O_4/TiO_2$/DIW nanofluids were explored over volume fractions ranging from 0.00625 to 0.3 wt%. The results revealed a heat transfer enhancement of 26.33% at 0.0125% volume fraction and 24.30% at 0.00625% volume fraction. The addition of nanoparticles significantly improved the thermal conductivity of the fluid, contributing to higher convective heat transfer rates. The study suggests that even at lower nanoparticle concentrations, substantial improvements in heat transfer can be achieved, highlighting the potential of these nanofluids for applications requiring efficient thermal management [192].

The use of nanofluids to enhance turbulent heat transfer in channel flows has been widely studied. Several numerical investigations have focused on the forced convection of $Al_2O_3$-water nanofluids, with volume fractions ranging from 0% (pure water) to 4%, and Reynolds numbers exceeding 20,000. These studies have shown that the heat transfer rate increases with larger nanoparticle sizes and higher Reynolds numbers. However, this improvement in heat transfer is accompanied by higher energy consumption, emphasizing the trade-off between enhanced thermal performance and increased energy demands [193]. The study found that using single nanofluids (Cu, CuO, $Al_2O_3$) with volume fractions ($\phi$) ranging from 0.3% to 1.5% significantly enhanced turbulent heat transfer, with Nusselt number increases ranging from 5.06% to 386.63% compared to water. The friction coefficient increased slightly by 6.71–15.84%, 7.46–14.42%, and 8.25–15.84% for Cu, CuO, and $Al_2O_3$, respectively. The Cu-$Al_2O_3$-water hybrid nanofluid exhibited the best performance, with Nu reductions of 20.85–30.61% and energy efficiency coefficient (EEC) reductions of 20.08–29.02% compared to Cu-water nanofluids at the same $\phi$. Nanofluids demonstrated poor heat transfer enhancement at low Reynolds numbers ($Re \leq 1500$), with optimal performance observed at $Re \geq 2640$. Furthermore, total entropy production decreased by 100.83–405.95% for Cu, 5.82–28.99% for CuO, and 11.28–53.51% for $Al_2O_3$ at $\phi$ = 0.3–1.5% [194].

The turbulent heat transfer performance of Aviation Turbine Fuel (ATF) with Multi-wall Carbon Nanotube (MWCNT) nanofluids at concentrations of 0–1% and temperatures of 30 °C and 50 °C has been investigated. Results show that the heat transfer coefficient increases with particle concentration, reaching a maximum enhancement of 23% at 30 °C

and 50% at 50 °C at 1% concentration. Two numerical models (single-phase and Eulerian–Lagrangian) were used, and both showed good agreement with experimental data. The enhanced heat transfer performance demonstrates the potential advantages of nanofluids for regenerative heat transfer in turbulent heat transfer applications [195]. A computational study on turbulent heat transfer was conducted for water and $Al_2O_3$ nanofluids in a horizontal corrugated pipe. The study varied parameters such as corrugation height, Kármán number, corrugation frequency, and nanoparticle volume fraction. The results showed that the highest thermal efficiency occurred at $\phi$ = 2%, indicating optimal conditions for turbulent heat transfer [196]. Produced by pulsed discharge and ultrasound, graphene nanofluids demonstrate a 35% improvement in turbulent heat transfer performance compared to water. The numerical results indicate a notable 8% increase in turbulent kinetic energy and velocity gradients near the wall, attributed to the physical interaction between the continuous phase (water) and the dispersed graphene nanoparticles [197].

The hybrid $Al_2O_3$-CuO/water nanofluid significantly enhances turbulent heat transfer performance in a circular tube. Experimental results show a 2–35% increase in heat transfer with mass concentrations ranging from 0.5% to 3%, while pressure drop increases by up to 12%. CFD simulations using various models (Discrete Phase Model, mixture, Eulerian multiphase) reveal that the choice of thermophysical property model impacts heat transfer and pressure drop predictions, with the Eulerian model showing the smallest deviation. The thermal performance factor increases with concentration and decreases with Reynolds number [198]. Forced turbulent heat transfer in a grooved cylinder with varying groove spacings (A = 1, 1.1, 1.3) and groove depth-to-cylinder diameter ratios (e/D = 0.1 and 0.2) was analyzed using CuO nanoparticles at volume fractions of 0–4%. Lower Reynolds numbers resulted in better thermal performance, while higher Reynolds numbers showed less significant growth in Nusselt number [199]. Nanofluids display notable improvements in heat transfer performance in turbulent flows due to several mechanisms [183]; their advantages and limitations at both microscopic and macroscopic levels are as follows:

- Enhanced Thermal Conductivity—Nanoparticles have higher thermal conductivity compared to normal base fluids, like water or ethylene glycol. When added to a base fluid, even at low concentrations, these nanoparticles significantly increase the thermal conductivity, which enables more efficient conduction of heat in the system. This improvement is significant at higher temperatures, at which the thermal conductivity of the base fluid increases.
- Boundary Layer Disruption—In turbulent flow, the thermal boundary layer plays a critical role in heat transfer. The introduction of nanoparticles alters the flow characteristics near the boundary layer, increasing turbulence intensity and reducing its thickness. This disruption enhances the temperature gradient at the wall-fluid interface, leading to improved convective heat transfer coefficients.
- Brownian Motion-Induced Convection—Nanoparticles in suspension exhibit continuous random motion (Brownian motion) due to collisions with surrounding fluid molecules. This motion generates localized micro-convection, which enhances the overall convective heat transfer process. The intensity of Brownian motion increases with smaller particle size and higher temperatures.
- Particle Aggregation Effects—Nanoparticles may form clusters or aggregates, especially at higher concentrations. While aggregation is often considered a limitation, small-scale clusters can create secondary turbulence structures within the flow, which further enhance the mixing of fluid layers and increase heat transfer rates.
- Thermophoresis and Diffusiophoresis—Thermophoresis refers to the movement of nanoparticles under temperature gradients, while diffusiophoresis results from con-

centration gradients. Both phenomena contribute to the redistribution of nanoparticles, leading to improved thermal performance in turbulent systems.

- Turbulence Intensification—The addition of nanoparticles modifies the flow behavior, increasing Reynolds stresses and intensifying turbulence. This effect becomes more pronounced in high Reynolds number flows, where turbulence dominates the heat transfer mechanism.
- Reduced Thermal Boundary Resistance—At the nanoparticle–fluid interface, thermal boundary resistance is reduced due to the high surface area-to-volume ratio of nanoparticles. This reduction facilitates efficient energy exchange between the particles and the surrounding fluid.
- Advantages of Nanofluids in Turbulent Systems—Nanofluids exhibit significantly higher Nusselt numbers and convective heat transfer coefficients compared to base fluids under turbulent conditions, due to enhanced thermal conductivity, boundary layer disruption, and increased turbulence. This results in improved heat dissipation capabilities, making nanofluids ideal for high-performance applications such as heat exchangers, cooling systems, and energy systems. Additionally, nanofluids show consistent performance improvements across various flow velocities and turbulence intensities, offering versatility for a wide range of engineering applications.
- Limitations of Nanofluids in Turbulent Systems—The addition of nanoparticles to fluids increases their effective viscosity, leading to higher pumping power requirements, creating a trade-off between enhanced heat transfer and increased flow resistance. Furthermore, the stability of nanofluids can be compromised over time as nanoparticles aggregate or settle, requiring stabilizing agents or surfactants to maintain thermal performance. Additionally, existing predictive models, such as the Dittus-Boelter and Gnielinski equations, may not accurately capture nanofluid behavior under turbulent conditions, highlighting the need for the development of more accurate models to ensure reliable performance predictions.

#### 3.3.5. Heat Transfer Behavior of Hybrid Nanofluids

Hybrid nanofluids are advanced heat transfer fluids that consist of a base fluid combined with two or more types of nanoparticles, offering enhanced thermal conductivity and improved performance in various engineering applications. Table 11 offers a summary of the applications of hybrid nanofluids in natural, forced and mixed convective systems. Hybrid nanofluids have not been widely reviewed in natural convection heat transfer systems in the literature. While various studies focus on mono-nanofluids as HTF in solar-based thermal energy storage systems, where natural HTF flow is essential, hybrid nanofluids present a feasible alternative for such systems. Moreover, research has shown that hybrid nanofluids perform well with natural convection systems in solar applications. Consequently, more investigation is desirable to explore the practical application of hybrid nanofluids in natural convection systems.

Hybrid nanofluids in forced convective heat transfer systems emphasize their increasing role in enhancing heat transfer performance. The findings indicate that the addition of hybrid nanoparticles substantially improves system efficiency. Forced convective heat transfer is essential in a wide range of applications, and hybrid nanofluids, with their superior thermal properties, are increasingly used as heat transfer fluids (HTFs) to achieve higher heat transfer rates and greater overall system efficiency.

**Table 11.** Hybrid nanofluids in natural, forced and mixed convective systems proposed in previous studies.

| | Ref No | Hybrid Nanofluid | Base Fluid | ϕ (%) | EXP/NUM | Key Findings |
|---|---|---|---|---|---|---|
| Natural Convection | [93] | $Al_2O_3$-Cu | Water | $0 \leq \phi \leq 0.12$ | NUM | Compared to the $Al_2O_3$/water nanofluid, the $Al_2O_3$-Cu/water hybrid nanofluid provides better thermal performance. The buoyancy effect related to the hybrid nanofluid improves the mean Nusselt number, hence enhancing the heat transfer efficiency compared to mono nanofluids. |
| | [161] | $TiO_2$-Cu | Water | $0 \leq \phi \leq 0.02$ | NUM | The introduction of hybrid nanoparticles to the base fluid enhances its thermal conductivity, resulting in an increment in surface temperature. At high Rayleigh numbers (*Ra*), the streamline functions deteriorate, indicating a decrease in fluid flow efficiency under these conditions. |
| | [200] | Cu-SWCNT | Sodium alginate | $0.01 \leq \phi \leq 1$ | NUM | Hybrid fluid models are appropriate when the nanomaterial concentration reaches 0.3% of the volume. Also, the heat transfer rate for SWCNT-Cu nanofluids increases with increasing nanoparticle volume fraction and Prandtl number, resulting in thermal performance enhancement. |
| | [201] | $Al_2O_3$-Cu | Water | $0 \leq \phi \leq 0.2$ | NUM | As the size of the heating element decreases, the Nusselt number increases, indicating improved heat transfer efficiency. |
| | [115] | $SiO_2$-Graphite | Water | $0.5 \leq \phi \leq 1$ | EXP & NUM | At moderate Reynolds numbers (4500 < Re < 7000), a 1% hybrid nanoparticle concentration increases the Nusselt number by up to 6%, while at higher Reynolds numbers (7500 < Re < 10,000), Nusselt numbers rise consistently with higher concentrations. |
| | [191] | $Fe_3O_4$-MWCNT | Water | $0.1 \leq \phi \leq 0.3$ | EXP | Experimental testing of MWCNT–$Fe_3O_4$ nanofluids showed that Nusselt numbers increased with higher particle concentrations and Reynolds numbers, with enhancements ranging from 9.35% to 31.10%. The improved heat transfer performance was due to the nanoparticles' high thermal conductivity, Brownian motion, and increased surface area. |
| | [202] | Ag-GNP | Water | $0.5 \leq \phi \leq 1$ | EXP | Nusselt number for GNP–Ag nanofluids increased with both Reynolds number and nanoparticle concentration, due to the higher conductivity and Brownian motion of the nanoparticles. The enhancements ranged from 8.29% to 32.70%, depending on particle fraction and Reynolds number. |
| | [203] | $TiO_2$-CuO | Water | $0 \leq \phi \leq 0.06$ | NUM | The local Nusselt number increases with the Falkner-Skan power law parameter and nanoparticle mass, with moving wedges enhancing heat transfer more than static ones. The highest nanoparticle mass in hybrid nanofluids results in the best thermal performance, while spherical nanoparticles led to the lowest local Nusselt number. |
| | [204] | Cu-$TiO_2$ | Aqueous | $0.1 \leq \phi \leq 2$ | EXP | At 1.0 vol.% concentration of Cu-$TiO_2$, the Nusselt number increased, reaching its maximum, but a decrease was observed at 2.0 vol.%, with a drop ranging from 2.3% to 11.2%. This reduction is attributed to the higher dynamic viscosity and increased thermal boundary layer thickness at higher particle loading. |
| | [205] | $Al_2O_3$-Cu | Water | $\phi = 0.1$ | NUM | The hybrid nanofluids showed a notable increase in the average Nusselt number, with an enhancement of 4.73% compared to $Al_2O_3$/water and 13.46% compared to pure water, demonstrating their superior heat transfer performance. |
| Mixed Convection | [110] | $Al_2O_3$-Cu | Water | $0 \leq \phi \leq 0.05$ | NUM | A small rise in the mean Nusselt number was observed in $Al_2O_3$-Cu/water hybrid nanofluids compared with regular nanofluids. This augmentation resulted in enhanced heat transfer performance, contributing to higher overall thermal efficiency in heat transfer applications. |
| | [179] | $Al_2O_3$-Cu | Water | $0.01 \leq \phi \leq 0.05$ | NUM | At a volume fraction of 0.05, the maximum heat transmission was observed. |

Studies on mixed convective heat transfer systems incorporating hybrid nanofluids have been discussed. $Al_2O_3$ has been used as an important constituent for producing hybrid nanoparticles in the reviewed literature, though other elements have been explored less. To optimize the performance of a system, it is recommended to select the hybrid nanoparticle that offers the highest performance. Further studies focusing on all three types of convective heat transfer systems using hybrid nanoparticle types are also recommended for better results.

#### 3.3.6. Role of Nanoparticle Concentration in Heat Transfer Optimization

In terms of heat transfer, the concentration of nanoparticles plays a significant role. It is influenced by various thermophysical properties like thermal conductivity, viscosity and stability. Based on the type of nanoparticles, size and base fluid, the effect of nanoparticle concentration on heat transfer performance varies [206]. Hence, it is critical to consider the advantages and limitations involved with concentration variation in various applications.

Effect of Nanoparticle Concentration on Heat Transfer: Increasing the nanoparticle concentration normally improves the thermal conductivity of a nanofluid due to the greater surface area available for heat transfer. However, this improvement is not continuously linear. As the concentration rises, the viscosity of the nanofluid also increases, which can undesirably affect the flow behavior and lead to a reduction in heat transfer efficiency. Furthermore, at higher concentrations, the nanoparticles may lead to agglomeration or sedimentation, resulting in instability patterns in the nanofluid and a potential decrease in thermal conductivity [207].

Range of Volumetric Concentration Leading to Slurry Formation: Nanofluids naturally change to a slurry-like state when the nanoparticle concentration surpasses a certain level, at which point the particles start to cluster and hinder dispersion. The exact concentration at which slurry formation occurs depends on the material, size and the effectiveness of the nanoparticles [208]. The development of a slurry in nanofluids is not only exhibited by the volumetric concentration but also influenced by nanoparticle size, shape and surface details [209]. Smaller nanoparticles need a higher concentration to reach the slurry state due to their increased surface area. But, when the concentration rises, even well-dispersed smaller nanoparticles may commence to agglomerate. Meanwhile, the larger nanoparticles may reach the slurry formation level even at lower concentrations, because they have a lower surface area, which leads to clustering. The use of surfactants can enlarge the concentration range at which nanoparticles remain well-dispersed, which can delay slurry formation and enhance the overall stability of the nanofluid [210].

Influence of Volumetric Concentration in Temperature-Dependent Thermo-Physical Properties Systems: Thermophysical properties of nanofluids like viscosity and thermal conductivity are temperature-dependent; here, the impact of nanoparticle concentration is highly complex. At low concentrations, the dispersion of nanoparticles improves thermal conductivity because of the increased surface area, which helps to improve heat transfer. When the concentration of nanoparticles increases, the properties display non-linear characteristics [211]. Initially, the thermal conductivity continues to improve, but when a certain concentration level is reached, aggregation of nanoparticles occurs. This aggregation decreases the effective surface area for heat conduction, leading to a decrement in thermal conductivity. Concurrently, the viscosity of the fluid increases, which also reduces the convective heat transfer characteristics; this is especially significant in forced convection systems where fluid movement is essential for effective heat transfer [212].

In systems characterized by large temperature gradients, such as heat exchangers or solar thermal applications, the influence of nanoparticle concentration on thermophysical properties plays a vital role. As the temperature increases, the viscosity of the base

fluid decreases, which would improve heat transfer [213]. Meanwhile, higher concentrations of nanoparticles lead to an increase in viscosity, which counters this effect, obscuring the relationship between temperature and heat transfer performance. Also, higher nanoparticle concentrations worsen the potential for aggregation, resulting in instability and sedimentation, which hinder the nanofluid's capability to uphold high thermal conductivity. Thus, defining the optimum nanoparticle concentration that maximize heat transfers is challenging.

Advantages: Higher nanoparticle concentrations can improve the thermal conductivity of nanofluids, which leads to higher heat transfer performance in applications such as heat exchangers, cooling systems and thermal energy storage. Especially in those operating at lower temperatures, even a small increase in nanoparticle concentration can result in prominent improvements in performance [214].

Limitations: However, increased nanoparticle concentration frequently leads to higher fluid viscosity, which can increase the pumping power required to circulate the nanofluid inside the system, resulting in a reduction of overall efficiency of the system. Also, nanoparticle agglomeration at higher concentrations can lead to instability. In temperature-dependent systems, these variations in nanoparticle behavior can introduce additional complexity in the system's performance [215].

## 4. Nanofluids in Thermal Energy Storage Systems

For TES applications, nanocomposites composed of nanoparticles and PCMs are being widely investigated in the literature. These nano-enhanced PCMs (NEPCMs) undergo characterization and optimization to achieve desired thermal properties. They are then integrated into TES systems to facilitate efficient charging and discharging cycles. NEPCMs are emerging as a promising solution for storing both sensible and latent heat in TES systems. The key findings from earlier investigations of NEPCMs are presented below. Previous studies have shown that NEPCMs are fabricated by dispersing nanoparticles or nanocomposites into PCMs. These NEPCMs are considered promising materials for TES applications. NEPCMs can significantly improve their overall performance by affecting three key properties [216]: thermal conductivity, storage capacity and phase change temperature in LHS systems.

### *4.1. Effect on Thermal Conductivity*

Nanoparticles with higher thermal conductivity can augment the heat transfer rate within PCM. This is mainly useful in applications where quick heat transfer is required, such as TES systems. Several investigations have been conducted to study such effects in LHS systems. In [217], graphene nanoparticles at a concentration of 0.3% by weight were incorporated into a beeswax-based PCM. This strategic addition resulted in a substantial enhancement in the thermal conductivity of around 0.25–2.89 W/mK. Nanoparticles with larger surface area enhance heat transfer, thereby improving thermal conductivity of PCMs. A myristic acid PCM was modified by incorporating 1.0 wt% $SiO_2$ nanoparticles. This addition led to a substantial 87.27% increase in the thermal conductivity compared to the original material. The latent heat remained largely unaffected, and the phase transition kinetics were slightly altered, with a minor increase in melting and solidification temperatures of 1.13% and 1.30%, respectively [218]. Qu et al. conducted experiments using EG-MWCNT and EG-CNF with Paraffin wax. The key findings demonstrated that EG-MWCNT/PCM exhibited greater thermal conductivity compared with EG-CNF/PCM [219]. Paraffin waxes (PW) were enhanced with the addition of aluminum oxide ($Al_2O_3$) and carbon black nanoparticles in [220].

Incorporating a 1% concentration of carbon black nanoparticles significantly improved thermal conductivity by more than 35%, outperforming $Al_2O_3$ in terms of augmenting thermal conductivity. Lin et al. investigated the impact of incorporating hexagonal-shaped copper nanoparticles, ranging in size from 15 to 125 nm, into paraffin wax. The investigation found that increasing the nanoparticle concentration to around 0.5–2% resulted in a significant improvement in thermal conductivity, ranging from 14% to 46.3% [221]. The impact of nanoparticles, including copper (Cu), aluminum (Al), nickel (Ni), silver (Ag), copper oxide (CuO), aluminum oxide ($Al_2O_3$), titanium dioxide ($TiO_2$), silica ($SiO_2$), and graphene nanoplatelets, on eutectic salt have been evaluated by Singh et al. [222]. They found that graphene had the least detrimental effect on latent heat in the NEPCM and exhibited improved thermal conductivity. A stearic acid-based PCM was modified with expanded graphite nanoparticles. The thermal conductivity increased significantly by 9.6 times compared with pure PCM when 6% wt of nanoparticles were added. The latent heat of NEPCM decreased slightly, from 189.7 J/g to 163.5 J/g, while the phase transition kinetics and temperature effects remained largely unaffected, with a variation of less than 1 °C in melting and freezing temperatures [223].

Incorporating graphite-based nanoparticles into paraffin wax significantly enhanced thermal conductivity, as described in [224]. Paraffin wax with graphene nanoparticles exhibited the highest thermal conductivity among all the tested samples [225]. Krishna et al. incorporated aluminum oxide ($Al_2O_3$) nanoparticles into tricosane ($C_{23}H_{48}$) at 0.5% to 2% by volume. The investigation found that the incorporation of nanoparticles significantly enhanced the thermal conductivity of the PCM, increasing it by up to 32% [226].

In [227], erythritol was modified with the addition of $Al_2O_3$, Cu, $TiO_2$ and $SiO_2$ nanoparticles. Copper and aluminum nanoparticles were found to have significantly higher thermal conductivity compared to the others tested, improving thermal conductivity by approximately 8%. In [228], the thermal properties of ethyl trans-cinnamate were improved by incorporating silver and titanium nanoparticles at concentrations between 0.1 and 1.5 wt%. Singh et al. demonstrated that incorporating $SiO_2$, $Al_2O_3$, and MgO nanoparticles with paraffin wax at 0.5 wt% significantly improves thermal conductivity [229]. This enhancement raises the thermal conductivity from an initial value of 0.20–0.26 W/m·K, which can contribute to faster heat transfer and potentially increase the efficiency of TES systems.

Moein-Jahromi et al. also proved that incorporating 3 wt% of graphene nanoplatelets (GNP) and CuO nanoparticles into polyethylene glycol PCM significantly enhances thermal conductivity, augmenting it from 0.234 W/m·K to 0.45 W/m·K [230]. In another investigation [231], nano-graphene nanoparticles, at a concentration of 3% by weight, were dispersed within a paraffin wax-based PCM. This specific formulation resulted in a notable enhancement in thermal conductivity from 0.123 to 0.303 W/mK. Maher et al. demonstrated that in paraffin wax PCM, the addition of 15 wt% silicon carbide and silver nanoparticles significantly enhances thermal conductivity, augmenting it from 0.248 W/m·K to 0.392 W/m·K [232]. Moreover, Qian et al. proved that in polyethylene glycol PCM, the integration of 2 wt% SWCNT leads to a notable improvement in thermal conductivity, increasing it from 0.24 W/m·K to 0.87 W/m·K [233]. This significant enhancement in thermal conductivity could facilitate more efficient heat transfer, making the modified PCM particularly advantageous for applications in TES and management, where rapid thermal response is essential. Figure 6 illustrates similar studies on the thermal conductivity variation for various PCMs incorporating nanomaterials.

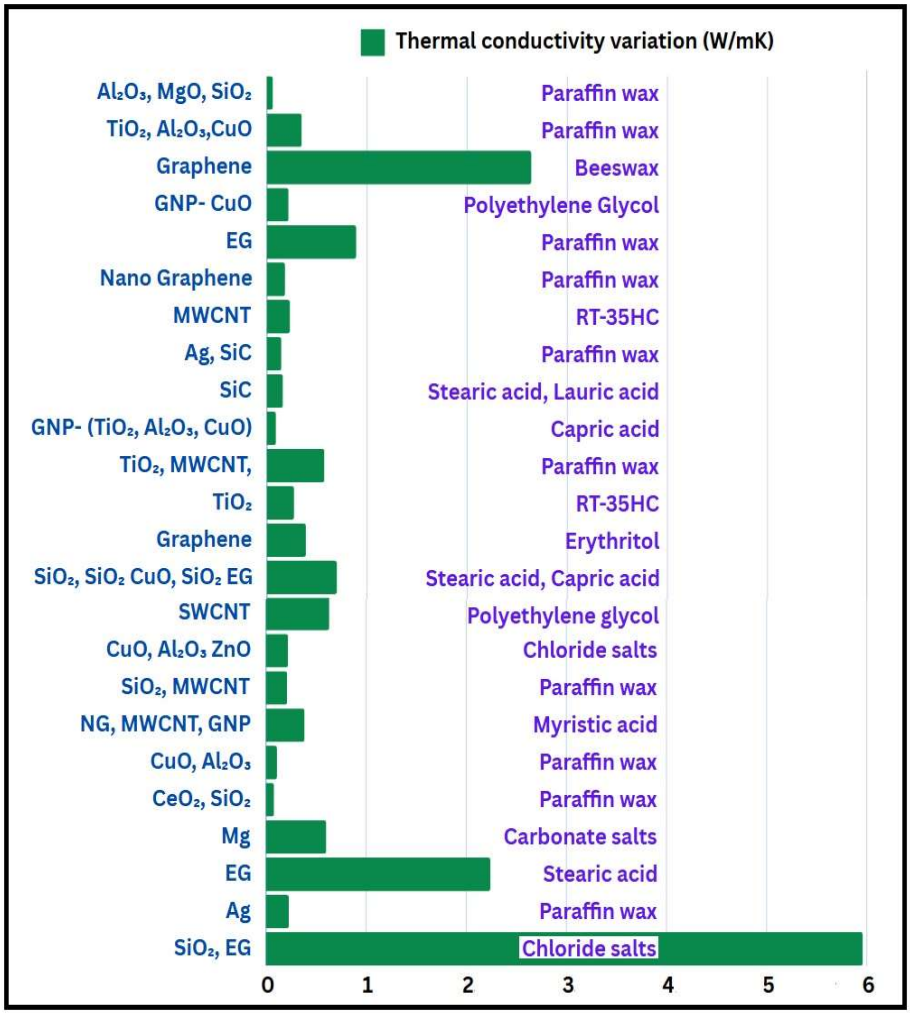


**Figure 6.** Studies on variation of thermal conductivity (W/mK) with PCM–nanomaterials.

### *4.2. Effect on the Latent Heat*

Overall, the incorporation of nanoparticles into PCMs offers a viable method of enhancing their thermal performance and increasing their suitability in various fields. While some studies have recommended that the addition of nanoparticles can enhance latent heat capacity, others have found that the existence of nanoparticles can reduce the quantity of PCMs, leading to a reduction in latent heat capacity. However, the impact of nanoparticles on latent heat capacity can be complex, with small proportions potentially benefiting latent heat capacity while larger proportions may have the opposite effect [234].

For instance, in paraffin wax PCM, the addition of $SiO_2$, $Al_2O_3$, and MgO nanoparticles at 0.5 wt% resulted in a slight decrease in latent heat, reducing it from 260 J/g to 258.30 J/g [229]. This minor reduction suggests that while the nanoparticles affect thermal conductivity, their impact on LHS capacity is minimal, preserving the PCM's effectiveness in TES applications. In [230], GNP and CuO nanoparticles, at a concentration of 3% by weight, were dispersed within a polyethylene glycol-based PCM. This specific formulation led to a slight reduction in latent heat, ranging from 178.35 to 168.70 J/g. While this alteration in LHS capacity may influence the overall thermal performance of a PCM, further investigation is required to fully understand the implications of these changes. Similarly, Ali et al. demonstrated that the addition of 3 wt% nano-graphene to paraffin wax PCM results in a decrease in latent heat, lowering it from 230.08 J/g to 216.1 J/g [231]. In [232], a paraffin wax-based PCM was enhanced with a combination of silicon carbide (SiC) and silver (Ag) nanoparticles at a 15% weight concentration. This specific formulation led to a

reduction in latent heat, ranging from 206.94 to 170 J/g. However, the authors highlighted that while this alteration in LHS capacity may influence overall thermal performance of PCM, further investigation is mandatory to understand the implications of these changes, particularly considering the potential benefits of enhanced thermal conductivity and other properties that may arise from the addition of these nanoparticles. The thermal properties of paraffin were enhanced by adding $TiO_2$, CuO, and GO nanoparticles, as investigated.

The study found that graphene oxide decreased thermal latency, while other research has indicated that nanoparticles can increase thermal latency [235]. In [236], the thermal properties of palmitic acid ($C_{17}H_{34}O_2$) and lauric acid ($C_{12}H_{24}O_2$) were enhanced by the addition of graphene platelets at a concentration of 10% by weight. It has been detected that incorporation of nanoparticles changed latent heat from 177.9 J/g to 165.6 J/g. Copper oxide nanoparticles were added to d-mannitol, a PCM. The addition of 0.5 wt% CuO improved the thermal conductivity of PCM from 1.308 W/mK to 1.637 W/mK. However, the latent heat (melting point) reduced slightly from 281.89 kJ/kg to 273.20 kJ/kg [237]. In study [238], paraffin combined with graphene demonstrated highest phase change enthalpy for both melting and solidification when compared with the pure PCM and other tested nanocomposites having MWCNT, aluminum, and $TiO_2$ at a concentration of 20 vol% [238]. Incorporating $Al_2O_3$, CuO, and $TiO_2$ nanoparticles into paraffin wax PCM reduces its latent heat from 116.75 J/g to 110.78 J/g [239].

MWCNTs, at 1% by weight, were dispersed within an RT-35HC PCM. This specific formulation led to a slight reduction in latent heat, ranging from 255.88 to 230.82 J/g [240]. The addition of GNP-$Al_2O_3$, GNP-CuO, and GNP-$TiO_2$ nanoparticles to a PCM composed of a blend of lauryl alcohol and capric acid resulted in reduction of latent heat, lowering it from 170.7–159.1 J/g [241]. The incorporation of $Al_2O_3$, CuO, and ZnO nanoparticles into a chloride salt mixture of $MgCl_2$, KCl, and NaCl caused a decrement in latent heat, reducing it from 283.3 J/g to 276.5 J/g. This reduction indicates that while the nanoparticles may enhance other thermal properties, they also slightly diminish the LHS capacity of PCMs, which could affect their overall efficiency in TES applications [242]. Figure 7 represents similar research on the latent heat variation for various PCM incorporated with nanomaterials.

### *4.3. Effect on the Phase Change Temperature*

The phase change temperature (PCT) of a PCM could be slightly varied by the addition of nanoparticles, depending on the specific nanoparticle and PCM combination. While the improved thermal conductivity enhances heat transfer efficiency, the lower phase change temperature may influence the PCM's performance in specific applications where precise temperature control is necessary.

For instance, as proved in one study [232], incorporating 15 wt% silicon carbide and silver nanoparticles in paraffin wax resulted in significant augmentation of its thermal conductivity, increasing from 0.248 W/mK to 0.392 W/mK. However, this modification also led to a decrease in phase change temperature, reducing it from 53 °C to 49.3 °C. A similar result was observed in [233], in which a polyethylene glycol-based PCM was enhanced with SWCNTs at a 2% weight concentration. This specific formulation resulted in a decrease in the phase change temperature, from 62.1 °C to 59.6 °C. In [241], a PCM composed of lauryl alcohol and capric acid was enhanced with graphene nanoparticle–metal oxide composites (GNP-$Al_2O_3$, GNP-CuO, and GNP-$TiO_2$). This specific formulation resulted in a decrease in the phase change temperature, from 4 °C to 3.8 °C. In another analysis [242], a PCM composed of magnesium chloride, potassium chloride, and sodium chloride was enhanced with aluminum oxide, copper oxide, and zinc oxide nanoparticles. This specific formulation resulted in a decrease in the phase change temperature, from 399.7 °C to 398.8 °C.

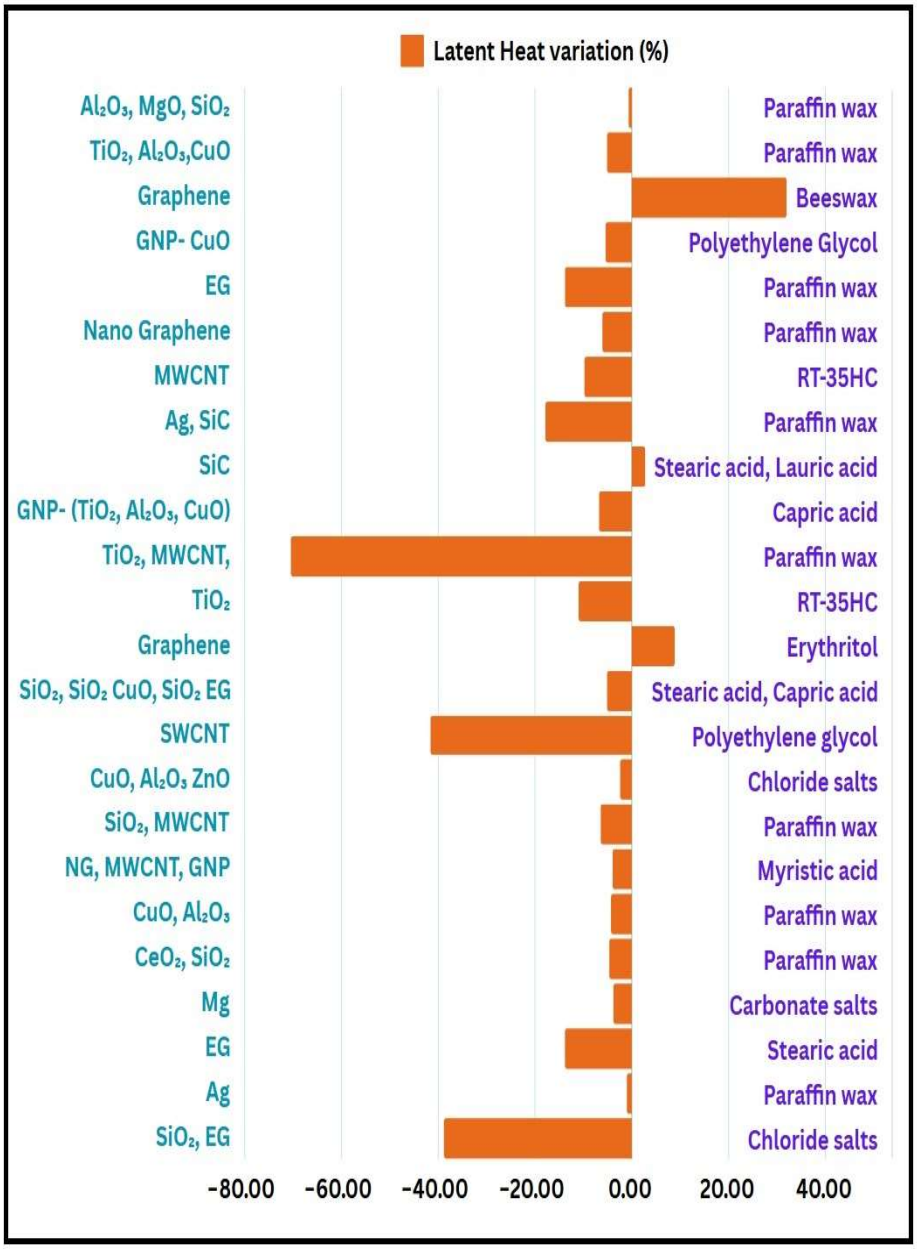


**Figure 7.** Studies on variation of latent heat (%) with PCM-nanomaterials.

Conversely, the PCT of the PCM remained nearly unchanged after dosing with CuO, as observed in [237]. In other cases, an increase in PCT was observed, as in [239], in which the dosing of $Al_2O_3$, CuO, and $TiO_2$ nanoparticles to paraffin wax PCM resulted in a small rise in phase change temperature, from 62.54 °C to 63.56 °C. The addition of 1 wt% MWCNT into RT-35HC PCM led to a minor increase in phase change temperature, rising from 36.09 °C to 36.17 °C. This slight adjustment may improve the thermal stability of the PCM, potentially improving its performance [240].

Paraffin wax was determined to be less effective for TES applications due to its lower operating temperature and limited heat absorption. Erythritol is well-suited for temperatures near 150 °C, while nitrate salt is preferable for temperatures between 200 °C and 230 °C [243]. The addition of MWCNTs to paraffin wax was found to lower the phase change temperature by about 1 °C, as reported by Wang et al. [244]. An experimental study on thermal performance of a cold TES system employing Ni-ZnO nanocomposites added to oleic acid has been performed. This study found that incorporating 0.3, 0.6 and 1.2 wt% of nanocomposites improved heat transfer properties of a heat transfer

fluid (HTF), resulting in a decrease of melting and also solidification times by around 29.69% and 28.52%, respectively [245]. The addition of alpha-aluminum oxide ($\alpha$-$Al_2O_3$) to petroleum wax was found to lower the phase change temperature by 2.2 °C, as reported by Mohamed et al. [246].

The combination of MWCNT-CuO nanoparticles and paraffin wax in a parabolic dish-type solar collector has been investigated using both theoretical and experimental approaches. The study compared both charging and discharging rates of NEPCM to pure paraffin wax, and found that the NEPCM's phase change time was reduced by 66.6% [247]. Adding 0.3 wt% graphene nanoparticles to beeswax PCM resulted in a slight increase in phase change temperature, from 62.28 °C to 62.42 °C. This small adjustment in temperature could increase the thermal stability of the PCM, making it more suitable for applications that benefit from precise phase transition control [248]. Figure 8 represents similar studies on the phase change temperature variation for various PCMs incorporating nanomaterials.

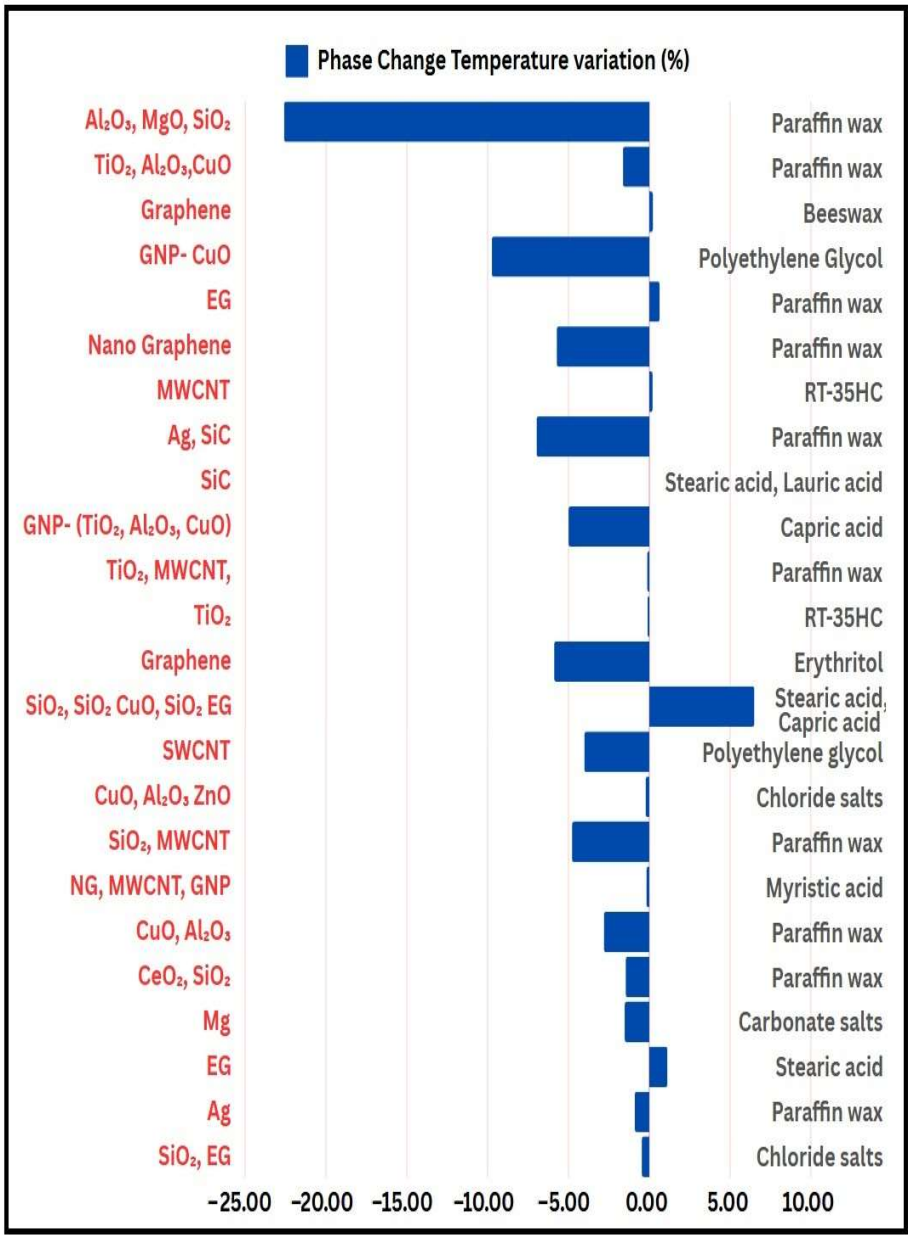


**Figure 8.** Studies on variation of phase change temperature (%) with PCM–nanomaterials.

The application of nanomaterials has led to the following impacts:
Increase in Thermal Conductivity

- Enhanced heat transfer because of the presence of nanoparticles that provide a larger surface area for conduction [239].
- Improved dispersion of nanoparticles increases the effective thermal conductivity of the PCM [232,238–243].
- Nanoparticles can generate a network that facilitates thermal energy transfer [249]. No evidence of decrease in thermal conductivity has been found from previous studies.

Potential increase in Latent Heat

- Improved microstructural properties of the PCM due to nanoparticles can lead to a higher latent heat of fusion [248].
- Some nanoparticles can enhance the energy storage capability of the PCM by stabilizing the phase change process [250].
- Nanoparticles may create a composite structure that can absorb more energy during phase transitions [251,252].

Potential decrease in Latent Heat

- Increased thermal conductivity may result in faster phase transitions, reducing the amount of energy stored as latent heat [223].
- Presence of nanoparticles can disrupt the crystallization process, resulting in lower latent heat of fusion [232,239].
- Some nanoparticles may change the thermodynamic properties of PCM, resulting in lower energy storage efficiency [253,254].

Potential increase in Phase Change Temperature

- Nanoparticles can modify the nucleation sites and promote a more uniform phase change, shifting the melting temperature upwards [240].
- Improved thermal stability of the PCM due to the incorporation of nanoparticles can lead to a higher phase change temperature [255].
- The interaction between nanoparticles and the PCM can result in enhanced thermal stability under varying temperature conditions [256].

Potential decrease in Phase Change Temperature

- Addition of nanoparticles may lower the PCT by altering the intermolecular forces within the PCM [229,247].
- Certain nanoparticles can introduce impurities that destabilize the solid phase, leading to a lower melting point [240].
- The modified thermal behavior of the PCM caused by nanoparticles can lead to earlier phase transitions [233,242,257].

Table 12 represents the various studies on thermophysical properties of nanomaterials incorporated PCM.

### *4.4. Influence of Nanoparticles on Latent Heat and Temperature Control in PCM Systems: Beneficial and Adverse Effects*

As highlighted in the comparative Table 12, adding nanoparticles to PCMs can have both beneficial and unfavorable effects on the latent heat capacity of the material, which determines the energy stored or released during phase transitions. The primary advantage of nanoparticle incorporation is the enhancement of thermal conductivity, leading to improved heat transfer during the charging and discharging cycles. However, this improvement does not always correlate with an increase in latent heat. In some cases, the presence of nanoparticles can lead to adverse effects, such as the following:

- Premature Phase Change: Nanoparticles can act as nucleation sites, which may cause the PCM to solidify or melt prematurely. This disrupts the desired phase change process, leading to a reduction in the amount of energy that can be stored or retrieved.
- Increased Viscosity: Higher concentrations of nanoparticles can increase the viscosity of the PCM, impeding heat transfer by slowing down the movement of the material. This can result in less efficient charging and discharging cycles, reducing the overall performance of the PCM.
- Thermal Conductivity vs. Latent Heat: While nanoparticles enhance thermal conductivity, this does not always correlate with an increase in energy storage capacity. In some cases, the higher thermal conductivity can lead to faster melting or solidification, thus reducing the time the PCM stays in the phase change state and impacting its overall latent heat capacity.

**Table 12.** Review of studies on nanoparticle-enhanced thermophysical properties of TES.

| Ref No | EXP/NUM | Nanoparticle | | PCM | Variation in Latent Heat | | Variation in Phase Change Temperature | | Variation in Thermal Conductivity | |
|---|---|---|---|---|---|---|---|---|---|---|
| | | Material | Concentration | | (J/g) ↑ or ↓ | (%) ↑ or ↓ | (°C) ↑ or ↓ | (%) ↑ or ↓ | (W/m K) ↑ or ↓ | (%) ↑ or ↓ |
| [193] | EXP | Graphene | 0.3 wt% | Beeswax | 45.25 ↑ | 31.98 ↑ | 0.14 ↑ | 0.22 ↑ | 2.64 ↑ | ≈150 ↑ |
| [223] | EXP | EGr | - | Stearic acid | 26.2 ↓ | 13.81 ↓ | 0.6 ↑ | 1.13 ↑ | 2.24 ↑ | ≈800 ↑ |
| [229] | EXP & NUM | $Al_2O_3$, MgO, $SiO_2$ | 0.5 wt% | Paraffin wax | 1.7 ↓ | 0.65 ↓ | 9.72 ↓ | 22.6 ↓ | 0.06 ↑ | 30 ↑ |
| [230] | EXP | GNP-CuO | 3 wt% | Polyethylene Glycol | 9.65 ↓ | 5.41 ↓ | 4.2 ↓ | 9.74 ↓ | 0.216 ↑ | 92.31 ↑ |
| [231] | EXP | Nano Graphene | 3 wt% | Paraffin wax | 13.98 ↓ | 6.08 ↓ | 1.71 ↓ | 5.73 ↓ | 0.18 ↑ | ≈150 ↑ |
| [232] | EXP | Ag, SiC | 15 wt% | Paraffin wax | 36.94 ↓ | 17.85 ↓ | 3.7 ↓ | 6.98 ↓ | 0.144 ↑ | 58.06 ↑ |
| [233] | EXP | SWCNT | 2 wt% | Polyethylene glycol | 78.3 ↓ | 41.62 ↓ | 2.5 ↓ | 4.02 ↓ | 0.63 ↑ | ≈250 ↑ |
| [239] | EXP & NUM | $TiO_2$, $Al_2O_3$,CuO | 3 wt% | Paraffin wax | 5.97 ↓ | 5.11 ↓ | 1.02 ↑ | 1.63 ↑ | 0.348 ↑ | 59.39 ↑ |
| [240] | EXP & NUM | MWCNT | 1 wt% | RT-35HC | 25.06 ↓ | 9.79 ↓ | 0.08 ↑ | 0.2 ↑ | 0.229 ↑ | ≈100 ↑ |
| [241] | EXP | GNP-($TiO_2$, $Al_2O_3$, CuO) | 0.3 wt% | Capric acid | 11.6 ↓ | 6.79 ↓ | 0.2 ↓ | 5 ↓ | 0.09 ↑ | 60.81 ↑ |
| [242] | EXP | CuO, $Al_2O_3$ ZnO | 0.5–3 wt% | Chloride salts | 6.8 ↓ | 2.4 ↓ | 0.9 ↓ | 0.23 ↓ | 0.22 ↑ | 62.86 ↑ |
| [248] | EXP & NUM | $TiO_2$ | 2 wt% | RT-35HC | 28.14 ↓ | 10.99 ↓ | 0.04 ↓ | 0.11 ↓ | 0.27 ↑ | ≈100 ↑ |
| [250] | EXP | Ag | 1 wt% | Paraffin wax | 1.6 ↑ | 1.01 ↑ | 0.5 ↓ | 0.9 ↓ | 0.228 ↑ | ≈100 ↑ |
| [251] | EXP | SiC | 0.075 wt% | Stearic acid, Lauric acid | 3.4 ↑ | 2.79 ↑ | No Change | No Change | 0.16 ↑ | 75.83 ↑ |
| [252] | EXP & NUM | Graphene | 1 wt% | Erythritol | 27.6 ↑ | 8.87 ↑ | 7.51 ↓ | 5.89 ↓ | 0.389 ↑ | 53.07 ↑ |
| [253] | EXP | $SiO_2$, EGr | - | Chloride salts | 78.5 ↓ | 38.82 ↓ | 1.8 ↓ | 0.46 ↓ | 5.96 ↑ | ≈1000 ↑ |
| [254] | EXP | Mg | 2 wt% | Carbonate salts | 6.3 ↓ | 3.79 ↓ | 5.99 ↓ | 1.52 ↓ | 0.602 ↑ | 45.33 ↑ |
| [255] | EXP | EGr | 15 wt% | Paraffin wax | 21.3 ↓ | 13.83 ↓ | 0.3 ↑ | 0.64 ↑ | 0.891 ↑ | ≈400 ↑ |
| [256] | EXP | $SiO_2$, $SiO_2$-CuO, $SiO_2$-EGr | 0.2–0.6 g | Stearic acid, Capric acid | 8.5 ↓ | 5.15 ↓ | 1.87 ↑ | 6.5 ↑ | 0.698 ↑ | ≈300 ↑ |
| [257] | EXP | NG, MWCNT, GNP | 3 wt% | Myristic acid | 7.71 ↓ | 3.96 ↓ | 0.1 ↓ | 0.18 ↓ | 0.385 ↑ | ≈150 ↑ |
| [258] | EXP | CuO, $Al_2O_3$ | 1 wt% | Paraffin wax | 6 ↓ | 4.3 ↓ | 1.8 ↓ | 2.81 ↓ | 0.109 ↑ | 60.56 ↑ |
| [259] | EXP | $TiO_2$, MWCNT, | 1 wt% | Paraffin wax | 17.5 ↓ | 70.45 ↓ | 0.04 ↓ | 0.14 ↓ | 0.574 ↑ | ≈200 ↑ |
| [260] | EXP | $SiO_2$, MWCNT | 1 wt% | Paraffin wax | 12.7 ↓ | 6.44 ↓ | 3 ↓ | 4.78 ↓ | 0.21 ↑ | 87.5 ↑ |
| [261] | EXP | $CeO_2$, $SiO_2$ | 1 wt% | Paraffin wax | 6.5 ↓ | 4.64 ↓ | 0.93 ↓ | 1.46 ↓ | 0.08 ↑ | 44.44 ↑ |

Note: ↑ Increment, ↓ Decrement.

The effect of temperature on PCM performance varies significantly depending on the system in which the PCM is applied:

- Systems with Beneficial Temperature Control: In systems where temperature control is less critical, the improved thermal conductivity from nanoparticles can enhance PCM performance by accelerating the melting and solidification processes. This is particularly useful in applications like thermal energy storage in solar power plants or industrial heat recovery systems, where quicker response times are beneficial.
- Systems Requiring Precise Temperature Control: In applications where maintaining a stable temperature is crucial, such as in electronic cooling, the addition of nanoparticles may cause instability. The faster melting and freezing induced by higher thermal conductivity could lead to unwanted temperature fluctuations, which can impair the effectiveness of the PCM in controlling temperature. In such cases, nanoparticle concentration must be carefully optimized to avoid these adverse effects.

## 5. Challenges

Integrating nanomaterials with PCM presents multifaceted challenges, including compatibility issues, thermal performance optimization, and scalability for practical applications.

- The release of nanoparticles into the environment can have serious detrimental effects, posing significant risks to human health and harming ecosystems [262]. These nanoparticles may exhibit toxic properties, potentially leading to respiratory issues, neurological damage, and other health concerns. Moreover, the introduction of heavy metals, often found in some nanoparticle formulations, can result in severe damage to vital organs. Given these consequences, it is imperative to explore sustainable methods for recycling and repurposing nanoparticles [262]. This not only helps mitigate the negative environmental impacts but also allows for the recovery of valuable materials. By prioritizing the development of recycling techniques, the scientific community can contribute to safer nanotechnology practices while enhancing the overall sustainability of nanomaterials [263].
- Preparing mono and hybrid nanofluids comes with several challenges. One of the key issues is achieving a stable and uniform dispersion of nanoparticles, as they tend to clump together due to Van der Waals forces, which can affect their stability and thermal performance. Another challenge is finding the right combination of nanoparticles and base fluids, as some combinations may react chemically, leading to instability. It is also tricky to determine the ideal nanoparticle concentration—higher concentrations can boost thermal conductivity, but they also make the fluid thicker, reducing flow efficiency. On top of this, advanced synthesis methods like the one-step technique are expensive and not always practical for large-scale applications. Preparing hybrid nanofluids, which use two or more types of nanoparticles, is even more complex, requiring careful methods to ensure stability, prevent separation, and maximize the combined benefits of the different materials.
- The disposal of nanomaterials poses significant environmental challenges, especially when these materials are deposited in landfills. The incineration of such materials can release harmful emissions into the atmosphere, contributing to air pollution and potentially affecting human health and local ecosystems [264]. Furthermore, the leaching of nanoparticles from landfills into soil and groundwater can lead to contamination, which poses long-term risks to environmental quality and public safety [265]. Research into alternative disposal methods and the development of biodegradable nanomaterials could play a vital role in addressing these issues and promoting a sustainable approach to the lifecycle of nanofluids in energy applications [266].

- Maintaining an optimal concentration of nanoparticles is vital for achieving high thermal conductivity in nanofluids, as excessive concentrations can lead to agglomeration. This clustering reduces the effective surface area for heat transfer and can increase viscosity, resulting in higher pumping power requirements and energy losses. Therefore, careful selection of nanoparticle concentration is essential, along with strategies to prevent agglomeration, such as using surfactants or stabilizers. By optimizing both concentration and dispersion, it becomes possible to enhance thermal conductivity effectively while minimizing the negative impacts of agglomeration, thereby improving the efficiency of TES systems and heat exchangers [267,268].
- Numerical studies of nanofluids come with their own set of challenges, largely due to the complex interactions between nanoparticles and the base fluid. This becomes even more difficult in turbulent or multiphase flows, where traditional models struggle to accurately capture the detailed dynamics. Adding to the complexity, factors like Brownian motion, thermophoresis, and sedimentation require advanced physical models, which not only increase computational demands but also make simulations harder to manage. Another hurdle is the temperature-dependent nature of nanofluid properties, like viscosity and thermal conductivity, which introduces uncertainties—especially since experimental data for validation are often limited. These studies are also highly sensitive to assumptions and boundary conditions, meaning that oversimplified models might not reflect real-world scenarios. Lastly, most numerical simulations are done on a lab scale, making it tough to apply the results to industrial systems, as experimental validation at larger scales is both expensive and complicated.
- The widespread application of nanoparticles is constrained by their high purchasing cost, which can deter manufacturers and investors from adopting this technology [266]. The cost of nanofluid PCMs increases with increasing nanoparticle concentration. The nanofluid's total cost (EUR) $C_T$ is calculated by previous researchers [269,270] as (Equation (8)):

$$C_T = C_{Base\text{-}fluid} + C_{Nano} + C_{Other} \quad (8)$$

where $C_{Base\text{-}fluid}$ is cost of the base fluid, $C_{Nano}$ is the cost of the nanoparticles, and $C_{Other}$ is the extra cost of preparing the nanofluid. As an example, Figure 9 shows the total nanofluid costs corresponding to different nanofluid volume fractions.

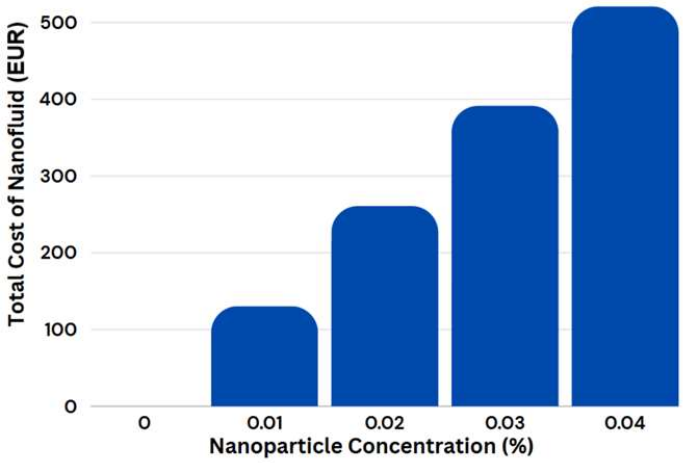


**Figure 9.** Nanofluid Cost (EUR) for various nanoparticle concentrations [271].

## 6. Limitations and Future Directions in Nanoparticle-Based PCM Systems and Thermal Storage Systems

Nanoparticle-based phase change materials (NPPCMs) and thermal storage systems utilizing nanofluids have garnered significant attention due to their potential to enhance thermal performance, particularly in renewable energy applications. However, despite their promising benefits, several challenges persist in their implementation. These challenges stem from issues related to the preparation of nanofluids, stability, optimal nanoparticle concentration, and the cost-effectiveness of large-scale production. Additionally, while theoretical and numerical advancements have contributed to a deeper understanding of these systems, practical limitations remain that hinder their widespread application. In this section, we explore the limitations of NPPCM systems, the challenges in nanoparticle integration for thermal storage, and the future directions that could potentially overcome these barriers.

### *6.1. Limitations of Nanoparticle-Based Phase Change Material (NPPCM) Systems*

- Thermal Conductivity Enhancement: While adding nanoparticles improves thermal conductivity, this enhancement is often limited and highly dependent on particle size, shape, and concentration.
- Agglomeration and Stability: Nanoparticles in PCM systems tend to aggregate over time, reducing the overall effectiveness and stability of the material.
- Cost and Scalability: The preparation and integration of NPPCMs are cost-intensive, limiting large-scale adoption in industrial applications.
- Environmental Concerns: Many nanoparticle materials are non-biodegradable and pose environmental and health risks during production, use, and disposal.
- PCM Compatibility: Ensuring compatibility between nanoparticles and the PCM matrix without altering its phase change properties is a persistent challenge.

### *6.2. Limitations of Nanoparticles in Thermal Storage Systems*

- Optimal Nanoparticle Concentration: The enhancement in thermal performance is concentration-dependent, but high nanoparticle volumes can lead to increased viscosity, sedimentation, and reduced system efficiency.
- Heat Transfer Limitations: While nanoparticles improve thermal conductivity, the actual enhancement in heat transfer rate may not always justify the added complexity and cost.
- Sedimentation Issues: In fluid-based systems, nanoparticles tend to sediment over time, requiring additional stabilization mechanisms.
- Compatibility with Existing Systems: Retrofitting thermal storage systems to accommodate nanoparticle-based fluids can be challenging due to potential chemical reactions, wear, or clogging issues.

### *6.3. Limitations of Volumetric Nanoparticle/Volume Fraction in Nanofluids*

- Viscosity Increase: Higher concentrations of nanoparticles significantly increase viscosity, leading to higher pumping power requirements and reduced flow efficiency.
- Clustering and Agglomeration: Beyond a certain threshold (often 5–10% by volume), nanoparticles begin to cluster, transitioning the nanofluid into a slurry state, which adversely affects heat transfer properties.
- Thermal Saturation: The thermal conductivity improvement plateaus at higher concentrations, reducing the benefit of adding more nanoparticles.

### 6.4. Numerical and Theoretical Developments in Thermal Storage Systems

Advantages:

- Predictive Insights: Numerical models provide valuable insights into nanoparticle behavior, phase change dynamics, and thermal properties, enabling optimization without costly experiments.
- Customizable Simulations: Advanced numerical tools allow researchers to simulate specific conditions and configurations, reducing the time and resources required for experimental validation.

Limitations:

- Complex Interactions: Capturing the full range of nanoparticle-fluid interactions (e.g., Brownian motion, thermophoresis) is computationally expensive and often requires simplifying assumptions.
- Validation Challenges: Numerical results are often based on idealized conditions, which may not match real-world scenarios, leading to discrepancies with experimental findings.
- Scalability Issues: Translating results from small-scale numerical studies to industrial-scale systems is fraught with uncertainties and requires extensive testing.

### 6.5. Future Directions

To comprehensively grasp the capabilities of nanofluids within TES systems, it is essential to conduct additional investigations. Future research directions suggested by the current literature include the following activities:

- A major challenge in using NEPCMs is the high cost of preparation and synthesis. To mitigate this issue, the authors suggest adopting the economical two-step process, where readily available nanoparticles are added into PCM and base fluid. However, this method can lead to sedimentation problems, which can be addressed through techniques like magnetic stirring, surfactant addition and ultrasonication, enhancing the stability of the dispersion.
- Research findings indicate that incorporating nanoparticles into PCM improves thermal conductivity, although in some instances, a higher concentration of nanoparticles resulted in reduction of latent heat. Therefore, extensive investigation is necessary to establish the optimal nanoparticle concentration, ensuring that the benefits of enhanced thermal conductivity outweigh any adverse effects, such as decreased latent heat.
- A key concern regarding the use of nanoparticles is their environmental impact, which can be mitigated through recycling processes. This issue is critical and requires further research to fully understand the risks associated with nanofluids and NEPCM. To ensure environmental sustainability, it is essential to develop and implement mitigation techniques before applying these materials in TES systems.
- Nanofluids and NEPCMs show promise in improving TES systems. However, their long-term stability remains a concern, limiting their widespread application. Further research is needed to ensure their durability and effectiveness in these systems.

## 7. Conclusions and Future Perspectives

This review has highlighted the significant findings related to the incorporation of nanofluids in TES systems. The integration of nanoparticles into LHS systems has demonstrated considerable potential for enhancing thermal conductivity, altering latent heat characteristics, and optimizing overall energy storage performance. By synthesizing current knowledge and identifying key trends, this review aims to deliver a comprehensive understanding of the role of nanofluids in TES, paving the way for future developments that

can contribute to more efficient and sustainable energy systems. The primary conclusions are as follows:

- Few studies indicate that the addition of nanoparticles can enhance latent heat of enthalpy, improving the efficiency of TES systems. This enhancement is often attributed to the increased surface area, and better thermal conductivity provided by the nanoparticles. However, in certain cases, particularly with the inclusion of carbon-based nanoparticles, a decline in latent heat has been observed. This reduction may be linked to factors such as nanoparticle agglomeration or changes in the microstructure of the PCM. Understanding these contrasting outcomes is essential for optimizing the formulation of nanofluids and ensuring the effective performance of TES systems. Further investigation into the interactions between nanoparticles and PCMs is needed to develop strategies that maximize the benefits while minimizing any potential drawbacks.
- The incorporation of nanoparticles has demonstrated significant improvements in the thermal conductivity of PCMs, making them more effective for TES applications. This enhancement in thermal conductivity allows for faster heat transfer, which is crucial for the efficiency of systems utilizing PCMs. Also, the addition of nanoparticles can help optimize the phase change process by facilitating quicker melting and solidification, ultimately leading to improved energy management. As research in this area progresses, the continued exploration of different types and concentrations of nanoparticles will be essential for maximizing the benefits of PCMs in various applications.
- The nanoparticles used in conjunction with the PCMs can either be fabricated in-house or sourced from commercial suppliers. It is important to assess the costs associated with integrating these nanoparticles with PCM, as this can lead to significant expenses. Nonetheless, a comprehensive economic analysis should be conducted, taking into account not only the initial investment but also the potential energy savings and overall efficiency improvements that the system may achieve. By evaluating these factors, one can determine the long-term financial viability of using nanoparticles in TES applications.
- Economic flexibility is significantly influenced by the market availability of nanoparticles. The accessibility of these materials directly impacts their pricing; when nanoparticles are readily available, costs tend to be lower, which suggests greater economic sustainability. This situation encourages the adoption of technologies that utilize nanoparticles, as it enhances reliability while making them more financially feasible for various applications. Thus, a stable supply chain for these materials is essential for promoting innovations in TES and other related technologies.
- Nano-based technology is currently experiencing widespread adoption across various fields, including medicine and solar applications, due to its significant potential. However, its extensive use also presents environmental challenges. The entire lifecycle of nanomaterials, from laboratory fabrication to disposal, involves multiple stages and can be costly. Improper disposal can lead to toxicity and harm ecosystems. Consequently, substantial research efforts are being directed towards developing methods for recycling used nanoparticles instead of discarding them. Ultimately, while the benefits of nano-based technology are considerable, addressing the associated risks through thorough research and innovation is essential to safely harness its full potential.

Although substantial progress has been made in understanding the thermophysical properties and operational efficiencies of nanofluids, challenges remain in achieving long-term stability, minimizing environmental impact, and improving cost-effectiveness. Continuous research is essential to address these issues, refine nanoparticle formulations, and establish sustainable recycling practices. Harnessing the benefits of these innovative materials can drive the expansion of more efficient and environmentally friendly energy solutions, fostering a sustainable energy future.

**Author Contributions:** Investigation, writing—original draft preparation, M.S.P.; conceptualization, writing—review and editing, validation, M.C.; conceptualization, writing—review and editing, supervision, L.M.; conceptualization, writing—review and editing, funding acquisition, M.P. All authors have read and agreed to the published version of the manuscript.

**Funding:** We acknowledge financial support under the National Recovery and Resilience Plan (NRRP), Mission 4, Component 2, Investment 1.1, Call for tender No. 1409 published on 14 September 2022 by the Italian Ministry of University and Research (MUR), funded by the European Union—NextGenerationEU—Project Title: Gases with nanoparticles as working fluid for CSP technologies (nanoCSP)—CUP F53D23009830001—Grant Assignment Decree No. 961 adopted on 30 June 2023 by the Italian Ministry of University and Research (MUR).

**Conflicts of Interest:** The authors declare that they have no known competing financial interests or personal relationships that could have appeared to influence the work reported in this paper.

## Nomenclature

Abbreviations

| | |
|---|---|
| AR | Aspect Ratio |
| BS | Benzene Sulfonate |
| CA | Capric Acid |
| CFD | Computational Fluid Dynamics |
| CNF | Cyanuric fluoride |
| CNT | Carbon Nano Tube |
| CHF | Constant heat flux |
| CSP | Concentrated Solar Power |
| CTAB | Cetyl Trimethyl Ammonium Bromide |
| CWT | Constant wall temperature (K) |
| DDC | Distearyl Dimethylammonium Chloride |
| DW | Distilled Water |
| EG | Ethylene Glycol |
| EG-CNF | Expanded Graphite-Carbon Nano-fiber |
| EG-MWCNT | Expanded Graphite-Multi-walled Carbon Nano-tubes |
| GNP | Graphene Nanoplates |
| GO | Graphene Oxide |
| HTF | Heat Transfer Fluid |
| LA | Lauric acid |
| LHS | Latent Heat Storage |
| MWCNT | Multi-Walled Carbon Nanotube |
| MS | Magnetic Stirring |
| NEPCM | Nano-Enhanced Phase Change Materials |
| NF | Nanofluid |
| NG | Nano graphene |
| PCM | Phase Change Material |

| | |
|---|---|
| PCT | Phase Change Temperature |
| PD | Particle Diameter (μm) |
| PV | Photovoltaic |
| PVP | Polyvinylpyrrolidone |
| PW | Paraffin Wax |
| RES | Renewable Energy Sources |
| SDS | Sodium Dodecyl Sulphate |
| SDBS | Sodium Dodecyl Benzene Sulfonate |
| SHS | Sensible Heat Storage |
| SWCNT | Single-Walled Carbon Nanotube |
| TES | Thermal Energy Storage |
| TCHS | Thermo-Chemical Heat Storage |
| US | Ultrasonication |
| USB | Ultrasonic Bath |
| Dimensionless Numbers | |
| *Gr* | Grashoff number |
| *Nu* | Nusselt number |
| *Pr* | Prandtl number |
| *Ra* | Rayleigh number |
| *Re* | Reynolds number |
| Symbols | |
| D | Diameter (m) |
| L | Length (m) |
| $\zeta$ | Zeta potential (volts) |
| $\beta$ | Coefficient of thermal expansion (1/°C or 1/K) |
| $\varepsilon$ | Eccentricity (no units) |
| $\phi$ | Volume concentration (%) |
| $\psi$ | Mass fraction (%) |
| $\mu$ | Viscosity ($N \cdot s/m^2$) |
| $\rho_P$ | Object density ($kg/m^3$) |
| $\rho_L$ | Liquid density ($kg/m^3$) |
| $g$ | Acceleration due to gravity ($m/s^2$) |
| $R$ | Spherical object radius (m) |
| $h$ | Convective heat transfer coefficient ($W/m^2 \cdot K$) |
| $k$ | Thermal conductivity ($W/m \cdot K$) |
| $\Delta H$ | Change in enthalpy (J) |
| $T$ | Temperature (K) |
| $R$ | Radius (m) |
| $m$ | Mass (kg) |
| $C_p$ | Specific capacity (J/kg.K) |
| Subscripts | |
| *bf* | Base fluid |
| *hw* | Hot wall |
| *nf* | Nanofluid |
| *p* | Particle |
| *np* | Nanoparticle |
| *f* | Fluid |
| *min* | Minimum |
| *max* | Maximum |
| *s* | Channel/tube surface |
| *con* | Convection |
| $N_t$ | Thermophoresis parameter |
| $N_b$ | Brownian diffusion parameter |

## References


1. Petrollese, M.; Cascetta, M.; Tola, V.; Cocco, D.; Cau, G. Pumped thermal energy storage systems integrated with a concentrating solar power section: Conceptual design and performance evaluation. *Energy* **2022**, *247*, 123516. [CrossRef]
2. Energy Institute—2024 Statistical Review of World Energy. June 2024. 73rd Edition. Available online: https://www.energyinst.org/statistical-review (accessed on 3 January 2025).
3. Cascetta, M.; Petrollese, M.; Oyekale, J.; Cau, G. Thermocline vs. two-tank direct thermal storage system for concentrating solar power plants: A comparative techno-economic assessment. *Int. J. Energy Res.* **2021**, *45*, 17721–17737. [CrossRef]
4. Cascetta, M.; Licheri, F.; Merchán, R.P.; Petrollese, M. Operating performance of a Joule-Brayton pumped thermal energy storage system integrated with a concentrated solar power plant. *J. Energy Storage* **2023**, *73*, 108865. [CrossRef]
5. Javadi, F.S.; Metselaar, H.S.C.; Ganesan, P. Performance improvement of solar thermal systems integrated with phase change materials (PCM): A review. *Sol. Energy* **2020**, *206*, 330–352. [CrossRef]
6. Zhang, P.; Li, K.; Liu, Q.; Zou, Q.; Liang, R.; Qin, L.; Wang, Y. Thermal stratification characteristics and cooling water shortage risks for pumped storage reservoir–green data centers under extreme climates. *Renew. Energy* **2024**, *229*, 120697. [CrossRef]
7. Vahidhosseini, S.M.; Rashidi, S.; Hsu, S.-H.; Yan, W.-M.; Rashidi, A. Integration of solar thermal collectors and heat pumps with thermal energy storage systems for building energy demand reduction: A comprehensive review. *J. Energy Storage* **2024**, *95*, 112568. [CrossRef]
8. Alva, G.; Liu, L.; Huang, X.; Fang, G. Thermal energy storage materials and systems for solar energy applications. *Renew. Sustain. Energy Rev.* **2017**, *68*, 693–706. [CrossRef]
9. Abolghasemi, M.; Keshavarz, A.; Mehrabian, M.A. Thermodynamic analysis of a thermal storage unit under the influence of nanoparticles added to the phase change material and/or the working fluid. *Heat Mass Transf.* **2012**, *48*, 1961–1970. [CrossRef]
10. Abdulateef, A.M.; Mat, S.; Abdulateef, J.; Sopian, K.; Al-Abidi, A.A. Thermal performance enhancement of triplex tube latent thermal storage using fins-nano-phase change material technique. *Heat Transf. Eng.* **2017**, *39*, 1067–1080. [CrossRef]
11. Akeiber, H.; Nejat, P.; Majid MZ, A.; Wahid, M.A.; Jomehzadeh, F.; Famileh, I.Z.; Zaki, S.A. A review on phase change material (PCM) for sustainable passive cooling in building envelopes. *Renew. Sustain. Energy Rev.* **2016**, *60*, 1470–1497. [CrossRef]
12. Peng, G.; Dou, G.; Hu, Y.; Sun, Y.; Chen, Z. Phase change material (PCM) microcapsules for thermal energy storage. *Adv. Polym. Technol.* **2020**, *2020*, 9490873. [CrossRef]
13. Sarbu, I.; Sebarchievici, C. A comprehensive review of thermal energy storage. *Sustainability* **2018**, *10*, 191. [CrossRef]
14. Al-Jethelah, M.; Tasnim, S.H.; Mahmud, S.; Dutta, A. Nano-PCM filled energy storage system for solar-thermal applications. *Renew. Energy* **2018**, *126*, 137–155. [CrossRef]
15. Al-Waeli, A.H.; Sopian, K.; Kazem, H.A.; Yousif, J.H.; Chaichan, M.T.; Ibrahim, A.; Ruslan, M.H. Comparison of prediction methods of PV/T nanofluid and nano-PCM system using a measured dataset and artificial neural network. *Sol. Energy* **2018**, *162*, 378–396. [CrossRef]
16. Magendran, S.S.; Khan, F.S.A.; Mubarak, N.M.; Vaka, M.; Walvekar, R.; Khalid, M.; Karri, R.R. Synthesis of organic phase change materials (PCM) for energy storage applications: A review. *Nano-Struct. Nano-Objects* **2019**, *20*, 100399. [CrossRef]
17. Das, N.; Takata, Y.; Kohno, M.; Harish, S. Effect of carbon nano inclusion dimensionality on the melting of phase change nanocomposites in vertical shell-tube thermal energy storage unit. *Int. J. Heat Mass Transf.* **2017**, *113*, 423–431. [CrossRef]
18. Nazir, H.; Batool, M.; Osorio FJ, B.; Isaza-Ruiz, M.; Xu, X.; Vignarooban, K.; Kannan, A.M. Recent developments in phase change materials for energy storage applications: A review. *Int. J. Heat Mass Transf.* **2019**, *129*, 491–523. [CrossRef]
19. Zhang, L.; Zhou, K.; Wei, Q.; Ma, L.; Ye, W.; Li, H.; Gan, X. Thermal conductivity enhancement of phase change materials with 3D porous diamond foam for thermal energy storage. *Appl. Energy* **2019**, *233–234*, 208–219. [CrossRef]
20. Shojaeefard, M.H.; Jourabian, M.; Ali Rabienataj Darzi, A.; Bayat, A. Inward melting inside a horizontal multilobed capsule with conductive wall affected by Ag-MgO/water hybrid and MgO/water nanofluids. *J. Heat Mass Transf. Res.* **2021**, *8*, 205–223. [CrossRef]
21. Rahman, M.M.; Khan, I.; Alameh, K. The role of energy storage technologies for sustainability in developing countries. In *Renewable Energy and Sustainability*; Elsevier: Amsterdam, The Netherlands, 2022; pp. 347–376. [CrossRef]
22. Alva, G.; Lin, Y.; Fang, G. An overview of thermal energy storage systems. *Energy* **2018**, *144*, 341–378. [CrossRef]
23. Dahash, A.; Ochs, F.; Janetti, M.B.; Streicher, W. Advances in seasonal thermal energy storage for solar district heating applications: A critical review on large-scale hot-water tank and pit thermal energy storage systems. *Appl. Energy* **2019**, *239*, 296–315. [CrossRef]
24. Mohan, G.; Venkataraman, M.; Gomez-Vidal, J.; Coventry, J. Assessment of a novel ternary eutectic chloride salt for next generation high-temperature sensible heat storage. *Energy Convers. Manag.* **2018**, *167*, 156–164. [CrossRef]
25. Nallusamy, N.; Sampath, S.; Velraj, R. Experimental investigation on a combined sensible and latent heat storage system integrated with constant/varying (solar) heat sources. *Renew. Energy* **2007**, *32*, 1206–1227. [CrossRef]
26. Barbhuiya, S.; Das, B.B.; Idrees, M. Thermal energy storage in concrete: A comprehensive review on fundamentals, technology and sustainability. *J. Build. Eng.* **2024**, *82*, 108302. [CrossRef]

27. El Alami, K.; Asbik, M.; Agalit, H. Identification of natural rocks as storage materials in thermal energy storage (TES) system of concentrated solar power (CSP) plants—A review. *Sol. Energy Mater. Sol. Cells* **2020**, *217*, 110599. [CrossRef]
28. Calderón-Vásquez, I.; Segovia, V.; Cardemil, J.M.; Barraza, R. Assessing the use of copper slags as thermal energy storage material for packed-bed systems. *Energy* **2021**, *227*, 120370. [CrossRef]
29. Vijjapu, R.; Tiwari, S. Thermodynamics of sensible thermal energy storage systems. *Encycl. Energy Storage* **2022**, *1*, 171–185. [CrossRef]
30. Rahjoo, M.; Goracci, G.; Gaitero, J.J.; Martauz, P.; Rojas, E.; Dolado, J.S. Thermal energy storage (TES) prototype based on Geopolymer concrete for high-temperature applications. *Materials* **2022**, *15*, 7086. [CrossRef]
31. Hua, W.; Lv, X.; Zhang, X.; Ji, Z.; Zhu, J. Research progress of seasonal thermal energy storage technology based on supercooled phase change materials. *J. Energy Storage* **2023**, *67*, 107378. [CrossRef]
32. Ren, Q.; Xu, H.; Luo, Z. PCM charging process accelerated with combination of optimized triangle fins and nanoparticles. *Int. J. Therm. Sci.* **2019**, *140*, 466–479. [CrossRef]
33. Sharma, A.; Chauhan, R.; Ali Kallioğlu, M.; Chinnasamy, V.; Singh, T. A review of phase change materials (PCMs) for thermal storage in solar air heating systems. *Mater. Today Proc.* **2021**, *44*, 4357–4363. [CrossRef]
34. Malik, F.K.; Khan, M.M.; Ahmed, H.F.; Irfan, M.; Ahad, I.U. Performance characteristics of PCM based thermal energy storage system for fluctuating waste heat sources. *Therm. Eng.* **2022**, *34*, 102012. [CrossRef]
35. Yang, H.; Bai, Y.; Ge, C.; He, L.; Liang, W.; Zhang, X. Polyethylene glycol-based phase change materials with high photothermal conversion efficiency and shape stability in an aqueous environment for solar water heater. *Compos. Part A Appl. Sci. Manuf.* **2022**, *154*, 106778. [CrossRef]
36. Lingayat, A.; Das, P.; Gilago, M.C.; Chandramohan, V.P. A detailed assessment of paraffin waxed thermal energy storage medium for solar dryers. *Sol. Energy* **2023**, *261*, 14–27. [CrossRef]
37. Xie, Z.; Yan, H.; Dai, H.; Kou, Y.; Yan, X.; Tian, Y.; Shi, Q. Heat capacity study of fatty acids as phase change materials for thermal energy storage. *J. Chem. Thermodyn.* **2024**, *197*, 107338. [CrossRef]
38. Anand, A.; Mansor, M.; Sharma, K.; Shukla, A.; Sharma, A.; Siddiqui, M.I.H.; Sadasivuni, K.K.; Priyadarshi, N.; Twala, B. A comprehensive review on eutectic phase change materials: Development, thermophysical properties, thermal stability, reliability, and applications. *Alex. Eng. J.* **2025**, *112*, 254–280. [CrossRef]
39. Lee, S.H.; Luvnish, A.; Su, X.; Meng, Q.; Liu, M.; Kuan, H.C.; Saman, W.; Bostrom, M.; Ma, J. Advancements in polymer (Nano)composites for phase change material-based thermal storage: A focus on thermoplastic matrices and ceramic/carbon fillers. *Smart Mater. Manuf.* **2024**, *2*, 100044. [CrossRef]
40. Sarı, A.; Karaipekli, A. Fatty acid esters-based composite phase change materials for thermal energy storage in buildings. *Appl. Therm. Eng.* **2012**, *37*, 208–216. [CrossRef]
41. Liu, H.; Jing, J.; Liu, J.; Wang, X. Sugar alcohol-based phase change materials for thermal energy storage: Optimization design and applications. *Renew. Sust. Energ. Rev.* **2024**, *199*, 114528. [CrossRef]
42. Ensari, Ö.F.; Alkan, C. 1,12-dodecanediol among similar fatty alcohols as a phase change material for thermal energy storage. *Sol. Energy Adv.* **2025**, *5*, 100079. [CrossRef]
43. Wong-Pinto, L.S.; Milian, Y.; Ushak, S. Progress on use of nanoparticles in salt hydrates as phase change materials. *Renew. Sust. Energy Rev.* **2020**, *122*, 109727. [CrossRef]
44. Shamberger, P.J.; Bruno, N.M. Review of metallic phase change materials for high heat flux transient thermal management applications. *Appl. Energy* **2020**, *258*, 113955. [CrossRef]
45. Mohamed, S.A.; Al-Sulaiman, F.A.; Ibrahim, N.I.; Zahir, M.H.; Al-Ahmed, A.; Saidur, R.; Yılbaş, B.S.; Sahin, A.Z. A review on current status and challenges of inorganic phase change materials for thermal energy storage systems. *Renew. Sust. Energy Rev.* **2017**, *70*, 1072–1089. [CrossRef]
46. Liu, M.; Saman, W.; Bruno, F. Review on storage materials and thermal performance enhancement techniques for high temperature phase change thermal storage systems. *Renew. Sust. Energ. Rev.* **2012**, *16*, 2118–2132. [CrossRef]
47. Liu, H.; Awbi, H.B. Performance of phase change material boards under natural convection. *Build. Environ.* **2009**, *44*, 1788–1793. [CrossRef]
48. Zalba, B.; Marín, J.M.; Cabeza, L.F.; Mehling, H. Review on thermal energy storage with phase change: Materials, heat transfer analysis and applications. *Appl. Therm. Eng.* **2003**, *23*, 251–283. [CrossRef]
49. Aydin, D.; Casey, S.P.; Riffat, S. The latest advancements on thermochemical heat storage systems. *Renew. Sust. Energ. Rev.* **2015**, *41*, 356–367. [CrossRef]
50. Kuznik, F.; Opel, O.; Osterland, T.; Ruck, W.K.L. Thermal energy storage for space heating and domestic hot water in individual residential buildings. In *Advances in Thermal Energy Storage Systems*, 2nd ed.; Woodhead Publishing: Cambridge, UK, 2021; pp. 567–594. [CrossRef]

51. Sarbu, I.; Sebarchievici, C. General review of solar-powered closed sorption refrigeration systems. *Energy Convers. Manag.* **2015**, *105*, 403–422. [CrossRef]
52. Li, G. Sensible heat thermal storage energy and exergy performance evaluations. *Renew. Sustain. Energy Rev.* **2016**, *53*, 897–923. [CrossRef]
53. Malinauskaite, J.; Jouhara, H. A theoretical analysis of waste heat recovery technologies. In *Sustainable Energy Technology, Business Models, and Policies: Theoretical Peripheries and Practical Implications*; Elsevier: Amsterdam, The Netherlands, 2024; pp. 99–144. [CrossRef]
54. Wu, S.; Zhou, C.; Doroodchi, E.; Nellore, R.; Moghtaderi, B. A review on high-temperature thermochemical energy storage based on metal oxides redox cycle. *Energy Convers. Manag.* **2018**, *168*, 421–453. [CrossRef]
55. Long, X.F.; Dai, L.; Lou, B.; Wu, J. The kinetics research of thermochemical energy storage system $Ca(OH)_2/CaO$. *Int. J. Energy Res.* **2017**, *41*, 1004–1013. [CrossRef]
56. Mukherjee, A.; Majumdar, R.; Saha, S.K.; Kumar, L.; Subramaniam, C. Assessment of open thermochemical energy storage system performance for low temperature heating applications. *Appl. Therm. Eng.* **2019**, *156*, 453–470. [CrossRef]
57. Ma, Z.; Lin, W.; Sohel, M.I. Nano-enhanced phase change materials for improved building performance. *Renew. Sustain. Energy Rev.* **2016**, *58*, 1256–1268. [CrossRef]
58. Alshuhail, L.A.; Shaik, F.; Sundar, L.S. Thermal efficiency enhancement of mono and hybrid nanofluids in solar thermal applications—A review. *Alex. Eng. J.* **2023**, *68*, 365–404. [CrossRef]
59. Satti, J.R.; Das, D.K.; Ray, D. Investigation of the thermal conductivity of propylene glycol nanofluids and comparison with correlations. *Int. J. Heat Mass Transf.* **2017**, *107*, 871–881. [CrossRef]
60. He, Q.; Wang, S.; Tong, M.; Liu, Y. Experimental study on thermophysical properties of nanofluids as phase-change material (PCM) in low temperature cool storage. *Energy Convers. Manag.* **2012**, *64*, 199–205. [CrossRef]
61. Said, Z.; Pandey, A.K.; Tiwari, A.K.; Kalidasan, B.; Jamil, F.; Thakur, A.K.; Tyagi, V.V.; Sarı, A.; Ali, H.M. Nano-enhanced phase change materials: Fundamentals and applications. *Prog. Energy Combust. Sci.* **2024**, *104*, 101162. [CrossRef]
62. Pereira, J.; Souza, R.; Moreira, A.; Moita, A. A review on the nanofluids-PCMs integrated solutions for solar thermal heat transfer enhancement purposes. *Technologies* **2023**, *11*, 166. [CrossRef]
63. Saleh, H.M.; Hassan, A.I. Synthesis and characterization of nanomaterials for application in cost-effective electrochemical devices. *Sustainability* **2023**, *15*, 10891. [CrossRef]
64. Moreira, T.A.; Moreira, D.C.; Ribatski, G. Nanofluids for heat transfer applications: A review. *J. Braz. Soc. Mech. Sci. Eng.* **2018**, *40*, 303. [CrossRef]
65. Liu, F.; Cai, Y.; Wang, L.; Zhao, J. Effects of nanoparticle shapes on laminar forced convective heat transfer in curved ducts using two-phase model. *Int. J. Heat Mass Transf.* **2018**, *116*, 292–305. [CrossRef]
66. Choi, S.U.S.; Eastman, J.A. Enhancing thermal conductivity of fluids with nanoparticles. *ASME FED* **1995**, *231*, 99–105. Available online: https://www.researchgate.net/publication/236353373_Enhancing_thermal_conductivity_of_fluids_with_nanoparticles/references (accessed on 3 January 2025).
67. Özerinç, S.; Kakaç, S.; Yazıcıoğlu, A.G. Enhanced thermal conductivity of nanofluids: A state-of-the-art review. *Microfluid Nanofluid* **2010**, *8*, 145–170. [CrossRef]
68. Papuga, K.; Kaszubkiewicz, J.; Kawałko, D. Do we have to use suspensions with low concentrations in determination of particle size distribution by sedimentation methods? *Powder Technol.* **2021**, *388*, 92–99. [CrossRef]
69. Lo, C.H.; Tsung, T.T.; Chen, L.C.; Su, C.H.; Lin, H.M. Fabrication of copper oxide nanofluid using submerged arc nanoparticle synthesis system (SANSS). *J. Nanopart. Res.* **2005**, *7*, 313–320. [CrossRef]
70. Teng, T.P.; Wang, W.P.; Hsu, Y.C. Fabrication and characterization of nanocarbon-based nanofluids by using an oxygen–acetylene flame synthesis system. *Nanoscale Res. Lett.* **2016**, *11*, 266. [CrossRef]
71. Bhat, D.; Kumar, S.P.; Shenoy, U.S. Enhancing the thermal conductivity and stability of cuprous oxide nanofluids: Ribose-mediated single-step chemical synthesis for solar energy applications. *Nano Trends* **2025**, *9*, 100071. [CrossRef]
72. Botha, S.S.; Ndungu, P.; Bladergroen, B.J. Physicochemical properties of oil-based nanofluids containing hybrid structures of silver nanoparticles supported on silica. *Ind. Eng. Chem. Res.* **2011**, *50*, 3071–3077. [CrossRef]
73. Aberoumand, S.; Jafarimoghaddam, A.; Moravej, M.; Aberoumand, H.; Javaherdeh, K. Experimental study on the rheological behavior of silver-heat transfer oil nanofluid and suggesting two empirical based correlations for thermal conductivity and viscosity of oil based nanofluids. *Appl. Therm. Eng.* **2016**, *101*, 362–372. [CrossRef]
74. Ma, B.; Shin, D.; Banerjee, D. One-step synthesis of molten salt nanofluid for thermal energy storage application: A comprehensive analysis on thermophysical property, corrosion behavior, and economic benefit. *J. Energy Storage* **2021**, *35*, 102278. [CrossRef]
75. Aberoumand, S.; Jafarimoghaddam, A. Experimental study on synthesis, stability, thermal conductivity, and viscosity of Cu–engine oil nanofluid. *J. Taiwan Inst. Chem. Eng.* **2017**, *71*, 315–322. [CrossRef]
76. Zheng, N.; Wang, L.; Wan, M.; Fan, R.; Sun, Z. Experimental investigation on the static and dynamic stability of water-based graphene nanofluids prepared by one-step liquid phase shear exfoliation of graphite. *J. Mol. Liq.* **2023**, *381*, 121848. [CrossRef]

77. Kumar, S.P.; Shenoy, U.S.; Bhat, D.K. A direct approach towards synthesis of copper nanofluid by one-step solution phase method. *J. Cryst. Growth* **2024**, *630*, 127591. [CrossRef]
78. Alrowaili, Z.A.; Ezzeldien, M.; Shaaalan, N.M.; Hussein, E.; Sharafeldin, M.A. Investigation of the effect of hybrid CuO-Cu/water nanofluid on the solar thermal energy storage system. *J. Energy Storage* **2022**, *50*, 104675. [CrossRef]
79. Chen, X.; Xiong, Z.; Chen, M.; Zhou, P. Ultra-stable carbon quantum dot nanofluids for direct absorption solar collectors. *Sol. Energy Mater. Sol. Cells* **2022**, *240*, 111720. [CrossRef]
80. RM Mostafizur, M.G.; Rasul, M.N. Nabi. Effect of surfactant on stability, thermal conductivity, and viscosity of aluminium oxide–methanol nanofluids for heat transfer applications. *Therm. Sci. Eng. Progr.* **2022**, *31*, 101302. [CrossRef]
81. Parsa, S.M.; Yazdani, A.; Aberoumand, H.; Farhadi, Y.; Ansari, A.; Aberoumand, S.; Ali, H.M. A critical analysis on the energy and exergy performance of photovoltaic/thermal (PV/T) system: The role of nanofluids stability and synthesizing method. *Sustain. Energy Technol. Assess.* **2022**, *51*, 101887. [CrossRef]
82. Roy, A.; Venkitaraj, K.P.; Vigneshwaran, P.; Saboor, S.; Cuce, E.; Saxena, K.K. Enhanced convective heat transfer with Al2O3-water nanofluid in a PCM-based thermal energy storage system. *J. Energy Storage* **2024**, *97*, 112853. [CrossRef]
83. Sepehrnia, M.; Farrokh, M.J.; Karimi, M.; Mohammadzadeh, K. Experimental study and development of mathematical model using surface response method to predict the rheological performance of $CeO_2$-CuO/10W40 hybrid nanolubricant. *Arab. J. Chem.* **2023**, *16*, 104721. [CrossRef]
84. Srinivasan, N.K.; Ponnusamy, C. Stability, thermal and solidification behaviour of oxygen functionalized GNPs–CuO/water-based hybrid nanofluid phase change materials for cool thermal energy storage system. *J. Energy Storage* **2024**, *98*, 113107. [CrossRef]
85. Zeng, Z.; Lu, L.; Cao, X.; Xie, T.; Lu, X.; Zhou, L.; Cheng, J.; Ma, L.; Jing, D. Influence of particle morphology on solar thermal conversion performance and sensible heat storage capacity: A case study of TiO2@Go binary nanofluid. *J. Colloid Interface Sci.* **2025**, *682*, 502–518. [CrossRef] [PubMed]
86. Hadadian, M.; Goharshadi, E.K.; Youssefi, A. Electrical conductivity, thermal conductivity, and rheological properties of graphene oxide-based nanofluids. *J. Nanopart. Res.* **2014**, *16*, 2788. [CrossRef]
87. Asadi, A.; Pourfattah, F. Heat transfer performance of two oil-based nanofluids containing ZnO and MgO nanoparticles; a comparative experimental investigation. *Powder Technol.* **2019**, *343*, 296–308. [CrossRef]
88. Giwa, S.O.; Sharifpur, M.; Ahmadi, M.H.; Sohel Murshed, S.M.; Meyer, J.P. Experimental investigation on stability, viscosity, and electrical conductivity of water-based hybrid nanofluid of MWCNT-$Fe_2O_3$. *Nanomaterials* **2021**, *11*, 136. [CrossRef]
89. Yılmaz Aydın, D.; Gürü, M. Nanofluids: Preparation, stability, properties, and thermal performance in terms of thermo-hydraulic, thermodynamics and thermo-economic analysis. *J. Therm. Anal. Calorim.* **2022**, *147*, 7631–7664. [CrossRef]
90. Kumar, P.G.; Sakthivadivel, D.; Thangapandian, N.; Salman, M.; Thakur, A.K.; Sathyamurthy, R.; Kim, S.C. Effects of ultasonication and surfactant on the thermal and electrical conductivity of water–solar glycol mixture based $Al_2O_3$ nanofluids for solar-thermal applications. *Sustain. Energy Technol. Assess.* **2021**, *47*, 101371. [CrossRef]
91. Mehryan, S.A.M.; Ghalambaz, M.; Kalantar Feeoj, R.; Hajjar, A.; Izadi, M. Free convection in a trapezoidal enclosure divided by a flexible partition. *Int. J. Heat Mass Transf.* **2020**, *149*, 119186. [CrossRef]
92. Mansour, M.A.; Siddiqa, S.; Gorla, R.S.R.; Rashad, A.M. Effects of heat source and sink on entropy generation and MHD natural convection of $Al_2O_3$-Cu/water hybrid nanofluid filled with square porous cavity. *Therm. Sci. Eng. Prog.* **2018**, *6*, 57–71. [CrossRef]
93. Takabi, B.; Salehi, S. Augmentation of the heat transfer performance of a sinusoidal corrugated enclosure by employing hybrid nanofluid. *Adv. Mech. Eng.* **2014**, *6*, 147059. [CrossRef]
94. Hemmat Esfe, M.; Abbasian Arani, A.A.; Rezaie, M.; Yan, W.M.; Karimipour, A. Experimental determination of thermal conductivity and dynamic viscosity of Ag–MgO/water hybrid nanofluid. *Int. Commun. Heat Mass Transf.* **2015**, *66*, 189–195. [CrossRef]
95. Wole-Osho, I.; Okonkwo, E.C.; Adun, H.; Kavaz, D.; Abbasoglu, S. An intelligent approach to predicting the effect of nanoparticle mixture ratio, concentration and temperature on thermal conductivity of hybrid nanofluids. *J. Therm. Anal. Calorim.* **2021**, *144*, 671–688. [CrossRef]
96. Amani, M.; Amani, P.; Kasaeian, A.; Mahian, O.; Wongwises, S. Thermal conductivity measurement of spinel-type ferrite $MnFe_2O_4$ nanofluids in the presence of a uniform magnetic field. *J. Mol. Liquids* **2017**, *230*, 121–128. [CrossRef]
97. Esfe, M.H.; Rejvani, M.; Karimpour, R.; Abbasian Arani, A.A. Estimation of thermal conductivity of ethylene glycol-based nanofluid with hybrid suspensions of SWCNT–$Al_2O_3$ nanoparticles by correlation and ANN methods using experimental data. *J. Therm. Anal. Calorim.* **2017**, *128*, 1359–1371. [CrossRef]
98. Pourrajab, R.; Noghrehabadi, A.; Behbahani, M.; Hajidavalloo, E. An efficient enhancement in thermal conductivity of water-based hybrid nanofluid containing MWCNTs-COOH and Ag nanoparticles: Experimental study. *J. Therm. Anal. Calorim.* **2021**, *143*, 3331–3343. [CrossRef]
99. Yu, W.; Choi, S. The role of interfacial layers in the enhanced thermal conductivity of nanofluids: A renovated Maxwell model. *J. Nanopart. Res.* **2003**, *5*, 167–171. [CrossRef]

100. Parsian, A.; Akbari, M. New experimental correlation for the thermal conductivity of ethylene glycol containing $Al_2O_3$–Cu hybrid nanoparticles. *J. Therm. Anal. Calorim.* **2018**, *131*, 1605–1613. [CrossRef]
101. Roy, G.; Nguyen, C.T.; Lajoie, P.-R. Numerical investigation of laminar flow and heat transfer in a radial flow cooling system with the use of nanofluids. *Superlattices Microstruct.* **2004**, *35*, 497–511. [CrossRef]
102. Ho, C.J.; Huang, J.B.; Tsai, P.S.; Yang, Y.M. Preparation and properties of hybrid water-based suspension of $Al_2O_3$ nanoparticles and MEPCM particles as functional forced convection fluid. *Int. Commun. Heat Mass Transf.* **2010**, *37*, 490–494. [CrossRef]
103. Murali Krishna, V.; Sandeep Kumar, M.; Mahesh, O.; Senthil, K.P. Numerical investigation of heat transfer and pressure drop for cooling of microchannel heat sink using MWCNT-CuO-water hybrid nanofluid with different mixture ratio. *Mater. Today Proc.* **2021**, *42*, 969–974. [CrossRef]
104. Alnaqi, A.A. Numerical analysis of pressure drop and heat transfer of non-Newtonian nanofluids in a Li-ion battery thermal management system (BTMS) using bionic geometries. *J. Energy Storage* **2022**, *45*, 103670. [CrossRef]
105. Baghbanzadeh, M.; Rashidi, A.; Soleimanisalim, A.H.; Rashtchian, D. Investigating the rheological properties of nanofluids of water/hybrid nanostructure of spherical silica/MWCNT. *Thermochim. Acta* **2014**, *578*, 53–58. [CrossRef]
106. Bellos, E.; Tzivanidis, C. Thermal analysis of parabolic trough collector operating with mono and hybrid nanofluids. *Sustain. Energy Technol. Assess.* **2018**, *26*, 105–115. [CrossRef]
107. Alklaibi, A.M.; Syam Sundar, L.; Chandra Mouli, K.V.V. Experimental investigation on the performance of hybrid $Fe_3O^4$ coated MWCNT/water nanofluid as a coolant of a plate heat exchanger. *Int. J. Therm. Sci.* **2022**, *171*, 107249. [CrossRef]
108. Okonkwo, E.C.; Wole-Osho, I.; Kavaz, D.; Abid, M. Comparison of experimental and theoretical methods of obtaining the thermal properties of alumina/iron mono and hybrid nanofluids. *J. Mol. Liq.* **2019**, *292*, 111377. [CrossRef]
109. Sundar, L.S.; Mesfin, S.; Ramana, E.V.; Said, Z.; Sousa, A.C.M. Experimental investigation of thermo-physical properties, heat transfer, pumping power, entropy generation, and exergy efficiency of nanodiamond + $Fe_3O_4$/60:40% water-ethylene glycol hybrid nanofluid flow in a tube. *Therm. Sci. Eng. Prog.* **2021**, *21*, 100799. [CrossRef]
110. Zahan, I.; Nasrin, R.; Alim, M.A. Hybrid nanofluid flow in combined convective lid-driven sinusoidal triangular enclosure. *AIP Conf. Proc.* **2019**, *2121*, 070001. [CrossRef]
111. Saleh, B.; Syam Sundar, L. Entropy generation and exergy efficiency analysis of ethylene glycol-water-based nanodiamond + $Fe_3O_4$ hybrid nanofluids in a circular tube. *Powder Technol.* **2021**, *380*, 430–442. [CrossRef]
112. Ghalambaz, M.; Doostani, A.; Izadpanahi, E.; Chamkha, A.J. Conjugate natural convection flow of Ag–MgO/water hybrid nanofluid in a square cavity. *J. Therm. Anal. Calorim.* **2020**, *139*, 2321–2336. [CrossRef]
113. Ghadikolaei, S.S.; Yassari, M.; Sadeghi, H.; Hosseinzadeh, K.H.; Ganji, D.D. Investigation on thermophysical properties of $TiO_2$–Cu/$H_2O$ hybrid nanofluid transport dependent on shape factor in MHD stagnation point flow. *Powder Technol.* **2017**, *322*, 428–438. [CrossRef]
114. Aghili Yegane, S.P.; Kasaeian, A. Thermal performance assessment of a flat-plate solar collector considering porous media, hybrid nanofluid, and magnetic field effects. *J. Therm. Anal. Calorim.* **2020**, *141*, 1969–1980. [CrossRef]
115. Dalkılıç, A.S.; Türk, O.A.; Mercan, H.; Nakkaew, S.; Wongwises, S. An experimental investigation on heat transfer characteristics of graphite-$SiO_2$/water hybrid nanofluid flow in horizontal tube with various quad-channel twisted tape inserts. *Int. Commun. Heat Mass Transf.* **2019**, *107*, 1–13. [CrossRef]
116. Said, Z.; Sundar, L.S.; Tiwari, A.K.; Ali, H.M.; Sheikholeslami, M.; Bellos, E.; Babar, H. Recent advances on the fundamental physical phenomena behind stability, dynamic motion, thermophysical properties, heat transport, applications, and challenges of nanofluids. *Phys. Rep.* **2022**, *946*, 1–94. [CrossRef]
117. Li, H.; Wang, L.; He, Y.; Hu, Y.; Zhu, J.; Jiang, B. Experimental investigation of thermal conductivity and viscosity of ethylene glycol based ZnO nanofluids. *Appl. Therm. Eng.* **2015**, *88*, 363–368. [CrossRef]
118. Loulijat, H.; Moustabchir, H. Numerical study of the effects of Brownian motion and interfacial layer on the viscosity of nanofluid (Au-$H_2O$). *J. Mol. Liq.* **2022**, *350*, 118221. [CrossRef]
119. Zhang, H.; Qing, S.; Zhai, Y.; Zhang, X.; Zhang, A. The changes induced by pH in $TiO_2$/water nanofluids: Stability, thermophysical properties and thermal performance. *Powder Technol.* **2021**, *377*, 748–759. [CrossRef]
120. Hossein Karimi Darvanjooghi, M.; Nasr, E.M. Experimental investigation of the effect of nanoparticle size on thermal conductivity of in-situ prepared silica–ethanol nanofluid. *Int. Commun. Heat Mass Transf.* **2016**, *77*, 148–154. [CrossRef]
121. Afrand, M.; Nazari Najafabadi, K.; Akbari, M. Effects of temperature and solid volume fraction on viscosity of $SiO_2$-MWCNTs/SAE40 hybrid nanofluid as a coolant and lubricant in heat engines. *Appl. Therm. Eng.* **2016**, *102*, 45–54. [CrossRef]
122. Hemmat Esfe, M.; Afrand, M.; Rostamian, S.H.; Toghraie, D. Examination of rheological behavior of MWCNTs/ZnO-SAE40 hybrid nano-lubricants under various temperatures and solid volume fractions. *Exp. Therm. Fluid. Sci.* **2017**, *80*, 384–390. [CrossRef]
123. Sahoo, R.R.; Kumar, V. Development of a new correlation to determine the viscosity of ternary hybrid nanofluid. *Int. Commun. Heat Mass Transf.* **2020**, *111*, 104451. [CrossRef]

124. Dalkılıç, A.S.; Açıkgöz, Ö.; Küçükyıldırım, B.O.; Akdoğan Eker, A.; Lüleci, B.; Jumpholkul, C.; Wongwises, S. Experimental investigation on the viscosity characteristics of water-based $SiO_2$-graphite hybrid nanofluids. *Int. Commun. Heat Mass Transf.* **2018**, *97*, 30–38. [CrossRef]
125. Esfe, M.H.; Afrand, M.; Yan, W.M.; Yarmand, H.; Toghraie, D.; Dahari, M. Effects of temperature and concentration on rheological behavior of MWCNTs/SiO2(20–80)-SAE40 hybrid nano-lubricant. *Int. Commun. Heat Mass Transf.* **2016**, *76*, 133–138. [CrossRef]
126. Nabil, M.F.; Azmi, W.H.; Abdul Hamid, K.; Mamat, R.; Hagos, F.Y. An experimental study on the thermal conductivity and dynamic viscosity of TiO2-SiO2 nanofluids in water: Ethylene glycol mixture. *Int. Commun. Heat Mass Transf.* **2017**, *86*, 181–189. [CrossRef]
127. Zareie, A.; Akbari, M. Hybrid nanoparticles effects on rheological behavior of water-EG coolant under different temperatures: An experimental study. *J. Mol. Liquids* **2017**, *230*, 408–414. [CrossRef]
128. Asadi, M.; Asadi, A. Dynamic viscosity of MWCNT/ZnO–engine oil hybrid nanofluid: An experimental investigation and new correlation in different temperatures and solid concentrations. *Int. Commun. Heat Mass Transf.* **2016**, *76*, 41–45. [CrossRef]
129. Alade, I.O.; Abd Rahman, M.A.; Saleh, T.A. Modeling and prediction of the specific heat capacity of $Al_2O_3$/water nanofluids using hybrid genetic algorithm/support vector regression model. *Nano-Struct. Nano-Objects* **2019**, *17*, 103–111. [CrossRef]
130. Li, X.; Chen, W.; Zou, C. An experimental study on β-cyclodextrin modified carbon nanotubes nanofluids for the direct absorption solar collector (DASC): Specific heat capacity and photo-thermal conversion performance. *Sol. Energy Mater. Sol. Cells* **2020**, *204*, 110240. [CrossRef]
131. Rizvi, S.M.M.; Shin, D. Specific heat capacity, viscosity, and thermal stability of carbonate-based molten salt nanofluids. *J. Energy Storage* **2021**, *43*, 103192. [CrossRef]
132. Yarmand, H.; Gharehkhani, S.; Shirazi SF, S.; Amiri, A.; Montazer, E.; Arzani, H.K.; Kazi, S.N. Nanofluid based on activated hybrid of biomass carbon/graphene oxide: Synthesis, thermo-physical and electrical properties. *Int. Commun. Heat Mass Transf.* **2016**, *72*, 10–15. [CrossRef]
133. Khanafer, K.; Vafai, K. A critical synthesis of thermophysical characteristics of nanofluids. *Int. J. Heat Mass Transfer.* **2011**, *54*, 4410–4428. [CrossRef]
134. Barbés, B.; Páramo, R.; Blanco, E.; Pastoriza-Gallego, M.J.; Pineiro, M.M.; Legido, J.L.; Casanova, C. Thermal conductivity and specific heat capacity measurements of $Al_2O_3$ nanofluids. *J. Therm. Anal. Calorim.* **2013**, *111*, 1615–1625. [CrossRef]
135. Pak, B.C.; Cho, Y.I. Hydrodynamic and heat transfer study of dispersed fluids with submicron metallic oxide particles. *Exp. Heat Transf.* **1998**, *11*, 151–170. [CrossRef]
136. Sekhar, Y.R.; Sharma, K.V. Study of viscosity and specific heat capacity characteristics of water-based $Al_2O_3$ nanofluids at low particle concentrations. *J. Exp. Nanosci.* **2013**, *10*, 86–102. [CrossRef]
137. Xuan, Y.; Roetzel, W. Conceptions for heat transfer correlation of nanofluids. *Int. J. Heat Mass Transfer.* **2000**, *43*, 3701–3707. [CrossRef]
138. Cabaleiro, D.; Gracia-Fernández, C.; Legido, J.L.; Lugo, L. Specific heat of metal oxide nanofluids at high concentrations for heat transfer. *Int. J. Heat Mass Transfer.* **2015**, *88*, 872–879. [CrossRef]
139. Chakraborty, S.; Panigrahi, P.K. Stability of nanofluid: A review. *Appl. Therm. Eng.* **2020**, *174*, 115259. [CrossRef]
140. Jiang, W.; Song, J.; Jia, T.; Yang, L.; Li, S.; Li, Y.; Du, K. A comprehensive review on the pre-research of nanofluids in absorption refrigeration systems. *Energy Rep.* **2022**, *8*, 3437–3464. [CrossRef]
141. Farzaneh, H.; Behzadmehr, A.; Yaghoubi, M.; Samimi, A.; Sarvari, S.M.H. Stability of nanofluids: Molecular dynamic approach and experimental study. *Energy Convers. Manag.* **2016**, *111*, 1–14. [CrossRef]
142. Lei, J.; Luo, Z.; Qing, S.; Huang, X.; Li, F. Effect of surfactants on the stability, rheological properties, and thermal conductivity of $Fe_3O_4$ nanofluids. *Powder Technol.* **2022**, *399*, 117197. [CrossRef]
143. Zare, P.; Keshavarz, P.; Mowla, D. Membrane absorption coupling process for $CO_2$ capture: Application of water-based ZnO, $TiO_2$, and multi-walled carbon nanotube nanofluids. *Energy Fuels* **2019**, *33*, 1392–1403. [CrossRef]
144. Sarsam, W.S.; Amiri, A.; Kazi, S.N.; Badarudin, A. Stability and thermophysical properties of non-covalently functionalized graphene nanoplatelets nanofluids. *Energy Convers. Manag.* **2016**, *116*, 101–111. [CrossRef]
145. Ghadimi, A.; Metselaar, I.H. The influence of surfactant and ultrasonic processing on improvement of stability, thermal conductivity and viscosity of titania nanofluid. *Exp. Therm. Fluid. Sci.* **2013**, *51*, 1–9. [CrossRef]
146. Akash, A.R.; Abraham, S.; Pattamatta, A.; Das, S.K. Experimental assessment of the thermo-hydraulic performance of automobile radiator with metallic and nonmetallic nanofluids. *Heat Trans. Eng.* **2020**, *41*, 235–251. [CrossRef]
147. Elminshawy, A.; Morad, K.; Elminshawy, N.A.S.; Elhenawy, Y. Performance enhancement of concentrator photovoltaic systems using nanofluids. *Int. J. Energy Res.* **2021**, *45*, 2959–2979. [CrossRef]
148. Almanassra, I.W.; Manasrah, A.D.; Al-Mubaiyedh, U.A.; Al-Ansari, T.; Malaibari, Z.O.; Atieh, M.A. An experimental study on stability and thermal conductivity of water/CNTs nanofluids using different surfactants: A comparison study. *J. Mol. Liq.* **2020**, *304*, 111025. [CrossRef]

149. Islam, M.F.; Rojas, E.; Bergey, D.M.; Johnson, A.T.; Yodh, A.G. High weight fraction surfactant solubilization of single-wall carbon nanotubes in water. *Nano Lett.* **2003**, *3*, 269–273. [CrossRef]
150. Sarafraz, M.M.; Safaei, M.R.; Tian, Z.; Goodarzi, M.; Bandarra Filho, E.P.; Arjomandi, M. Thermal assessment of nano-particulate graphene-water/ethylene glycol (WEG 60:40) nano-suspension in a compact heat exchanger. *Energies* **2019**, *12*, 1929. [CrossRef]
151. Abdelrazik, A.S.; Tan, K.H.; Aslfattahi, N.; Saidur, R.; Al-Sulaiman, F.A. Optical properties and stability of water-based nanofluids mixed with reduced graphene oxide decorated with silver and energy performance investigation in hybrid photovoltaic/thermal solar systems. *Int. J. Energy Res.* **2020**, *44*, 11487–11508. [CrossRef]
152. Tiwari, A.K.; Pandya, N.S.; Said, Z.; Öztop, H.F.; Abu-Hamdeh, N. 4S consideration (synthesis, sonication, surfactant, stability) for the thermal conductivity of $CeO_2$ with MWCNT and water based hybrid nanofluid: An experimental assessment. *Colloids Surf. Physicochem. Eng. Asp.* **2021**, *610*, 125918. [CrossRef]
153. Khoshvaght-Aliabadi, M.; Nouri, M.; Sartipzadeh, O.; Salami, M. Performance of agitated serpentine heat exchanger using metallic nanofluids. *Chem. Eng. Res. Des.* **2016**, *109*, 53–64. [CrossRef]
154. Chakraborty, S.; Sarkar, I.; Ashok, A.; Sengupta, I.; Pal, S.K.; Chakraborty, S. Thermophysical properties of Cu-Zn-Al LDH nanofluid and its application in spray cooling. *Appl. Therm. Eng.* **2018**, *141*, 339–351. [CrossRef]
155. Everts, M.; Meyer, J.P. Laminar hydrodynamic and thermal entrance lengths for simultaneously hydrodynamically and thermally developing forced and mixed convective flows in horizontal tubes. *Exp. Therm. Fluid. Sci.* **2020**, *118*, 110153. [CrossRef]
156. Guzman-Urbina, A.; Fukushima, K.; Ohno, H.; Fukushima, Y. Deriving local Nusselt number correlations for heat transfer of nanofluids by genetic programming. *Int. J. Therm. Sci.* **2023**, *192*, 108382. [CrossRef]
157. Khanafer, K.; Vafai, K.; Lightstone, M. Buoyancy-driven heat transfer enhancement in a two-dimensional enclosure utilizing nanofluids. *Int. J. Heat Mass Transf.* **2003**, *46*, 3639–3653. [CrossRef]
158. Mahdy, A.; El-Zahar, E.R.; Rashad, A.M.; Saad, W.; Al-Juaydi, H.S. The magneto-natural convection flow of a micropolar hybrid nanofluid over a vertical plate saturated in a porous medium. *Fluids* **2021**, *6*, 202. [CrossRef]
159. Acharya, N. On the hydrothermal behavior and entropy analysis of buoyancy-driven magnetohydrodynamic hybrid nanofluid flow within an octagonal enclosure fitted with fins: Application to thermal energy storage. *J. Energy Storage* **2022**, *53*, 105198. [CrossRef]
160. Mokaddes, A.; Akhter, R.; Alim, M.A. Hydromagnetic natural convection in a wavy-walled enclosure equipped with hybrid nanofluid and heat generating cylinder. *Alex. Eng. J.* **2021**, *60*, 5245–5264. [CrossRef]
161. Nayak, M.K.; Karimi, N.; Chamkha, A.J.; Dogonchi, A.S.; El-Sapa, S.; Galal, A.M. Efficacy of diverse structures of wavy baffles on heat transfer amplification of double-diffusive natural convection inside a C-shaped enclosure filled with hybrid nanofluid. *Sustain. Energy Technol. Assess.* **2022**, *52*, 102180. [CrossRef]
162. Sheikholeslami, M.; Ziabakhsh, Z.; Ganji, D.D. Transport of Magnetohydrodynamic nanofluid in a porous media. *Colloids Surf. A Physicochem. Eng. Asp.* **2017**, *520*, 201–212. [CrossRef]
163. Rahimpour, N.; Keshavarz Moraveji, M. Free convection of water–$Fe_3O_4$ nanofluid in an inclined cavity subjected to a magnetic field: CFD modeling, sensitivity analysis. *Adv. Powder Technol.* **2017**, *28*, 1573–1584. [CrossRef]
164. Ho, C.J.; Liu, W.K.; Chang, Y.S.; Lin, C.C. Natural convection heat transfer of alumina-water nanofluid in vertical square enclosures: An experimental study. *Int. J. Therm. Sci.* **2010**, *49*, 1345–1353. [CrossRef]
165. Khosravi, R.; Rabiei, S.; Khaki, M.; Safaei, M.R.; Goodarzi, M. Entropy generation of graphene–platinum hybrid nanofluid flow through a wavy cylindrical microchannel solar receiver by using neural networks. *J. Therm. Anal. Calorim.* **2021**, *145*, 1949–1967. [CrossRef]
166. Abdelrazek, A.H.; Alawi, O.A.; Kazi, S.N.; Yusoff, N. Thermal performance evaluation for alumina coated MWCNTs composite nanofluid in annular passage of various eccentricities. *Powder Technol.* **2021**, *391*, 114–132. [CrossRef]
167. Xuan, Y.; Li, Q. Investigation on convective heat transfer and flow features of nanofluids. *J. Heat Transf.* **2003**, *125*, 151–155. [CrossRef]
168. Anoop, K.B.; Sundararajan, T.; Das, S.K. Effect of particle size on the convective heat transfer in nanofluid in the developing region. *Int. J. Heat Mass Transf.* **2009**, *52*, 2189–2195. [CrossRef]
169. Hejazian, M.; Moraveji, M.K. A comparative analysis of single and two-phase models of turbulent convective heat transfer in a tube for TiO2 nanofluid with CFD. *Numer. Heat Transf. Part A Appl.* **2013**, *63*, 795–806. [CrossRef]
170. Yang, Y.; Zhang, Z.G.; Grulke, E.A.; Anderson, W.B.; Wu, G. Heat transfer properties of nanoparticle-in-fluid dispersions (nanofluids) in laminar flow. *Int. J. Heat Mass Transf.* **2005**, *48*, 1107–1116. [CrossRef]
171. Vajjha, R.S.; Das, D.K.; Kulkarni, D.P. Development of new correlations for convective heat transfer and friction factor in turbulent regime for nanofluids. *Int. J. Heat Mass Transf.* **2010**, *53*, 4607–4618. [CrossRef]
172. Ravi Kumar, N.T.; Bhramara, P.; Addis, B.M.; Syam Sundar, L.; Singh, M.K.; Sousa, A.C.M. Heat transfer, friction factor and effectiveness analysis of Fe3O4/water nanofluid flow in a double pipe heat exchanger with return bend. *Int. Commun. Heat Mass Transf.* **2017**, *81*, 155–163. [CrossRef]

173. Asirvatham, L.G.; Raja, B.; Lal, D.M.; Wongwises, S. Convective heat transfer of nanofluids with correlations. *Particuology* **2011**, *9*, 626–631. [CrossRef]
174. Huang, D.; Wu, Z.; Sunden, B. Effects of hybrid nanofluid mixture in plate heat exchangers. *Exp. Therm. Fluid. Sci.* **2016**, *72*, 190–196. [CrossRef]
175. Agarwal, D.K.; Vaidyanathan, A.; Kumar, S.S. Experimental investigation on thermal performance of kerosene–graphene nanofluid. *Exp. Therm. Fluid. Sci.* **2016**, *71*, 126–137. [CrossRef]
176. Hussain, S.; Ahmed, S.E.; Akbar, T. Entropy generation analysis in MHD mixed convection of hybrid nanofluid in an open cavity with a horizontal channel containing an adiabatic obstacle. *Int. J. Heat Mass Transf.* **2017**, *114*, 1054–1066. [CrossRef]
177. Khan, U.; Zaib, A.; Ishak, A. Non-similarity solutions of radiative stagnation point flow of a hybrid nanofluid through a yawed cylinder with mixed convection. *Alex. Eng. J.* **2021**, *60*, 5297–5309. [CrossRef]
178. Jamaludin, A.; Nazar, R.; Naganthran, K.; Pop, I. Mixed convection hybrid nanofluid flow over an exponentially accelerating surface in a porous media. *Neural Comput. Appl.* **2021**, *33*, 15719–15729. [CrossRef]
179. Hussain, S.; Jamal, M.; Maatki, C.; Ghachem, K.; Kolsi, L. MHD mixed convection of $Al_2O_3$ –Cu–water hybrid nanofluid in a wavy channel with incorporated fixed cylinder. *J. Therm. Anal. Calorim.* **2021**, *144*, 2219–2233. [CrossRef]
180. Xia, W.F.; Ahmad, S.; Khan, M.N.; Ahmad, H.; Rehman, A.; Baili, J.; Gia, T.N. Heat and mass transfer analysis of nonlinear mixed convective hybrid nanofluid flow with multiple slip boundary conditions. *Case Stud. Therm. Eng.* **2022**, *32*, 101893. [CrossRef]
181. Ahmad, A.; Asghar, S.; Afzal, S. Flow of nanofluid past a Riga plate. *J. Magn. Magn. Mater.* **2016**, *402*, 44–48. [CrossRef]
182. Ben Mansour, R.; Galanis, N.; Nguyen, C.T. Experimental study of mixed convection with water–$Al_2O_3$ nanofluid in inclined tube with uniform wall heat flux. *Int. J. Therm. Sci.* **2011**, *50*, 403–410. [CrossRef]
183. Yu, W.; France, D.M.; Timofeeva, E.V.; Singh, D.; Routbort, J.L. Comparative review of turbulent heat transfer of nanofluids. *Int. J. Heat Mass Transf.* **2012**, *55*, 5380–5396. [CrossRef]
184. Fotukian, S.M.; Nasr Esfahany, M. Experimental investigation of turbulent convective heat transfer of dilute $\gamma$-$Al_2O_3$/water nanofluid inside a circular tube. *Int. J. Heat Fluid Flow* **2010**, *31*, 606–612. [CrossRef]
185. Fotukian, S.M.; Nasr Esfahany, M. Experimental study of turbulent convective heat transfer and pressure drop of dilute CuO/water nanofluid inside a circular tube. *Int. Commun. Heat Mass Transf.* **2010**, *37*, 214–219. [CrossRef]
186. Demir, H.; Dalkilic, A.S.; Kürekci, N.A.; Duangthongsuk, W.; Wongwises, S. Numerical investigation on the single-phase forced convection heat transfer characteristics of $TiO_2$ nanofluids in a double-tube counter flow heat exchanger. *Int. Commun. Heat Mass Transf.* **2011**, *38*, 218–228. [CrossRef]
187. Ajeel, R.K.; Salim, W.S.-I.; Sopian, K.; Yusoff, M.Z.; Hasnan, K.; Ibrahim, A.; Al-Waeli, A.H.A. Turbulent convective heat transfer of silica oxide nanofluid through corrugated channels: An experimental and numerical study. *Int. J. Heat Mass Transf.* **2019**, *145*, 118806. [CrossRef]
188. Albadr, J.; Tayal, S.; Alasadi, M. Heat transfer through heat exchanger using $Al_2O_3$ nanofluid at different concentrations. *Case Stud. Therm. Eng.* **2013**, *1*, 38–44. [CrossRef]
189. Montazer, E.; Shafii, M.B.; Salami, E.; Muhamad, M.R.; Yarmand, H.; Gharehkhani, S.; Chowdhury, Z.Z.; Kazi, S.N.; Badarudin, A. Heat transfer in turbulent nanofluids: Separation flow studies and development of novel correlations. *Adv. Powder Technol.* **2020**, *31*, 3120–3133. [CrossRef]
190. Fu, R.; Liu, Z.; Chen, Y.; Yan, Y. Experimental investigation of turbulent forced heat transfer of $Fe_3O_4$ ethylene glycol–water nanofluid with highly disaggregated particles. *Therm. Sci. Eng. Prog.* **2019**, *10*, 1–9. [CrossRef]
191. Sundar, L.S.; Singh, M.K.; Sousa, A.C.M. Enhanced heat transfer and friction factor of MWCNT–$Fe_3O_4$/water hybrid nanofluids. *Int. Commun. Heat Mass Transf.* **2014**, *52*, 73–83. [CrossRef]
192. Adogbeji, V.O.; Sharifpur, M.; Meyer, J.P. Experimental investigation into heat transfer and flow characteristics of magnetic hybrid nanofluid ($Fe_3O_4$/$TiO_2$) in turbulent region. *Appl. Therm. Eng.* **2025**, *258*, 124630. [CrossRef]
193. Andreozzi, A.; Manca, O.; Nardini, S.; Ricci, D. Forced convection enhancement in channels with transversal ribs and nanofluids. *Appl. Therm. Eng.* **2016**, *98*, 1044–1053. [CrossRef]
194. Yu, Y.; Li, D.; Meng, H.; Zhang, J.; Xiang, K.; Li, W. Enhancement study of turbulent heat transfer performance of nanofluids in the clover static mixer. *Int. J. Therm. Sci.* **2024**, *198*, 108900. [CrossRef]
195. Sonawane, S. Investigation of turbulent heat transfer performance of aviation turbine fuel multi-wall carbon nanotube nanofluid. *Adv. Powder Technol.* **2023**, *34*, 104079. [CrossRef]
196. Shuvo, M.S.; Ruvo, T.H.; Saha, S. Characteristics of turbulent forced convective nanofluid flow and heat transfer in a 2D axisymmetric corrugated pipe. *Therm. Sci. Eng. Prog.* **2023**, *41*, 101838. [CrossRef]
197. Fujimoto, K.; Shibata, A.; Torii, S. An experimental and numerical study of turbulent heat transfer enhancement for graphene nanofluids produced by pulsed discharge. *Int. J. Thermofluids* **2022**, *16*, 100219. [CrossRef]
198. Zhang, S.; Lu, L.; Wen, T.; Dong, C. Turbulent heat transfer and flow analysis of hybrid $Al_2O_3$-CuO/water nanofluid: An experiment and CFD simulation study. *Appl. Therm. Eng.* **2021**, *188*, 116589. [CrossRef]

199. Karami, F.; Abbasian Arani, A.A.; Akbari, O.A.; Pourfattah, F.; Toghraie, D. Numerical study of location and depth of rectangular grooves on the turbulent heat transfer performance and characteristics of CuO-water nanofluid flow. *Heliyon* **2023**, *9*, e14239. [CrossRef]
200. Ahmad, F.; Waqas, H.; Ayed, H.; Hussain, S.; Farooq, S.; Khan, S.A.; Almatroud, A.O. Numerical treatment with Lobatto-IIIa scheme magneto-thermo-natural convection flow of casson nanofluid ($MoS_2$-Cu/SA) configured by a stretching cylinder in porous medium with multiple slips. *Case Stud. Therm. Eng.* **2021**, *26*, 101132. [CrossRef]
201. Rashad, A.M.; Chamkha, A.J.; Ismael, M.A.; Salah, T. Magnetohydrodynamics natural convection in a triangular cavity filled with a Cu-$Al_2O_3$/water hybrid nanofluid with localized heating from below and internal heat generation. *J. Heat Transf.* **2018**, *140*, 093701. [CrossRef]
202. Yarmand, H.; Gharehkhani, S.; Ahmadi, G.; Shirazi, S.F.; Baradaran, S.; Montazer, E.; Zubir, M.N.M.; Alehashem, M.S.; Kazi, S.N.; Dahari, M. Graphene nanoplatelets-silver hybrid nanofluids for enhanced heat transfer. *Energy Convers. Manag.* **2015**, *100*, 419–428. [CrossRef]
203. Dinarvand, S.; Rostami, M.N.; Pop, I. A novel hybridity model for $TiO_2$-CuO/water hybrid nanofluid flow over a static/moving wedge or corner. *Sci. Rep.* **2019**, *9*, 16290. [CrossRef]
204. Madhesh, D.; Parameshwaran, R.; Kalaiselvam, S. Experimental investigation on convective heat transfer and rheological characteristics of Cu-$TiO_2$ hybrid nanofluids. *Exp. Therm. Fluid. Sci.* **2014**, *52*, 104–115. [CrossRef]
205. Moghadassi, A.; Ghomi, E.; Parvizian, F. A numerical study of water-based $Al_2O_3$ and $Al_2O_3$-Cu hybrid nanofluid effect on forced convective heat transfer. *Int. J. Therm. Sci.* **2015**, *92*, 50–57. [CrossRef]
206. Ferrouillat, S.; Bontemps, A.; Poncelet, O.; Soriano, O.; Gruss, J.-A. Influence of nanoparticle shape factor on convective heat transfer and energetic performance of water-based $SiO_2$ and ZnO nanofluids. *Appl. Therm. Eng.* **2013**, *51*, 839–851. [CrossRef]
207. Li, S.; Yang, Q.; Ye, L.; Du, H.; Zhang, Z.; Huang, X.; Xu, J. Effect of nanoparticle concentration on physical and heat-transfer properties and evaporation characteristics of graphite/n-decane nanofluid fuels. *ACS Omega* **2022**, *7*, 3284–3292. [CrossRef] [PubMed]
208. Sujith, S.V.; Kim, H.; Lee, J. A Review on Thermophysical Property Assessment of Metal Oxide-Based Nanofluids: Industrial Perspectives. *Metals* **2022**, *12*, 165. [CrossRef]
209. Ali, N.; Teixeira, J.A.; Addali, A. A review on nanofluids: Fabrication, stability, and thermophysical properties. *J. Nanomater.* **2018**, *2018*, 6978130. [CrossRef]
210. Szczyglewska, P.; Feliczak-Guzik, A.; Nowak, I. Nanotechnology–General Aspects: A Chemical Reduction Approach to the Synthesis of Nanoparticles. *Molecules* **2023**, *28*, 4932. [CrossRef]
211. Moradi, A.; Zareh, M.; Afrand, M.; Khayat, M. Effects of temperature and volume concentration on thermal conductivity of MWCNTs (70-30)/EG-water hybrid nano-fluid. *Powder Technol.* **2020**, *362*, 578–585. [CrossRef]
212. Tahmooressi, H.; Kasaeian, A.; Tarokh, A.; Rezaei, R.; Hoorfar, M. Numerical simulation of aggregation effect on nanofluids thermal conductivity using the lattice Boltzmann method. *Int. Commun. Heat Mass Transf.* **2020**, *110*, 104408. [CrossRef]
213. Li, Q.; Wang, J.; Wang, J.; Baleta, J.; Min, C.; Sundén, B. Effects of gravity and variable thermal properties on nanofluid convective heat transfer using connected and unconnected walls. *Energy Convers. Manag.* **2018**, *171*, 1440–1448. [CrossRef]
214. Cieśliński, J.T.; Smolen, S.; Sawicka, D. Effect of Temperature and Nanoparticle Concentration on Free Convective Heat Transfer of Nanofluids. *Energies* **2021**, *14*, 3566. [CrossRef]
215. Ben Bacha, H.; Ullah, N.; Hamid, A.; Shah, N.A. A comprehensive review on nanofluids: Synthesis, cutting-edge applications, and future prospects. *Int. J. Thermofluids* **2024**, *22*, 100595. [CrossRef]
216. Bellos, E.; Said, Z.; Tzivanidis, C. Nanofluids in Linear Fresnel Reflector. In *Nanotechnology Applications for Solar Energy Systems*, 1st ed.; Wiley: Hoboken, NJ, USA, 2023; pp. 99–124. [CrossRef]
217. Yang, Z.L.; Walvekar, R.; Wong, W.P.; Sharma, R.K.; Dharaskar, S.; Khalid, M. Advances in phase change materials, heat transfer enhancement techniques, and their applications in thermal energy storage: A comprehensive review. *J. Energy Storage* **2024**, *87*, 111329. [CrossRef]
218. Harikrishnan, S.; Imran Hussain, S.; Devaraju, A.; Sivasamy, P.; Kalaiselvam, S. Improved performance of a newly prepared nano-enhanced phase change material for solar energy storage. *J. Mech. Sci. Technol.* **2017**, *31*, 4903–4910. [CrossRef]
219. Qu, Y.; Wang, S.; Zhou, D.; Tian, Y. Experimental study on thermal conductivity of paraffin-based shape-stabilized phase change material with hybrid carbon nano-additives. *Renew. Energy* **2020**, *146*, 2637–2645. [CrossRef]
220. Colla, L.; Fedele, L.; Mancin, S.; Danza, L.; Manca, O. Nano-PCMs for enhanced energy storage and passive cooling applications. *Appl. Therm. Eng.* **2017**, *110*, 584–589. [CrossRef]
221. Lin, S.C.; Al-Kayiem, H.H. Evaluation of copper nanoparticles–paraffin wax compositions for solar thermal energy storage. *Sol. Energy* **2016**, *132*, 267–278. [CrossRef]
222. Singh, R.P.; Xu, H.; Kaushik, S.C.; Rakshit, D.; Romagnoli, A. Charging performance evaluation of finned conical thermal storage system encapsulated with nanoenhanced phase change material. *Appl. Therm. Eng.* **2019**, *151*, 176–190. [CrossRef]

223. Li, C.; Zhang, B.; Xie, B.; Zhao, X.; Chen, J.; Chen, Z.; Long, Y. Stearic acid/expanded graphite as a composite phase change thermal energy storage material for tankless solar water heater. *Sustain. Cities Soc.* **2019**, *44*, 458–464. [CrossRef]
224. Bahiraei, F.; Fartaj, A.; Nazri, G.A. Experimental and numerical investigation on the performance of carbon-based nanoenhanced phase change materials for thermal management applications. *Energy Convers. Manag.* **2017**, *153*, 115–128. [CrossRef]
225. Kibria, M.G.; Mohtasim, M.S.; Paul, U.K.; Das, B.K.; Saidur, R. Impact of hybrid nano PCM (paraffin wax with $Al_2O_3$ and ZnO nanoparticles) on photovoltaic thermal system: Energy, exergy, exergoeconomic and enviroeconomic analysis. *J. Clean. Prod.* **2024**, *436*, 140577. [CrossRef]
226. Krishna, J.; Kishore, P.; Solomon, A.B. Heat pipe with nano enhanced-PCM for electronic cooling application. *Exp. Therm. Fluid Sci.* **2017**, *81*, 84–92. [CrossRef]
227. Soni, V.; Kumar, A.; Jain, V.K. Performance evaluation of nano-enhanced phase change materials during discharge stage in waste heat recovery. *Renew. Energy* **2018**, *127*, 587–601. [CrossRef]
228. Parameshwaran, R.; Deepak, K.; Saravanan, R.; Kalaiselvam, S. Preparation, thermal and rheological properties of hybrid nanocomposite phase change material for thermal energy storage. *Appl. Energy* **2014**, *115*, 320–330. [CrossRef]
229. Singh, S.K.; Verma, S.K.; Kumar, R. Thermal performance and behavior analysis of $SiO_2$, $Al_2O_3$, and MgO based nano-enhanced phase-changing materials, latent heat thermal energy storage system. *J. Energy Storage* **2022**, *48*, 103977. [CrossRef]
230. Moein-Jahromi, M.; Rahmanian-Koushkaki, H.; Rahmanian, S.; Pilban Jahromi, S. Evaluation of nanostructured GNP and CuO compositions in PCM-based heat sinks for photovoltaic systems. *J. Energy Storage* **2022**, *53*, 105240. [CrossRef]
231. Ali, M.A.; Fayaz Viegas, R.F.; Kumar, M.B.S.; Kannapiran, R.K.; Feroskhan, M. Enhancement of heat transfer in paraffin wax PCM using nano graphene composite for industrial helmets. *J. Energy Storage* **2019**, *26*, 100982. [CrossRef]
232. Maher, H.; Rocky, K.A.; Bassiouny, R.; Saha, B.B. Synthesis and thermal characterization of paraffin-based nanocomposites for thermal energy storage applications. *Therm. Sci. Eng. Prog.* **2021**, *22*, 100797. [CrossRef]
233. Qian, T.; Li, J.; Feng, W.; Nian, H.E. Enhanced thermal conductivity of form-stable phase change composite with single-walled carbon nanotubes for thermal energy storage. *Sci. Rep.* **2017**, *7*, 44710. [CrossRef]
234. Paul, U.K.; Mohtasim, M.S.; Kibria, M.G.; Das, B.K. Nano-material based composite phase change materials and nanofluid for solar thermal energy storage applications: Featuring numerical and experimental approaches. *J. Energy Storage* **2024**, *98*, 113032. [CrossRef]
235. Rufuss, D.D.W.; Kumar, V.R.; Suganthi, L.; Iniyan, S.; Davies, P. Techno-economic analysis of solar stills using integrated fuzzy analytical hierarchy process and data envelopment analysis. *Sol. Energy* **2018**, *159*, 820–833. [CrossRef]
236. Saeed, R.M.; Schlegel, J.P.; Castano, C.; Sawafta, R. Preparation and enhanced thermal performance of novel (solid to gel) form-stable eutectic PCM modified by nano-graphene platelets. *J. Energy Storage* **2018**, *15*, 91–102. [CrossRef]
237. Salyan, S.; Suresh, S. Study of thermo-physical properties and cycling stability of D-Mannitol-copper oxide nanocomposites as phase change materials. *J. Energy Storage* **2018**, *15*, 245–255. [CrossRef]
238. Warzoha, R.J.; Fleischer, A.S. Improved heat recovery from paraffin-based phase change materials due to the presence of percolating graphene networks. *Int. J. Heat. Mass. Transf.* **2014**, *79*, 314–323. [CrossRef]
239. Pethurajan, V.; Sivan, S. Fabrication, characterisation and heat transfer study on microencapsulation of nano-enhanced phase change material. *Chem. Eng. Process.* **2018**, *133*, 12–23. [CrossRef]
240. Arshad, A.; Jabbal, M.; Shi, L.; Yan, Y. Thermophysical characteristics and enhancement analysis of carbon-additives phase change mono and hybrid materials for thermal management of electronic devices. *J. Energy Storage* **2021**, *34*, 102231. [CrossRef]
241. Karthikeyan, K.; Mariappan, V.; Kalidoss, P.; Mohana Jai Ganesh, J.; Nanda Kishore, P.V.R.; Prathiban, S.; Anish, R. Characterization and thermal properties of lauryl alcohol-capric acid binary mixture with hybrid-nanoparticles as phase change material for vaccine storage applications. *J. Energy Storage* **2023**, *74*, 109442. [CrossRef]
242. Han, D.; Guene Lougou, B.; Xu, Y.; Shuai, Y.; Huang, X. Thermal properties characterization of chloride salts/nanoparticles composite phase change material for high-temperature thermal energy storage. *Appl. Energy* **2020**, *264*, 114674. [CrossRef]
243. Kalbande, V.P.; Walke, P.V.; Untawale, S.; Mohan, M. Performance evaluation of novel heat pipe-assisted thermal storage system with parabolic trough solar collector using nanofluid. *Energy Technol.* **2022**, *10*, 2200118. [CrossRef]
244. Wang, J.; Xie, H.; Xin, Z. Thermal properties of paraffin based composites containing multi-walled carbon nanotubes. *Thermochim. Acta* **2009**, *488*, 39–42. [CrossRef]
245. Harikrishnan, S.; Devaraju, A.; Rajesh Kumar, G.; Kalaiselvam, S. Improved thermal energy storage behavior of a novel nanofluid as phase change material (PCM). *Mater. Today Proc.* **2019**, *9*, 410–421. [CrossRef]
246. Mohamed, N.H.; Soliman, F.S.; El Maghraby, H.; Moustfa, Y. Thermal conductivity enhancement of treated petroleum waxes, as phase change material, by α nano alumina: Energy storage. *Renew. Sustain. Energy Rev.* **2017**, *70*, 1052–1058. [CrossRef]
247. Kalbande, V.P.; Fating, G.; Mohan, M.; Rambhad, K.; Sinha, A.K. Experimental and theoretical study for suitability of hybrid nano enhanced phase change material for thermal energy storage applications. *J. Energy Storage* **2022**, *51*, 104431. [CrossRef]

248. Amin, M.; Putra, N.; Kosasih, E.A.; Prawiro, E.; Luanto, R.A.; Mahlia, T.M.I. Thermal properties of beeswax/graphene phase change material as energy storage for building applications. *Appl. Therm. Eng.* **2017**, *112*, 273–280. [CrossRef]
249. Arshad, A.; Jabbal, M.; Shi, L.; Darkwa, J.; Weston, N.J.; Yan, Y. Development of $TiO_2$/RT–35HC based nanocomposite phase change materials (NCPCMs) for thermal management applications. *Sustain. Energy Technol. Assess.* **2021**, *43*, 100865. [CrossRef]
250. Gupta, N.; Kumar, A.; Dhasmana, H.; Kumar, V.; Kumar, A.; Shukla, P.; Verma, A.; Nutan, G.V.; Dhawan, S.K.; Jain, V.K. Enhanced thermophysical properties of metal oxide nanoparticles embedded magnesium nitrate hexahydrate based nanocomposite for thermal energy storage applications. *J. Energy Storage* **2020**, *32*, 101773. [CrossRef]
251. Pugalenthi, S.; Chellapandian, M.; Dharmaraj, J.J.; Devaraj, J.; Arunachelam, N.; Singh, S.B. Enhancing the thermal transport property of eutectic lauric-stearic acid based phase change material with silicon carbide nanoparticles for usage in battery thermal management system. *J. Energy Storage* **2024**, *84*, 110890. [CrossRef]
252. Mayilvelnathan, V.; Arasu, A.V. Characterisation and thermophysical properties of graphene nanoparticles dispersed erythritol PCM for medium temperature thermal energy storage applications. *Thermochim. Acta* **2019**, *676*, 94–103. [CrossRef]
253. Yu, Q.; Zhang, C.; Lu, Y.; Kong, Q.; Wei, H.; Yang, Y.; Sciacovelli, A. Comprehensive performance of composite phase change materials based on eutectic chloride with $SiO_2$ nanoparticles and expanded graphite for thermal energy storage system. *Renew. Energy* **2021**, *172*, 1120–1132. [CrossRef]
254. Tian, H.; Du, L.; Wei, X.; Deng, S.; Wang, W.; Ding, J. Enhanced thermal conductivity of ternary carbonate salt phase change material with Mg particles for solar thermal energy storage. *Appl. Energy* **2017**, *204*, 525–530. [CrossRef]
255. Islam, A.; Pandey, A.K.; Saidur, R.; Tyagi, V.V. Shape stable composite phase change material with improved thermal conductivity for electrical-to-thermal energy conversion and storage. *Mater. Today Sustain.* **2024**, *25*, 100678. [CrossRef]
256. Yin, S.; Lu, M.; Liu, C.; Tong, L.; Wang, L.; Ding, Y. Fabrication and thermal properties of capric–stearic acid eutectic/nano-$SiO_2$ phase change material with expanded graphite and CuO for thermal energy storage. *J. Energy Storage* **2024**, *77*, 110025. [CrossRef]
257. He, M.; Yang, L.; Lin, W.; Chen, J.; Mao, X.; Ma, Z. Preparation, thermal characterization and examination of phase change materials (PCMs) enhanced by carbon-based nanoparticles for solar thermal energy storage. *J. Energy Storage* **2019**, *25*, 100874. [CrossRef]
258. Kumar, P.M.; Sudarvizhi, D.; Michael Joseph Stalin, P.; Aarif, A.; Abhinandhana, R.; Renuprasanth, A.; Sathya, V.; Thirukkural Ezhilan, N. Thermal characteristics analysis of a phase change material under the influence of nanoparticles. *Mater. Today Proc.* **2021**, *45*, 7876–7880. [CrossRef]
259. Hayat, M.A.; Yang, Y.; Li, L.; Bevilacqua, M.; Chen, Y. Preparation and thermophysical characterisation analysis of potential nano-phase transition materials for thermal energy storage applications. *J. Mol. Liq.* **2023**, *376*, 121464. [CrossRef]
260. Bharathiraja, R.; Ramkumar, T.; Selvakumar, M. Studies on the thermal characteristics of nano-enhanced paraffin wax phase change material (PCM) for thermal storage applications. *J. Energy Storage* **2023**, *73*, 109216. [CrossRef]
261. Pasupathi, M.K.; Alagar, K.; Joseph Stalin, P.M.; Matheswaran, M.M.; Ghosh, A. Characterization of hybrid-nano/paraffin organic phase change material for thermal energy storage applications in solar thermal systems. *Energies* **2020**, *13*, 5079. [CrossRef]
262. Anika, U.A.; Kibria, M.G.; Kanka, S.D.; Mohtasim, M.S.; Paul, U.K.; Das, B.K. Exergy, exergo-economic, environmental and sustainability analysis of pyramid solar still integrated hybrid nano-PCM, black sand, and sponge. *Sol. Energy* **2024**, *274*, 112559. [CrossRef]
263. Hemmatian, A.; Kargarsharifabad, H.; Abedini Esfahlani, A.; Rahbar, N.; Shoeibi, S. Improving solar still performance with heat pipe/pulsating heat pipe evacuated tube solar collectors and PCM: An experimental and environmental analysis. *Sol. Energy* **2024**, *269*, 112371. [CrossRef]
264. Sathish, T.; Suresh, P.; Sharma, K.; Saravanan, R.; Saleel, C.A.; Shaik, S.; Khan, S.A.; Panchal, H. Zero emission/energy building heating through parabolic dish collector focused $KNO_3$–$NaNO_3$ and $KNO_3$–$NaNO_3$–$NaNO_2$ PCM absorber: A case study. *Case Stud. Therm. Eng.* **2023**, *44*, 102854. [CrossRef]
265. Nourizadeh, F.; Shekaari, H.; Mokhtarpour, M. High performance nano-enhanced phase change composites based on 2-hydroxyethylammonium stearate for efficient and environmentally friendly thermal energy storage and thermoelectric conversion. *J. Power Sources* **2024**, *614*, 235042. [CrossRef]
266. Tyagi, P.K.; Kumar, R. Comprehensive performance assessment of photovoltaic/thermal system using MWCNT/water nanofluid and novel finned multi-block nano-enhanced phase change material-based thermal collector: Energy, exergy, economic, and environmental (4E) perspectives. *Energy* **2024**, *312*, 133575. [CrossRef]
267. Yu, X.; He, G.; Wu, J.; Wu, Z.; Wang, Y.; Dong, L.; Xie, H. Enhancement of solar-to-thermal properties of multiple-point $Cu_2O$/TiN plasmonic nanofluids. *Chem. Eng. J.* **2024**, *498*, 155523. [CrossRef]
268. Aligholami, M.; Shafiei, S.; Akbari, M.; Moodley, M.K.; Veeredhi, V.R.; Mthunzi, P.; Maaza, M. $MoS_2$-based nanofluid using pulsed laser ablation in liquid for concentrating solar power plant: Thermophysical study. *Sol. Energy* **2024**, *280*, 112876. [CrossRef]
269. Seyyedi, S.M.; Dogonchi, A.S.; Hashemi-Tilehnoee, M.; Waqas, M.; Ganji, D.D. Entropy generation and economic analyses in a nanofluid filled L-shaped enclosure subjected to an oriented magnetic field. *Appl. Therm. Eng.* **2020**, *168*, 114789. [CrossRef]

270. Tayebi, T.; Dogonchi, A.S.; Karimi, N.; Hu, G.-J.; Chamkha, A.J.; Elmasry, Y. Thermo-economic and entropy generation analyses of magnetic natural convective flow in a nanofluid-filled annular enclosure fitted with fins. *Sustain. Energy Technol. Assess.* **2021**, *46*, 101274. [CrossRef]
271. Hu, J.-T.; Mei, S.-J. Natural convection in nanofluid enclosure under magnetic field: Entropy generation and economic analysis. *Propuls. Power Res.* **2024**, *13*, 273–293. [CrossRef]